Supplement of Geosci. Model Dev., 12, 4309–4346, 2019
https://doi.org/10.5194/gmd-12-4309-2019-supplement

Geoscientific Model Development
Open Access
EGU

Supplement of

The biophysics, ecology, and biogeochemistry of functionally diverse, vertically and horizontally heterogeneous ecosystems: the Ecosystem Demography model, version 2.2 – Part 1: Model description

Marcos Longo et al.

Correspondence to: Marcos Longo (mlongo@post.harvard.edu)

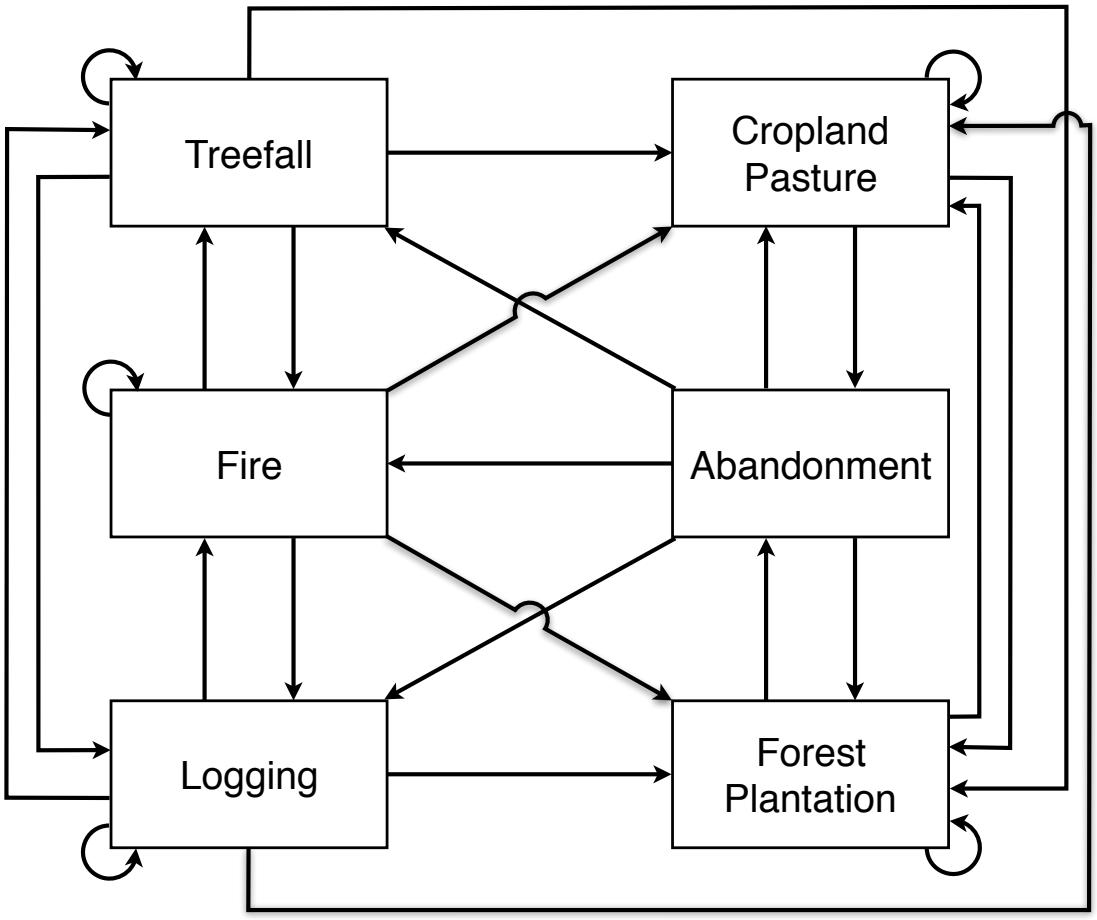

Figure S1: Schematic of disturbance types that generate new patches in ED-2.2. Patches are classified according to the last disturbance type (boxes), and new disturbances that create new patches are indicated by arrows (the arrow head points to the new disturbance type). The absence of arrows between some disturbance patches (e.g. from cropland to tree fall) indicate that such transition is not allowed. Arrows pointing to the same disturbance type indicate generation of new patches without change in the disturbance type.

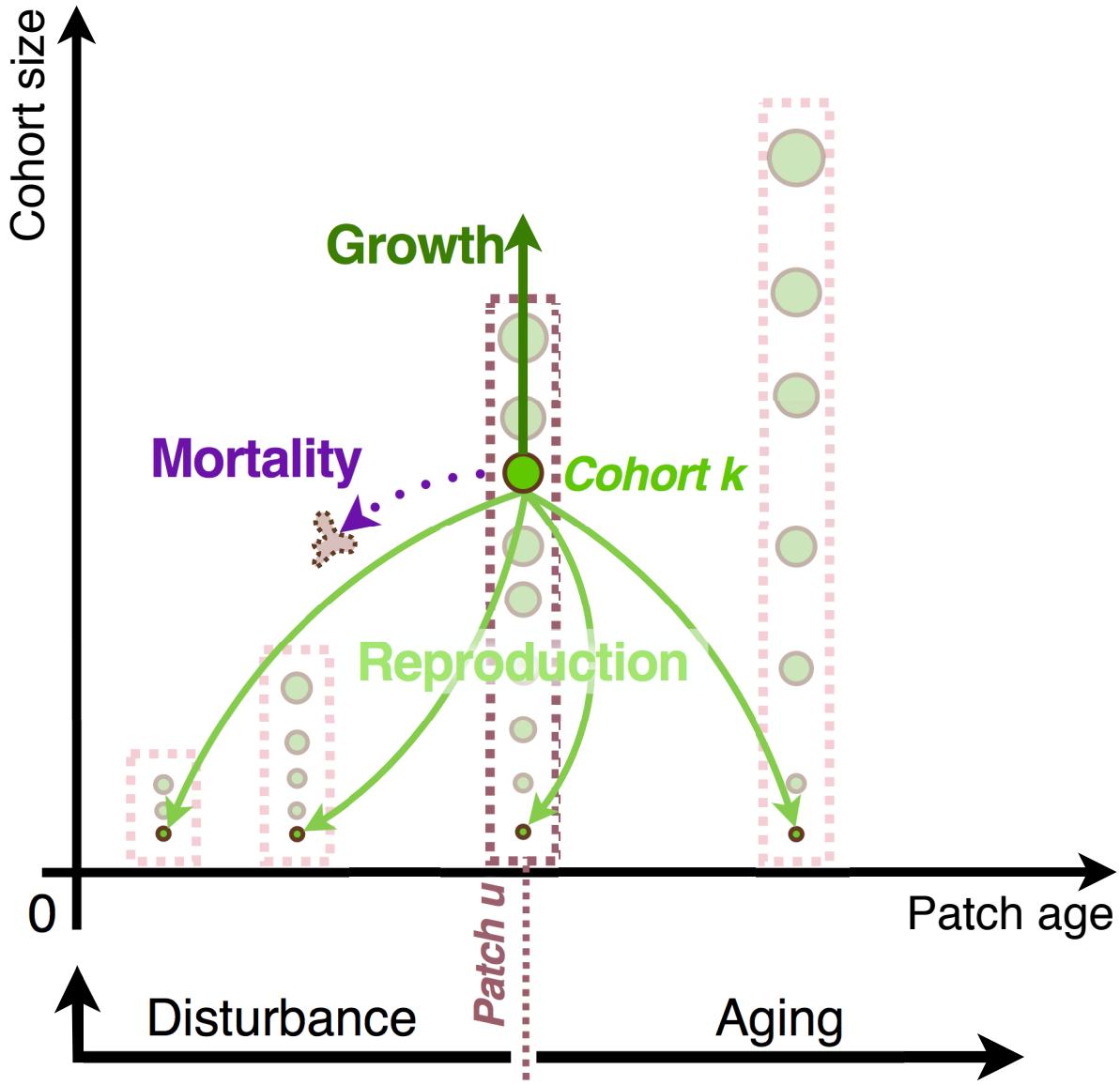

Figure S2: Schematics of ecosystem dynamics in ED-2.2, based on Fig. 5 of Moorcroft et al. (2001). The diagram shows a simplified case in which only of plant functional type and one disturbance type exist. Each dashed box corresponds to one patch, and each circle correspond to one cohort. Changes in the ecosystem structure are represented by arrows: green and purple arrows are associated with cohort dynamics, and black arrows are associated with patch dynamics. Every cohort time step, cohorts can grow in size, some of the cohort population is lost through mortality, and new cohorts are generated from reproduction. Every patch time step, patch age is increased linearly due to age, and a fraction of each patch is lost through disturbance, which resets patch age.

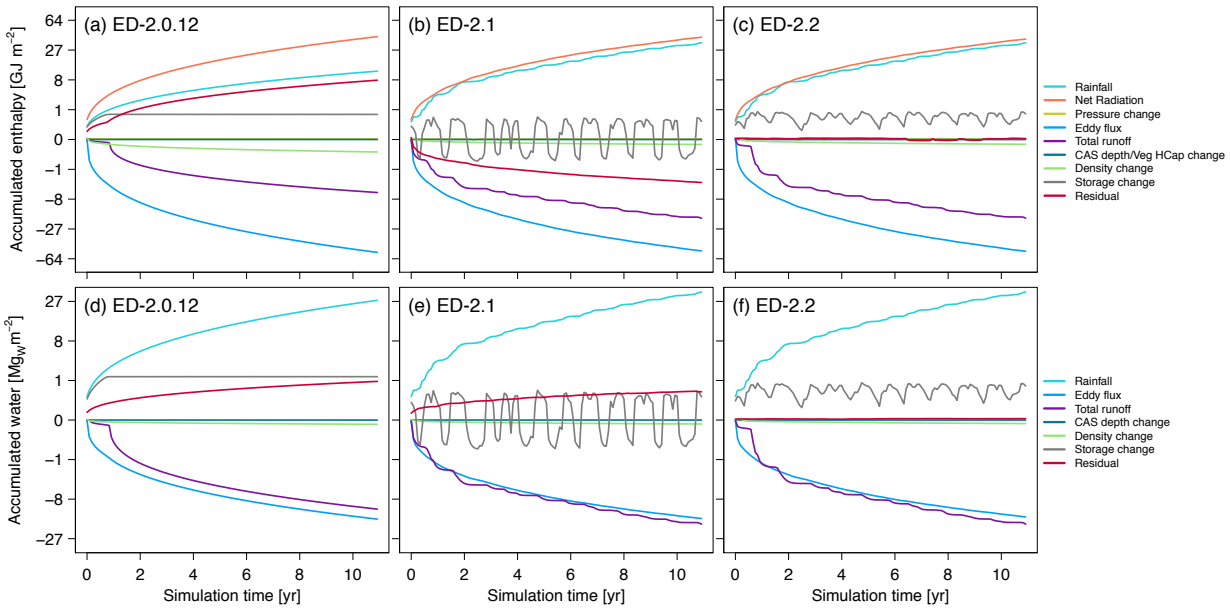

Figure S3: Comparison of budget closure for (a-c) enthalpy and (d-f) water between three different ED-2 versions: (a,d) ED-2.0.12 (`https://github.com/EDmodel/ED2/releases/tag/rev-12`), the first stable version of ED-2.0 (Medvigy et al., 2009) using the current model code structure; (b,e) ED-2.1 (`https://github.com/EDmodel/ED2/releases/tag/rev-64`); (c,f) ED-2.2. Simulations were carried out for a single-patch simulation at GYF for 11 years, without vegetation dynamics (earlier releases did not account for changes in energy and water when vegetation dynamics was active). Terms are presented as the cumulative contribution to the change storage. Total storage is the combination of canopy air space, cohorts, temporary surface water and soil layers. Positive (negative) values mean accumulation (loss) by the combined storage pool over the time. Pressure change accounts for changes in enthalpy when pressure from the meteorological forcing is updated, and density change accounts for changes in mass to ensure the ideal gas law. Canopy air space (CAS) change and vegetation heat capacity (Veg Hcap) change reflect the addition/subtraction of carbon, water, and enthalpy due to the vegetation dynamics modifying the canopy air space depth and the total heat capacity of the vegetation due to biomass accumulation or loss. Storage change is the net gain or loss of total storage, and residual corresponds to the deviation from the perfect closure. Note that we present the y axis in cube root scale to improve visualization of the smaller terms. Details on developments of ED-2.0.12, ED-2.1, and ED-2.2 are described in Supplement S1.

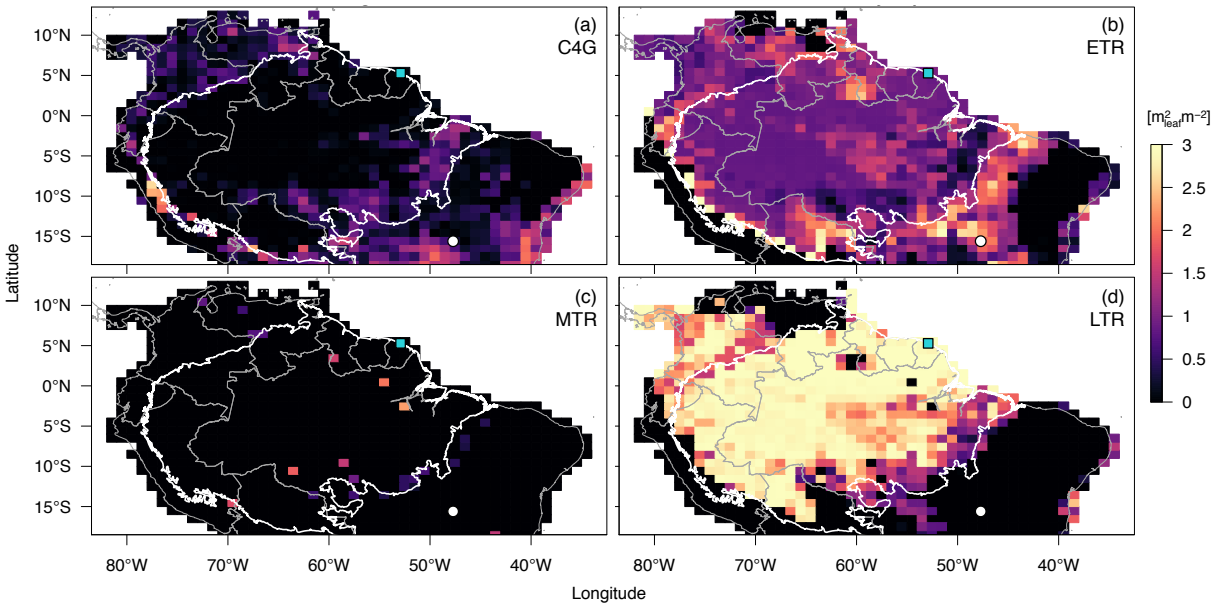

Figure S4: Simulated distribution of PFT-dependent leaf area index across tropical South America: (a) C_4 grasses (C4G); (b) Early-successional, tropical trees (ETR); (c) mid-successional, tropical trees (MTR); (d) late-successional, tropical trees (LTR). Maps were obtained from the final state of a 6-century simulation (1400–2002), initialized with near-bare ground conditions, active fires, and with prescribed land use changes between 1900 and 2002. Points indicate the location of the example sites (Fig. 8): (□) Paracou (GYF), a tropical forest site; (◯) Brasília (BSB), a woody savanna site. White contour is the domain of the Amazon biome, and grey contours are the political borders.

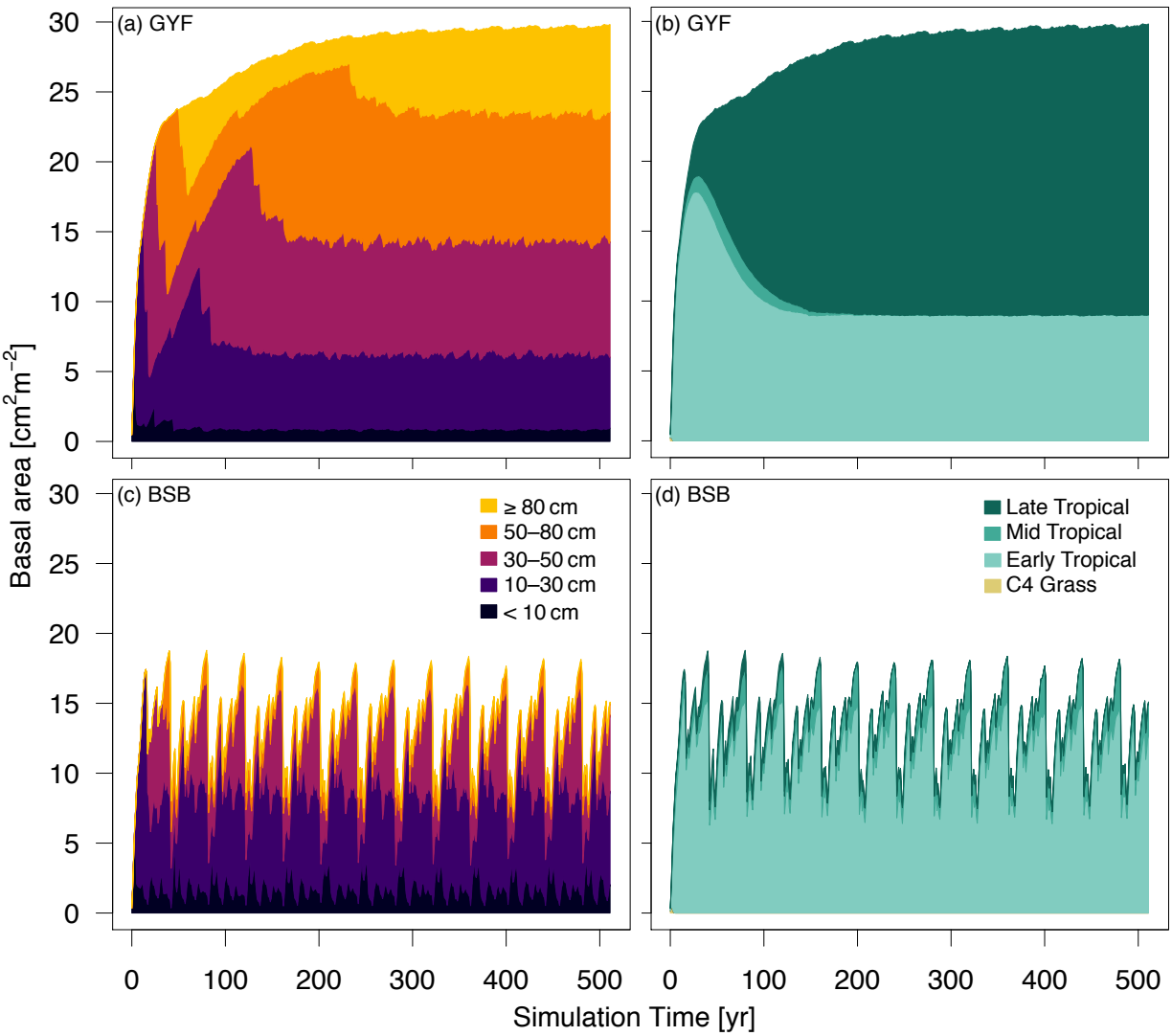

Figure S5: Simulated time series of basal area for near-bare ground simulations for (a,b) Paracou (GYF, tropical forest) and (c,d) Brasília (BSB, woody savanna), using local meteorological forcing and active fires, colored by the relative contribution of (a,c) plants of different sizes and (b,d) plants of different functional groups. See Fig. S4 for the location of both example sites.

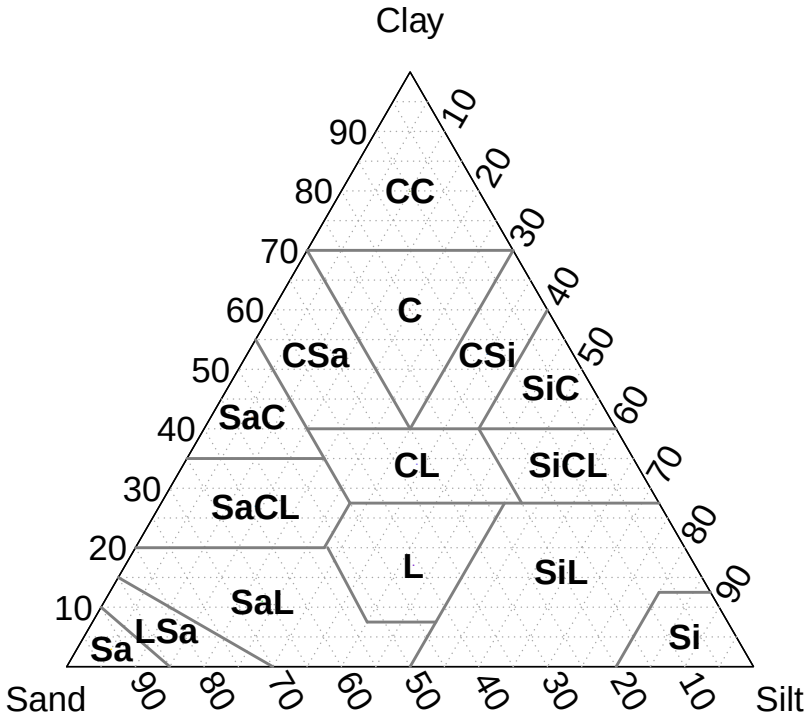

Figure S6: Barycentric diagram of volumetric percentage of soil particle sizes (sand, silt, and clay) along with the canonical soil texture classes in ED-2.2. Classes are: Sa – sand, LSa – loamy sand, SaL – sandy loam, SiL – silty loam, L – loam, SaCL – sandy clay loam, SiCL – silty clay loam, CL – clayey loam, SaC – sandy clay, SiC – silty clay, C – clay, Si – silt, CC – heavy clay, CSa – clayey sand, and CSi – clayey silt.

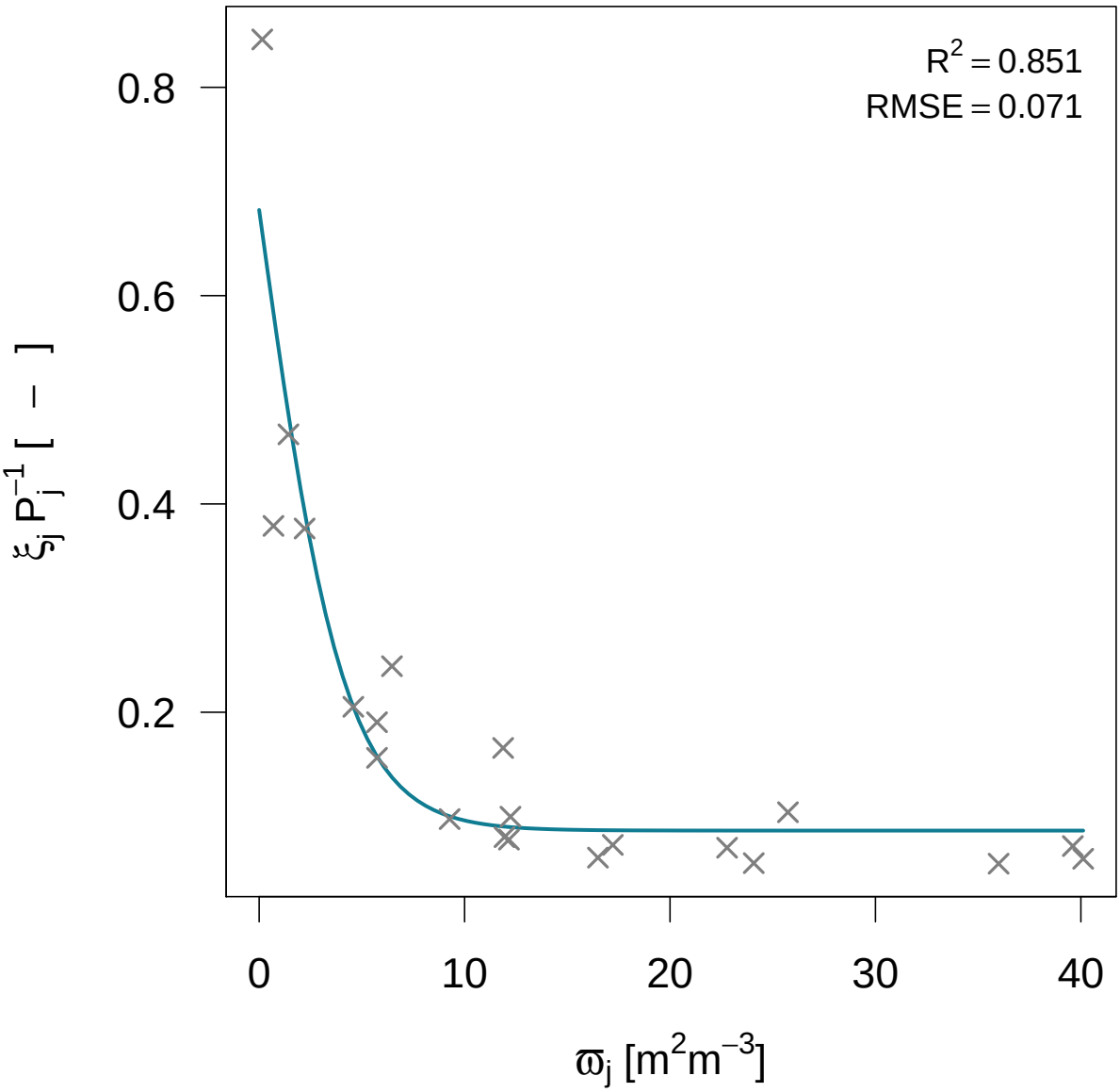

Figure S7: Fitted curve (Eq. S135) relating the effective drag coefficient ($\xi j \mathcal{P}_j^{-1}$) with plant area density (ϕ_j). Data points for fitting were extracted from Figure 3a of Wohlfahrt and Cernusca (2002) using a digitizer tool. Adjusted R^2 and the root mean square error (RMSE) are shown in the top right.

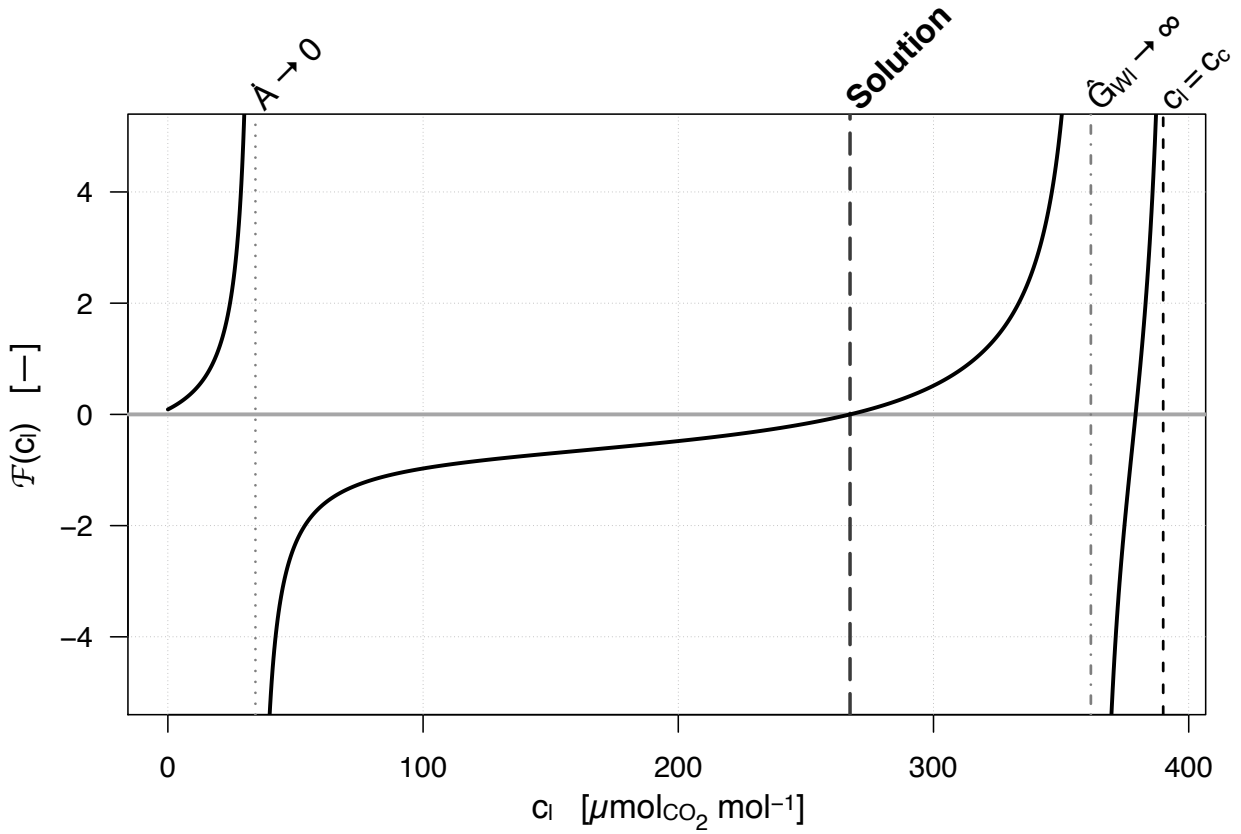

Figure S8: Example for the function $\mathcal{F}(c_{l_k})$ curve for the RuBP-saturated case for a mid-successional, tropical broadleaf tree when $Q_{\mathrm{PAR}:a,l_k} = 100\,\mathrm{W\,m^{-2}}$, $T_{t_k} = T_c = 301.15\,\mathrm{K}$, $w_c = 0.017\,\mathrm{kg_W\,kg_{Air}^{-1}}$, $u_{t_k} = 0.25\,\mathrm{m\,s^{-1}}$, and $c_c = 390\,\mu\mathrm{mol_C\,mol_{Air}^{-1}}$. Vertical lines shows the solution and the singularities within the plausible range.

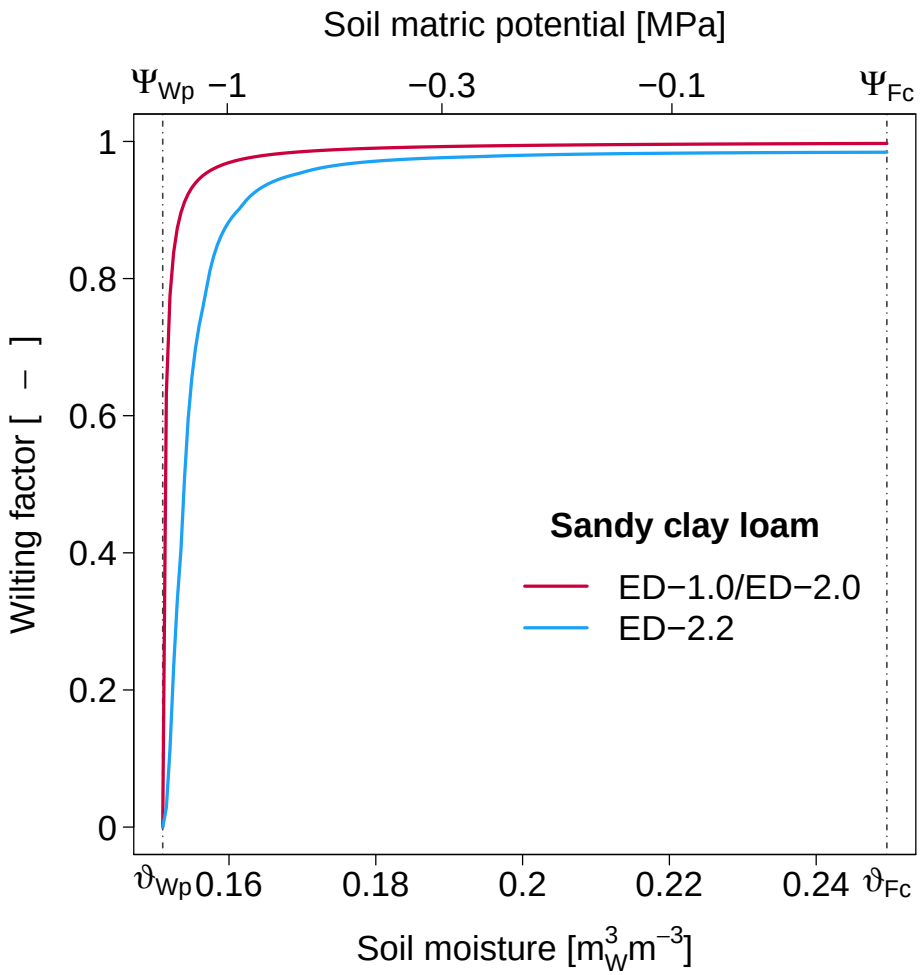

Figure S9: Example of the wilting factor (f_{Wl_k}, Eq. S201) response to soil moisture change for the original implementation in ED (ED-1.0 and ED-2.0, Moorcroft et al., 2001; Medvigy et al., 2009) and the ED-2.2 model approach. Results here are shown for the idealized case with constant soil moisture profile in a 3-m deep, sandy clay loam soil, for a mid-successional tropical cohort with default parameters (Table S5), with diameter at breast height of 30 cm and leaf area index of 1 $m^2_{Leaf} m^{-2}$, non-limited leaf-level transpiration rate $\dot{E}_k = 9.0\ kg_W\, m^{-2}_{Leaf}\, day^{-1}$. Values are shown for soil moisture columns ranging from wilting point ($\vartheta_{Wp}; \Psi_{Wp}$) to field capacity ($\vartheta_{Fc}; \Psi_{Fc}$).

Table S1: List of subscripts used in the manuscript. Fluxes are denoted by a dotted letter, and two subscripts separated with a comma: $\dot{X}_{m,n}$. This means positive (negative) flux going from thermodynamic system m (n) to thermodynamic system n (m). N_T is the total number of cohorts, N_G is the total number of soil (ground) layers, N_S is the total number of temporary surface water/snowpack layers, and N_C is the total number of canopy air space layers, currently only used to obtain properties related to canopy conductance.

Subscript	Description
X_3	Property at the water's triple point ($T_3 = 273.16$ K)
X_a	Air above canopy, from the meteorological forcing
X_{b_k}	Branch wood of cohort k ($k \in \{1,2,\ldots,N_T\}$)
$X_{\mathbf{C}}$	Size vector (leaves, fine roots, sapwood, heartwood, and non-structural storage)
X_C	Carbon component
X_c	Canopy air space (single layer)
X_{c_j}	Canopy air space, layer j ($j \in \{1,2,\ldots,N_C\}$)
X_d	Non-water component of thermodynamic system
X_{e_j}	Necromass pools: e_1, metabolic litter (fast); e_2, structural debris (intermediate); e_3, humified/dissolved (slow)
X_f	Plant functional type
X_{Fc}	Soil property at field capacity
X_{Fr}	Soil property at critical moisture for fire ignition
X_{g_j}	Soil (ground), layer j ($j \in \{1,2,\ldots,N_G\}$)
X_{h_k}	Structural (heartwood) of cohort k ($k \in \{1,2,\ldots,N_T\}$)
X_i	Ice
$X_{i\ell}$	Ice-liquid phase transition
X_{iv}	Ice-vapor phase transition
X_k	Cohort k ($k \in \{1,2,\ldots,N_T\}$), for variables that are only defined for cohorts
X_ℓ	Liquid water
$X_{\ell v}$	Liquid-vapor phase transition
X_{l_k}	Leaves of cohort k ($k \in \{1,2,\ldots,N_T\}$)
X_{Ld}	Soil property at critical moisture for leaf shedding (drought-deciduous phenology)
X_m	Spectral band: $m = 1$, PAR; $m = 2$, NIR; $m = 3$, TIR
X_{n_k}	Non-structural carbon storage (starch, sugars) of cohort k
X_o	Surface runoff
X_p	Property at constant pressure
X_{Po}	Soil property at soil porosity (water saturation)
X_q	Disturbance type
X_{r_k}	Roots of cohort k
X_{Re}	Soil property at residual soil moisture
X_{Sat}	Phase equilibrium (saturation)
X_{s_j}	Temporary surface water/snowpack, layer j ($j \in \{1,2,\ldots,N_S\}$)
X_{t_k}	Cohort k ($k \in \{1,2,\ldots,N_T\}$)
X_U	Property associated with momentum (forced convection)
X_u	Patch u ($u \in \{1,2,\ldots,N_P\}$)
X_v	Water vapor
X_w	Water component of thermodynamic system (any phase)

Table S1: (Continued)

Subscript	Description
X_{Wp}	Soil property at permanent wilting point
X_x	West-East direction
$X_{\mathbf{x}}$	Horizontal direction
X_y	South-north direction
X_z	Vertical direction
X_{α_k}	Total living tissues (leaves, fine roots, sapwood) of cohort k ($k \in \{1,2,\ldots,N_T\}$)
X_{β_k}	Branch boundary layer of cohort k ($k \in \{1,2,\ldots,N_T\}$)
X_{Δ_k}	Carbon balance of cohort k ($k \in \{1,2,\ldots,N_T\}$)Q
X_{Θ}	Property associated with buoyancy (free convection)
X_{κ}	Soil textural component: $\kappa = 0$, water; $\kappa = 1$, sand; $\kappa = 2$, silt; $\kappa = 3$, clay
X_{λ_k}	Leaf boundary layer of cohort k ($k \in \{1,2,\ldots,N_T\}$)
X_{ϱ_k}	Reproductive tissues (seeds, fruits, flowers, cones) of cohort k ($k \in \{1,2,\ldots,N_T\}$)
X_{σ_k}	Sapwood of cohort k ($k \in \{1,2,\ldots,N_T\}$)
X_{∞}	Fluxes that depend on air above layer a, such as radiation and rainfall
$X_{\varnothing}$	Bare ground equivalent
$X_{\ast}$	Frost
$X_{\circledast}$	Pure, fresh snow

Table S2: List of variables used in this manuscript. For variables used in various thermodynamic systems, the subscript is omitted (see Table S1 for a comprehensive list of subscripts). Variable dimensions are shown in standard units for reference. Units with subscript are specific to a single substance: $\mathrm{kg_W}$ means kilograms of water, and $\mathrm{kg_C}$ means kilograms of carbon, and $\mathrm{kg_D}$ means kilogram of non-water material.

Variable	Description	Units
A	Site area	—
$\dot{A}$	Net leaf-level CO_2 uptake rate	$\mathrm{mol_C\,m_{Leaf}^{-2}\,s^{-1}}$
$\mathcal{A}$	Mean leaf/branch inclination relative to horizontal plane	rad
a	Patch age since last disturbance	s
$æ$	Aging factor for density-independent mortality (temperate PFTs)	yr
B	Soil carbon decay rates under optimal conditions	$\mathrm{s^{-1}}$
$\mathcal{B}_C$	Carbon to oven-dry biomass ratio	$\mathrm{kg_C\,kg_{Bio}^{-1}}$
$\mathcal{B}_W$	Water to oven-dry biomass ratio	$\mathrm{kg_W\,kg_{Bio}^{-1}}$
b	Slope of the logarithm of the water retention curve	—
BA	Basal area	$\mathrm{cm^2}$
C	Carbon mass (area-based, extensive)	$\mathrm{kg_C\,m^{-2}}$
$\mathbf{C}$	Size (carbon mass) vector	$\mathrm{kg_C\,plant^{-1}}$
$\mathcal{C}$	Empirical coefficients for determining biomass of individual tissues	—
$C^{\bullet}$	Expected carbon mass given size, PFT, and demographic density	$\mathrm{kg_C\,m^{-2}}$
$C^{\circledcirc}$	Carbon mass needed to bring tissue to allometry given size and PFT	$\mathrm{kg_C\,m^{-2}}$
$\dot{C}$	Carbon flux	$\mathrm{kg_C\,m^{-2}\,s^{-1}}$
$\dot{C}^{\bigstar}$	Carbon flux to necromass pools due to mortality	$\mathrm{kg_C\,m^{-2}\,s^{-1}}$
CHD	Chilling days	day
c	Carbon mixing ratio (intensive)	$\mathrm{mol_C\,mol^{-1}}$
D	"Dry material" mass (area-based, extensive)	$\mathrm{kg_D\,m^{-2}}$
$\mathcal{D}$	"Dry material" mass (volume-based, extensive)	$\mathrm{kg_D\,m^{-3}}$
d	Specific mass of "dry material" (intensive)	$\mathrm{kg_D\,kg^{-1}}$
DBH	Diameter at breast height	cm
$Đ$	Auxiliary variable for solution of canopy radiation transfer	—
$ð$	Sub-surface drainage impediment parameter	—
E	Average projection of leaves and branches onto the horizontal	—
$\dot{E}$	Leaf-level transpiration rate	$\mathrm{mol_C\,m_{Leaf}^{-2}\,s^{-1}}$
$\mathcal{E}$	Penalty reduction function for extreme temperatures and soil moistures	—
Ein	Average photon specific energy in the PAR band	$\mathrm{J\,mol^{-1}}$
$\hat{e}_l$	Leaf elongation factor given environmental constraints	—
$\mathcal{F}$	Dimensionless function of intercellular carbon dioxide	—
f_{AG}	Fraction of woody biomass that is above ground	—
f_{Clump}	Clumping factor	—
f_{Gl}	Ratio between stomatal conductance of CO_2 and water	—
$f_{G\lambda}$	Ratio between leaf boundary layer conductance of CO_2 and water	—
f_h	Fraction of the decay of soil carbon pools that are respired	—
f_{LD}	Fraction of carbon reabsorption before leaf shedding	—
f_{lw}	Down-regulation factor for photosynthesis due to soil moisture limitation	—
f_R	Ratio between day respiration and maximum carboxylation	—
f_r	Ratio between fine root and leaf biomass on allometry given size and PFT	—

Table S2: (Continued)

Variable	Description	Units
f_{TSW}	Fraction of ground covered by water or snow	—
$f_{\mathcal{V}}$	Volumetric fraction	—
f_{δ}	Fraction of reproduction that is randomly dispersed	—
f_{σ}	Scaling factor between height, sapwood, and leaf biomass on allometry	m^{-1}
G	Conductance (rate form)	$\mathrm{m\,s}^{-1}$
$\hat{G}$	Conductance (flux form)	$\mathrm{kg\,m}^{-2}\,\mathrm{s}^{-1}$ or $\mathrm{mol\,m}^{-2}\,\mathrm{s}^{-1}$
g	Gravity acceleration	$\mathrm{m\,s}^{-2}$
$\mathbf{g}$	Net growth rate	$\mathrm{kg_C\,plant}^{-1}\,\mathrm{s}^{-1}$
GDD	Growing degree-days	$\mathrm{K\,day}$
Gr	Grashof number	—
$\mathcal{H}$	Bulk specific enthalpy	$\mathrm{J\,m}^{-3}$
H	Enthalpy (area-based, extensive)	$\mathrm{J\,m}^{-2}$
$\dot{H}$	Enthalpy flux associated with mass flux	$\mathrm{W\,m}^{-2}$
h	Specific enthalpy (intensive)	$\mathrm{J\,kg}^{-1}$
$\tilde{h}$	Specific enthalpy at reference height	$\mathrm{J\,kg}^{-1}$
$\mathcal{I}$	Fire intensity parameter	s^{-1}
i	Fraction of water in solid phase (ice)	—
K	Eddy diffusivity	$\mathrm{m}^2\,\mathrm{s}^{-1}$
$\mathcal{K}_{\mathrm{C}}$	Michaelis constant for carboxylation	$\mathrm{mol_C\,mol}^{-1}$
$\mathcal{K}_{\mathrm{ME}}$	Effective Michaelis constant	$\mathrm{mol_C\,mol}^{-1}$
$\mathcal{K}_{\mathrm{O}}$	Michaelis constant for oxygenation	$\mathrm{mol_{O_2}\,mol}^{-1}$
k_{PEP}	Slope of CO_2-limited carboxylation rate	$\mathrm{mol\,mol_C^{-1}}$
$\mathcal{L}$	Obukhov length scale	m
l	Specific latent heat	$\mathrm{J\,kg}^{-1}\,\mathrm{K}^{-1}$
$l_{i\ell 3}$	Specific latent heat of fusion at triple point temperature	$\mathrm{J\,kg}^{-1}\,\mathrm{K}^{-1}$
l_{iv3}	Specific latent heat of sublimation at triple point temperature	$\mathrm{J\,kg}^{-1}\,\mathrm{K}^{-1}$
ℓ	Fraction of water in liquid phase	—
£	Fraction of living tissues that are lignified	—
M	Slope of stomatal conductance function	—
$\mathcal{M}$	Molar mass	$\mathrm{kg\,mol}^{-1}$
MCWD	Maximum cumulative water deficit	mm
m	Mortality rate	s^{-1}
n	Cohort demographic density	$\mathrm{plant\,m}^{-2}$
N_C	Number of canopy air space layers	—
N_F	Number of plant functional types	—
N_G	Number of soil layers	—
N_P	Number of patches	—
N_Q	Number of disturbance types	—
N_S	Actual number of temporary surface water layers	—
$N_S^{\max}$	Maximum number of temporary surface water layers	—
N_T	Number of cohorts	—
$N_{T(\mathrm{canopy})}$	Number of canopy cohorts	—
Nu	Nusselt number	—
$\mathcal{O}$	Open canopy fraction	—
o	Oxygen mixing ratio	$\mathrm{mol_{O_2}\,mol}^{-1}$

Table S2: (Continued)

Variable	Description	Units
$\mathcal{P}$	Sheltering factor for momentum	—
p	Atmospheric pressure	Pa
$p_{vi}^{\equiv}$	Saturation pressure: vapor-ice	Pa
$p_{v\ell}^{\equiv}$	Saturation pressure: vapor-liquid	Pa
Pr	Prandtl number	—
$\dot{Q}$	Heat flux (no mass exchange involved)	$\mathrm{W\,m^{-2}}$
$\dot{Q}^{\odot}$	Downward direct irradiance	$\mathrm{W\,m^{-2}}$
$\dot{Q}^{\Downarrow}$	Downward hemispheric diffuse irradiance	$\mathrm{W\,m^{-2}}$
$\dot{Q}^{\Uparrow}$	Upward hemispheric diffuse irradiance	$\mathrm{W\,m^{-2}}$
$\dot{Q}^{\blacklozenge}$	Irradiance emitted by black body	$\mathrm{W\,m^{-2}}$
$\mathcal{Q}_{10}$	Temperature coefficient for temperature-response function	—
$\dot{q}^{\mathrm{PAR}}$	Photon flux absorbed by leaves	$\mathrm{W\,m^{-2}_{Leaf}}$
q	Specific heat (intensive)	$\mathrm{J\,kg^{-1}}$
$q^{(\mathrm{OD})}$	Specific heat of oven-dry tissue (intensive)	$\mathrm{J\,kg^{-1}}$
q_p	Specific heat at constant pressure (intensive)	$\mathrm{J\,kg^{-1}}$
$\dot{R}$	Leaf-level dark respiration rate	$\mathrm{mol_C\,m^{-2}_{Leaf}\,s^{-1}}$
$\mathcal{R}$	Gas constant for typical air	$\mathrm{J\,mol^{-1}\,K^{-1}}$
r	Decay rate associated with root respiration	$\mathrm{s^{-1}}$
Re	Reynolds number	—
Ri_B	Bulk Richardson number	—
S	Elements of the flux matrix for solving the canopy radiation transfer model	—
$\mathbf{S}$	Flux matrix for solving the canopy radiation transfer model	—
$\mathcal{S}$	Above-canopy velocity variance to momentum flux ratio	—
SLA	Specific leaf area	$\mathrm{m^2_{Leaf}\,kg_C^{-1}}$
s_g	Soil wetness function for ground evaporation	—
s_l	Soil wetness function for drought-deciduous phenology	—
β	Joint eddy mixing length scale (shear- and wake-driven turbulence)	—
TSW	Temporary surface water	—
T	Temperature	K
T_3	Temperature of water triple point	K
$T_{\ell 0}$	Zero-energy temperature of supercooled liquid water	K
T_{Phen}	Temperature threshold for cold-deciduous leaf phenology	K
T_{v0}	Zero-energy temperature of supercooled water vapor	K
$T_{\mathcal{V}}$	Virtual temperature	K
$\mathcal{T}$	Temperature coefficient function ($\mathcal{Q}_{10}$ function)	—
$\mathcal{T}'$	Penalty reduction function for extreme temperatures	—
$\mathfrak{T}_{\mathrm{GS}}$	Extended growing season (for cold-deciduous leaf phenology)	—
$\mathfrak{T}_{\mathrm{SS}}$	Extended senescing season (for cold-deciduous leaf phenology)	—
t	Time	s
t_{Runoff}	Runoff decay time	s
$t_{\odot}$	Daytime duration	min
TKE	(Specific) Turbulent kinetic energy	$\mathrm{m^2\,s^{-2}}$
$\mathbf{P}$	Auxiliary variable for solution of canopy radiation transfer	—
p	Number of leaf sides with stomata	—
$\dot{U}$	Momentum flux	$\mathrm{kg\,m^{-1}\,s^{-2}}$
$u_{\mathbf{x}}$	Horizontal wind speed	$\mathrm{m\,s^{-1}}$

Table S2: (Continued)

Variable	Description	Units
u_z	Vertical wind velocity	$\mathrm{m\,s^{-1}}$
$u^\star$	Friction velocity	$\mathrm{m\,s^{-1}}$
$\dot{V}_C$	Leaf-level carboxylation rates	$\mathrm{mol_C\,m_{Leaf}^{-2}\,s^{-1}}$
$\dot{V}_C^{\mathrm{RuBP}}$	RuBP-saturated carboxylation rates	$\mathrm{mol_C\,m_{Leaf}^{-2}\,s^{-1}}$
$\dot{V}_C^{\mathrm{CO_2}}$	CO_2-limited carboxylation rate	$\mathrm{mol_C\,m_{Leaf}^{-2}\,s^{-1}}$
$\dot{V}_C^{\mathrm{PAR}}$	Light-limited carboxylation rate	$\mathrm{mol_C\,m_{Leaf}^{-2}\,s^{-1}}$
$\dot{V}_O$	Leaf-level oxygenation (photorespiration) rate	$\mathrm{mol_{O_2}\,m_{Leaf}^{-2}\,s^{-1}}$
$\mathcal{V}$	Volume	$\mathrm{m^3}$
v	Fraction of water in gas phase (water vapor)	—
W	Water mass (area-based, extensive)	$\mathrm{kg_W\,m^{-2}}$
$\dot{W}$	Water flux	$\mathrm{kg_W\,m^{-2}\,s^{-1}}$
$\mathcal{W}$	Water mass (volume-based, extensive)	$\mathrm{kg_W\,m^{-3}}$
w	Specific humidity (intensive)	$\mathrm{kg_W\,kg^{-1}}$
$w^{\equiv}$	Saturation specific humidity (intensive)	$\mathrm{kg_W\,kg^{-1}}$
$\hat{w}_{\max}$	Cohort water holding capacity of rainfall interception, dew and frost	$\mathrm{kg_W\,m_{Leaf+Wood}^{-2}}$
X	Crown area index	$\mathrm{m_{Crown}^2\,m^{-2}}$
$x^\star$	Characteristic dimension for boundary-layer generating obstacle	m
Y	Auxiliary functions, used only in the sections where they are described	—
$\mathcal{Y}$	Boolean variable controlling fire ignition	—
y	Auxiliary constants, used only in the sections where they are described	—
Z	Zenith distance	rad
$\mathcal{Z}$	Empirical coefficients to determine height	—
z	Height ($z > 0$) or depth ($z < 0$)	m
$z^\star$	Height above displacement height	m
z^-	Height of crown base	m
z_0	Roughness length	m
z_d	Displacement height	m
α	Probability distribution of gap ages	—
β	Backscattering coefficient, diffuse irradiance	—
$\beta^\odot$	Backscattering coefficient, direct irradiance	—
Γ	CO_2 compensation point	$\mathrm{mol_C\,mol^{-1}}$
γ	Growth rate	$\mathrm{s^{-1}}$
Δt	Time step	s
Δw	Stomatal conductance control on severe leaf-level water vapor deficit	$\mathrm{kg_W\,kg^{-1}}$
Δz	Layer thickness	m
δ_{ij}	Kronecker delta (1 if $i = j$, 0 otherwise)	—
ϵ	Quantum yield	—
ε	Thermal dilatation coefficient	$\mathrm{K^{-1}}$
F	Coefficients for generic function of CO_2 uptake rate (Table S9)	—
ζ	Dimensionless Obukhov length	—
ζ_0	Dimensionless roughness length	—
η	Thermal diffusivity of air	$\mathrm{m^2\,s^{-1}}$
θ	Potential temperature	K
$\theta_{\mathcal{V}}$	Virtual potential temperature	K
$\theta_{\mathcal{V}}^\star$	Characteristic scale: Virtual potential temperature	K
ϑ	Volumetric soil moisture	$\mathrm{m_W^3\,m^{-3}}$

Table S2: (Continued)

Variable	Description	Units
ι_U	Turbulence intensity	—
κ	von Kármán constant	—
$\varkappa$	Auxiliary variable for solution of canopy radiation transfer	—
Λ	Leaf area index	$\mathrm{m}^2_{\mathrm{Leaf}}\,\mathrm{m}^{-2}$
λ	Disturbance rate	s^{-1}
μ	Inverse of optical depth per unit of plant area index	$\mathrm{m}^2_{\mathrm{Plant}}\,\mathrm{m}^{-2}$
$\mu^{\odot}$	Same as above, specific for direct radiation	$\mathrm{m}^2_{\mathrm{Plant}}\,\mathrm{m}^{-2}$
$\overline{\mu}$	Same as above, specific for diffuse radiation	$\mathrm{m}^2_{\mathrm{Plant}}\,\mathrm{m}^{-2}$
ν	Kinematic viscosity	$\mathrm{m}^2\,\mathrm{s}^{-1}$
Ξ	Cumulative cohort drag area per unit ground area	$\mathrm{m}^2_{\mathrm{Plant}}\,\mathrm{m}^{-2}$
ξ	Drag coefficient	—
ϖ	Oxygenase:Carboxylase ratio	$\mathrm{mol}_{\mathrm{O}_2}\,\mathrm{molC}^{-1}$
ρ	Density	$\mathrm{kg}\,\mathrm{m}^{-3}$
ϱ	Recruitment rate	s^{-1}
$\hat{\sigma}$	Survivorship fraction following disturbance	—
σ_{SB}	Stefan-Boltzmann constant	$\mathrm{W}\,\mathrm{m}^{-2}\,\mathrm{K}^{-4}$
σ_u	Standard deviation of wind speed	$\mathrm{m}\,\mathrm{s}^{-1}$
ς	Scattering coefficient, diffuse irradiance	—
$\varsigma^{\odot}$	Scattering coefficient, direct irradiance	—
ς_R	Reflectance coefficient	—
ς_T	Transmittance coefficient	—
τ	Turnover rate (active tissues or non-structural carbon)	s^{-1}
Υ_{Q}	Thermal conductivity	$\mathrm{W}\,\mathrm{m}^{-1}\,\mathrm{K}^{-1}$
Υ_{Ψ}	Hydraulic conductivity	$\mathrm{m}\,\mathrm{s}^{-1}$
Φ	Total plant area index	$\mathrm{m}^2_{\mathrm{Plant}}\,\mathrm{m}^{-2}$
$\tilde{\Phi}$	Clump-corrected, effective total plant area index	$\mathrm{m}^2_{\mathrm{Plant}}\,\mathrm{m}^{-2}$
ϕ	Plant area density	$\mathrm{m}^2_{\mathrm{Plant}}\,\mathrm{m}^{-3}$
φ_U	Dimensionless stability function of momentum (eddy flux)	—
φ_{Θ}	Dimensionless stability function of heat (eddy flux)	—
χ	Mean orientation factor	—
Ψ	Soil matric potential	m
ψ_U	Dimensionless flux profile function of momentum (eddy flux)	—
ψ_{Θ}	Dimensionless flux profile function of heat (eddy flux)	—
Ω	Branch wood area index	$\mathrm{m}^2_{\mathrm{Wood}}\,\mathrm{m}^{-2}$
ω	Leaf shedding rate	s^{-1}

Table S3: List of universal (physical) constants used in ED-2.2. For parameters that can be constrained and optimized, refer to Tables S4 (global) and S5-S6 (PFT-dependent).

Symbol	Value	Description
Ein	$2.17 \cdot 10^{-5}$ J mol^{-1}	Average photon specific energy in the PAR band
g	9.807 m s^{-2}	Gravity acceleration
$\mathcal{M}_C$	$1.201 \cdot 10^{-2}$ kg mol^{-1}	Molar mass of carbon
$\mathcal{M}_d$	$2.897 \cdot 10^{-2}$ kg mol^{-1}	Molar mass of dry air
$\mathcal{M}_w$	$1.802 \cdot 10^{-2}$ kg mol^{-1}	Molar mass of water
$l_{i\ell 3}$	$3.34 \cdot 10^{5}$ J kg^{-1}	Specific latent heat of melting at the water triple point
l_{iv3}	$l_{i\ell 3} + l_{\ell v3}$	Specific latent heat of sublimation at the water triple point
$l_{\ell v3}$	$2.50 \cdot 10^{6}$ J kg^{-1}	Specific latent heat of vaporization at the water triple point
$o_{\oplus}$	0.209 mol$_{O_2}$ mol^{-1}	Reference oxygen mixing ratio
p_0	10^5 Pa	Reference pressure for potential temperature
q_i	2093 J kg^{-1} K^{-1}	Specific heat of ice
q_ℓ	4186 J kg^{-1} K^{-1}	Specific heat of liquid water
q_{pd}	1005 J kg^{-1} K^{-1}	Specific heat of dry air at constant pressure
q_{pv}	1859 J kg^{-1} K^{-1}	Specific heat of water vapor at constant pressure
$\mathcal{R}$	8.315 J mol^{-1} K^{-1}	Ideal gas constant
T_0	273.15 K	Zero degrees Celsius
T_3	273.16 K	Water triple point
κ	0.40	von Kármán constant
ρ_*	200 kg m^{-3}	Density of frost
ρ_ℓ	1000 kg m^{-3}	Density of liquid water
$\rho_\circledast$	100 kg m^{-3}	Reference density of fresh snow
$\sigma_{\rm SB}$	$5.67 \cdot 10^{-8}$ W m^{-2} K^{-4}	Stefan-Boltzmann constant
Υ_{Q_ℓ}	0.57 W m^{-1} K^{-1}	Thermal conductivity of liquid water

Table S4: List of default values for global parameters used in ED-2.2. Soil carbon parameters $x_{\mathbf{e}}$ are shown as vectors $(x_{e_1};x_{e_2};x_{e_3})$ corresponding to the fast, intermediate, and slow pools, respectively. Optical parameters are shown as vectors $(x_{\mathrm{PAR}};x_{\mathrm{NIR}};x_{\mathrm{TIR}})$ corresponding to the photosynthetically active (PAR), near infrared and thermal infrared bands, respectively. For default PFT-specific parameters, refer to Tables S5-S6; physical constants are listed in Table S3.

Symbol	Value	Description
$B_{\mathbf{e}}$	$(11.0;4.5;0.2)$ yr^{-1}	Optimal decay rates of soil carbon pools
$\mathcal{B}_C$	0.5 $\mathrm{kg_C\,kg_{Bio}^{-1}}$	Carbon:oven-dry-biomass ratio
$\hat{f}_{\mathrm{Cold}}$	0.24	Decay parameter for decomposition at cold temperatures
$\hat{f}_{\mathrm{Dry}}$	0.60	Decay parameter for decomposition at dry conditions
$\hat{f}_{\mathrm{Hot}}$	12.0	Decay parameter for decomposition at hot temperatures
$\hat{f}_{\mathrm{Wet}}$	36.0	Decay parameter for decomposition at wet conditions
f_{Gl}	1.6	Water:CO_2 diffusivity ratio
$f_{G\lambda}$	1.4	Water:CO_2 leaf-boundary-layer conductance ratio
$f_{h\mathbf{e}}$	$(1.0;0.3;1.0)$	Fraction of decay due to heterotrophic respiration
f_{LD}	0.5	Fraction of carbon retained by plants when shedding leaves
$\mathcal{I}$	0.5 yr^{-1}	Fire intensity parameter
$\mathcal{K}_{C_{15}}$	214.2 $\mu\mathrm{mol_{CO_2}\,mol^{-1}}$	Michaelis constant for carboxylation at 15 °C
$\mathcal{K}_{O_{15}}$	0.2725 $\mathrm{mol_{O_2}\,mol^{-1}}$	Michaelis constant for oxygenation at 15 °C
k_{PEP}	17949 $\mathrm{mol_{Air}\,mol_{CO_2}^{-1}}$	Initial slope for the PEP carboxylase (C_4 photosynthesis)
Pr	0.74	Prandtl number
$\mathcal{Q}_{10}(\mathcal{K}_C)$	2.1	Temperature factor for Michaelis constant (carboxylation)
$\mathcal{Q}_{10}(\mathcal{K}_O)$	1.2	Temperature factor for Michaelis constant (oxygenation)
$\mathcal{Q}_{10}(\varpi)$	0.57	Temperature factor for carboxylase:oxygenase ratio
$T_{g\mathrm{Cold}}$	291.15 K	Temperature threshold for decomposition at cold temperatures
$T_{g\mathrm{Hot}}$	318.15 K	Temperature threshold for decomposition at hot temperatures
T_{Phen}	278.15 K	Temperature threshold for cold-deciduous leaf phenology
t_{Runoff}	3600 s	E-folding Decay time for surface runoff
$\hat{w}_{\max}$	0.11 $\mathrm{kg_W\,m^2_{Leaf+Wood}}$	Water holding capacity
$z_{0\varnothing}$	0.01 m	Roughness length of bare soil
z_{Fr}	-0.50 m	Soil depth used to evaluate fuel dryness
λ_{TF}	0.014 yr^{-1}	Tree fall disturbance rate
$\vartheta'_{\mathrm{Dry}}$	0.48	Relative moisture threshold for decomposition at dry conditions
$\vartheta'_{\mathrm{Wet}}$	0.98	Relative moisture threshold for decomposition at wet conditions
$\overline{\mu}_s$	0.05 m	Inverse of the optical depth of temporary surface water
ς_{3g}	0.02	Scattering coefficients (thermal infrared) for bare soil
$\varsigma^{\circledast}_{R_s}$	$(0.518;0.435;0.030)$	Reflectance coefficients for pure snow
ϖ_{15}	4561	Carboxylase:oxygenase ratio at 15 °C
$\tilde{\psi}_0$	0.190	Flux profile function of momentum at roughness height

Table S5: List of default parameters that depend on plant functional type (PFT) used in ED-2.2 for tropical and subtropical regions, for default ED-2.2 PFTs. The PFTs are C_4 tropical grass (C4G), C_3 tropical grass (C3G); early successional tropical tree (ETR); mid-successional tropical tree (MTR); late-successional tropical tree (LTR); subtropical conifers (ARC); additional PFTs can be specified by the user and provided directly to ED-2.2 through extensible markup language (XML). Spectral-dependent parameters x are provided as vectors ($x_{\mathrm{PAR}};x_{\mathrm{NIR}};x_{\mathrm{TIR}}$), corresponding to the visible (photosynthetically active), nearinfrared, and thermal infrared, respectively. The default parameters for temperate PFTs are shown in Table S6. The values of constants and default global parameters are shown in Table S3.

Symbol	PFT-specific value						Units	Description
	C4G	C3G	ETR	MTR	LTR	ARC		
$æ$	15.15	15.15	16.22	31.58	∞	900.09	yr	Aging factor for density-independent mortality
$\mathcal{B}_{Wl}$	1.85	1.85	1.85	1.85	1.85	1.85	—	Water:oven-dry-biomass ratio for leaves
$\mathcal{B}_{Wb}$	0.70	0.70	0.70	0.70	0.70	0.70	—	Water:oven-dry-biomass ratio for wood
$\mathcal{C}_{0l}$	0.158	0.158	0.418	0.560	0.701	0.410	—	Scaling coefficient for leaf biomass allometry
$\mathcal{C}_{1l}$	0.975	0.975	0.975	0.975	0.975	0.975	—	Exponent coefficient for leaf biomass allometry
$\mathcal{C}_{0h}$	0.0627	0.0627	0.166	0.222	0.282	0.163	—	Scaling coefficient for heartwood biomass allometry (sub-canopy)
$\mathcal{C}_{1h}$	2.432	2.432	2.432	2.432	2.432	2.432	—	Exponent coefficient for heartwood biomass allometry (sub-canopy)
$\mathcal{C}_{2h}$	0.0647	0.0647	0.172	0.230	0.291	0.168	—	Scaling coefficient for heartwood biomass allometry (canopy)
$\mathcal{C}_{3h}$	2.426	2.426	2.426	2.426	2.426	2.426	—	Exponent coefficient for heartwood biomass allometry (canopy)
f_{AG}	0.70	0.70	0.70	0.70	0.70	0.70	—	Fraction of above-ground biomass
f_{Cold}	0.40	0.40	0.40	0.40	0.40	0.40	—	Decay parameter to down-regulate metabolism at cold temperatures
f_{Clump}	1.00	1.00	0.80	0.80	0.80	0.735	—	Clumping index
f_{Hot}	0.40	0.40	0.40	0.40	0.40	0.40	—	Decay parameter to down-regulate metabolism at hot temperatures
f_n	0.00	0.00	0.10	0.10	0.10	0.10	—	Fraction of carbon storage retained in storage pool
f_r	1.00	1.00	1.00	1.00	1.00	1.00	—	Fine-root:leaf biomass ratio
f_R	0.035	0.015	0.015	0.015	0.015	0.015	—	Respiration:carboxylation ratio
f_ϱ	1.0	1.0	0.30	0.30	0.30	0.30	—	Fraction of carbon allocation to reproduction at maturity
f_σ	3900	3900	3900	3900	3900	3900	$m^3\,kg_C^{-1}$	Sapwood:leaf biomass scaling factor
$\hat{G}_{lw}^{\varnothing}$	0.01	0.01	0.01	0.01	0.01	0.001	$\mathrm{mol\,m^{-2}\,s^{-1}}$	Residual conductance (closed stomata)
$\hat{G}_r$	900	900	600	600	600	600	$\mathrm{m^2\,kg_C^{-1}\,yr^{-1}}$	Scaling factor for fine root conductance
$£_h$	1.0	1.0	1.0	1.0	1.0	0.79	—	Fraction of lignified tissues (sapwood and hardwood)
$£_l$	0.0	0.0	0.0	0.0	0.0	0.00	—	Fraction of lignified tissues (leaves and fine roots)
M	7.2	9.0	9.0	9.0	9.0	7.2	—	Slope factor for stomatal conductance
m_ϱ	0.95	0.95	0.95	0.95	0.95	0.95	$\mathrm{mo^{-1}}$	Loss rate of reproductive tissues
$\mathcal{Q}_{10}\left(\dot{V}_C\right)$	2.40	2.40	2.40	2.40	2.40	2.40	—	Temperature dependence factor for carboxylation rate
$\mathcal{Q}_{10}\left(r_r\right)$	2.40	2.40	2.40	2.40	2.40	2.40	—	Temperature dependence factor for fine root respiration

Table S5: (Continued)

Symbol	PFT-specific value						Units	Description
	C4G	C3G	ETR	MTR	LTR	ARC		
$q_l^{(\mathrm{OD})}$	3218	3218	3218	3218	3218	3218	$\mathrm{J\,kg^{-1}\,K^{-1}}$	Specific heat of oven-dry leaf biomass
$q_b^{(\mathrm{OD})}$	1217	1217	1217	1217	1217	1217	$\mathrm{J\,kg^{-1}\,K^{-1}}$	Specific heat of oven-dry wood biomass
$r_{r_{15}}$	0.246	0.246	0.246	0.246	0.246	0.246	$\mathrm{s^{-1}}$	Fine-root respiration rate at 15 °C
SLA	22.70	22.70	16.02	11.65	9.66	6.32	$\mathrm{m^2\,kg_C^{-1}}$	Specific leaf area
T_{Cold}	288.15	283.15	283.15	283.15	283.15	277.86	K	Cold temperature threshold for metabolic activity
T_F	275.65	275.65	275.65	275.65	275.65	258.15	K	Temperature threshold for plant hardiness to frost
T_{Hot}	318.15	318.15	318.15	318.15	318.15	318.15	K	Hot temperature threshold for metabolic activity
b	1	1	1	1	1	2	—	Number of sides of leaf with stomata
$\dot{V}_{C_{15}}^{\max}$	12.5	18.75	18.75	12.5	6.25	15.62	$\mu\mathrm{mol_C\,m^{-2}\,s^{-1}}$	Maximum carboxylation rate at 15 °C
$x_\beta^\star$	0.05	0.05	0.05	0.05	0.05	0.05	m	Typical obstacle size for branches and twigs
$x_\lambda^\star$	0.05	0.05	0.10	0.10	0.10	0.05	m	Typical leaf width
$\mathcal{Z}_0$	0	0	0	0	0	0	m	Offset parameter for tree height allometry
$\mathcal{Z}_1$	0.0352	0.0352	0.0352	0.0352	0.0352	0.0352	—	Slope coefficient for leaf biomass allometry
$\mathcal{Z}_2$	0.694	0.694	0.694	0.694	0.694	0.694	—	Exponent coefficient for leaf biomass allometry
$\mathcal{Z}_\infty$	61.7	61.7	61.7	61.7	61.7	61.7	m	Asymptote height (relative to Z_0 at $\lim_{\mathrm{DBH}\to\infty}$)
$z_{t_{\max}}$	1.5	1.5	35.0	35.0	35.0	35.0	m	Maximum attainable height
z_t^{Repro}	1.5	1.5	18.0	18.0	18.0	18.0	m	Plant height at reproductive maturity
$\Delta q_b^{\mathrm{Bond}}$	63.10	63.10	63.10	63.10	63.10	63.10	$\mathrm{J\,kg^{-1}\,K^{-1}}$	Specific heat associated with bonding between wood and water
Δw	0.016	0.016	0.016	0.016	0.016	0.016	$\mathrm{mol_W\,mol^{-1}}$	Leaf water deficit down-regulation parameter (stomatal conductance)
ϵ	0.055	0.080	0.080	0.080	0.080	0.08	—	Quantum yield
ρ_t	—	—	0.53	0.71	0.90	0.52	$\mathrm{g\,cm^{-3}}$	Wood density
$\hat{\sigma}^{\mathrm{FR}}$	0.0	0.0	0.0	0.0	0.0	0.00	—	Survivorship to fire disturbance
$\hat{\sigma}^{\mathrm{TF}}\,(z_t < 10\ \mathrm{m})$	0.25	0.25	0.10	0.10	0.10	0.10	—	Survivorship of small trees to tree fall disturbance
$\hat{\sigma}^{\mathrm{TF}}\,(z_t \geq 10\ \mathrm{m})$	0.0	0.0	0.0	0.0	0.0	0.0	—	Survivorship of large trees to tree fall disturbance
$\varsigma_R^{\mathrm{Leaf}}$	(0.100; 0.400, 0.040)		(0.100; 0.400; 0.050)			(0.090; 0.577; 0.030)	—	Leaf reflectance
$\varsigma_R^{\mathrm{Wood}}$	(0.160; 0.250; 0.040)		(0.110; 0.250; 0.100)			(0.110; 0.250; 0.100)	—	Wood reflectance
$\varsigma_T^{\mathrm{Leaf}}$	(0.050; 0.200; 0.000)		(0.050; 0.200; 0.000)			(0.050; 0.248; 0.000)	—	Leaf transmittance
$\varsigma_T^{\mathrm{Wood}}$	(0.028; 0.248; 0.000)		(0.001; 0.001; 0.000)			(0.001; 0.001; 0.000)	—	Wood transmittance
τ_l	2.0	2.0	1.0	0.50	0.33	0.042	$\mathrm{yr^{-1}}$	Leaf turnover rate
τ_n	0.333	0.333	0.167	0.167	0.167	0.167	$\mathrm{yr^{-1}}$	Storage turnover rate
τ_r	2.0	2.0	1.0	0.50	0.33	0.042	$\mathrm{yr^{-1}}$	Fine-root turnover rate
τ_Δ	0.333	0.333	0.333	0.333	0.333	0.450	$\mathrm{dy^{-1}}$	Growth respiration factor
χ	0.00	0.00	0.10	0.10	0.10	0.01	—	Mean orientation factor

Table S6: List of default parameters that depend on plant functional type (PFT) used in ED-2.2 for temperate regions, for default ED-2.2 PFTs. The PFTs are C_3 temperate grass (C3T); mid-latitude ("Northern") pines (NPN); subtropical ("Southern") pines (SPN); late-successional conifers (LCN), early-successional hardwood tree (EHW); mid-succesional hardwood tree (MHW), late-successional tropical tree (LHW); additional PFTs can be specified by the user and provided directly to ED-2.2 through extensible markup language (XML). Spectral-dependent parameters x are provided as vectors $(x_{\mathrm{PAR}}; x_{\mathrm{NIR}}; x_{\mathrm{TIR}})$, corresponding to the visible (photosynthetically active), nearinfrared, and thermal infrared, respectively. The default parameters for tropical and subtropical PFTs are shown in Table S5. The values of constants and default global parameters are shown in Table S3.

Symbol	PFT-specific value							Units	Description
	C3T	NPN	SPN	LCN	EHW	MHW	LHW		
$æ$	15.15	294.74	232.56	424.30	162.76	262.61	233.64	yr	Aging factor for density-independent mortality
$\mathcal{B}_{Wl}$	2.50	2.50	2.50	2.50	2.50	2.50	2.50	—	Water:oven-dry-biomass ratio for leaves
$\mathcal{B}_{Wb}$	0.7	0.7	0.7	0.7	0.7	0.7	0.7	—	Water:oven-dry-biomass ratio for wood
$\mathcal{C}_{0l}$	0.0800	0.0240	0.0240	0.0454	0.0129	0.0480	0.0170	—	Scaling coefficient for leaf biomass allometry
$\mathcal{C}_{1l}$	1.0000	1.8990	1.8990	1.6829	1.7477	1.4550	1.7310	—	Exponent coefficient for leaf biomass allometry
$\mathcal{C}_{0h}$	1×10^{-5}	0.1470	0.1470	0.1617	0.0265	0.1617	0.2350	—	Scaling coefficient for heartwood biomass allometry (sub-canopy)
$\mathcal{C}_{1h}$	1.0000	2.2380	2.2380	2.1536	2.9595	2.4572	2.2518	—	Exponent coefficient for heartwood biomass allometry (sub-canopy)
$\mathcal{C}_{2h}$	1×10^{-5}	0.1470	0.1470	0.1617	0.0265	0.1617	0.2350	—	Scaling coefficient for heartwood biomass allometry (canopy)
$\mathcal{C}_{3h}$	1.0000	2.2380	2.2380	2.1536	2.9595	2.4572	2.2518	—	Exponent coefficient for heartwood biomass allometry (canopy)
f_{AG}	0.70	0.70	0.70	0.70	0.70	0.70	0.70	—	Fraction of above-ground biomass
f_{Cold}	0.40	0.40	0.40	0.40	0.40	0.40	0.40	—	Decay parameter to down-regulate metabolism at cold temperatures
f_{Clump}	0.840	0.735	0.735	0.735	0.840	0.840	0.840	—	Clumping index
f_{Hot}	0.40	0.40	0.40	0.40	0.40	0.40	0.40	—	Decay parameter to down-regulate metabolism at hot temperatures
f_n	0.00	0.00	0.00	0.00	0.00	0.00	0.00	—	Fraction of carbon storage retained in storage pool
f_r	1.0000	0.3463	0.3463	0.3463	1.1274	1.1274	1.1274	—	Fine-root:leaf biomass ratio
f_R	0.02	0.02	0.02	0.02	0.02	0.02	0.02	—	Respiration:carboxylation ratio
f_{ϱ}	1.0	1.0	0.30	0.30	0.30	0.30	0.30	—	Fraction of carbon allocation to reproduction at maturity
f_σ	3900	3900	3900	3900	3900	3900	3900	$m^3\,kg_C^{-1}$	Sapwood:leaf biomass scaling factor
$\hat{G}_{lw}^{\varnothing}$	0.020	0.001	0.001	0.001	0.020	0.020	0.020	$\mathrm{mol\,m^{-2}\,s^{-1}}$	Residual conductance (closed stomata)
$\hat{G}_r$	160	150	150	150	150	150	150	$\mathrm{m^2\,kg_C^{-1}\,yr^{-1}}$	Scaling factor for fine root conductance
$£_h$	1.00	0.79	0.79	0.79	0.79	0.79	0.79	—	Fraction of lignified tissues (sapwood and hardwood)
$£_l$	0.0	0.0	0.0	0.0	0.0	0.0	0.0	—	Fraction of lignified tissues (leaves and fine roots)
M	8.0	6.4	6.4	6.4	6.4	6.4	6.4	—	Slope factor for stomatal conductance
m_{ϱ}	0.95	0.95	0.95	0.95	0.95	0.95	0.95	$\mathrm{mo^{-1}}$	Loss rate of reproductive tissues
$\mathcal{Q}_{10}\left(\dot{V}_C\right)$	2.40	2.40	2.40	2.40	2.40	2.40	2.40	—	Temperature dependence factor for carboxylation rate
$\mathcal{Q}_{10}\left(r_r\right)$	2.40	2.40	2.40	2.40	2.40	2.40	2.40	—	Temperature dependence factor for fine root respiration
$q_l^{(\mathrm{OD})}$	3218	3218	3218	3218	3218	3218	3218	$\mathrm{Jkg^{-1}\,K^{-1}}$	Specific heat of oven-dry leaf biomass
$q_b^{(\mathrm{OD})}$	1217	1217	1217	1217	1217	1217	1217	$\mathrm{Jkg^{-1}\,K^{-1}}$	Specific heat of oven-dry wood biomass
$r_{r_{15}}$	0.246	0.246	0.246	0.246	0.246	0.246	0.246	$\mathrm{s^{-1}}$	Fine-root respiration rate at 15 °C
SLA	22.70	6.0	9.0	10.0	30.0	24.2	60.0	$\mathrm{m^2\,kg_C^{-1}}$	Specific leaf area

Table S6: (Continued)

Symbol	PFT-specific value							Units	Description
	C3T	NPN	SPN	LCN	EHW	MHW	LHW		
T_{Cold}	277.86	277.86	277.86	277.86	277.86	277.86	277.86	K	Cold temperature threshold for metabolic activity
T_F	193.15	193.15	263.15	213.15	193.15	253.15	253.15	K	Temperature threshold for plant hardiness to frost
T_{Hot}	318.15	318.15	318.15	318.15	318.15	318.15	318.15	K	Hot temperature threshold for metabolic activity
$\flat$	1	2	2	2	1	1	1	—	Number of sides of leaf with stomata
$\dot{V}_{C_{15}}^{\max}$	18.30	11.35	11.35	4.54	20.39	17.45	6.98	$\mu\mathrm{mol_C\,m^{-2}\,s^{-1}}$	Maximum carboxylation rate at 15 °C
$x_\beta^\star$	0.05	0.05	0.05	0.05	0.05	0.05	0.05	m	Typical obstacle size for branches and twigs
$x_\lambda^\star$	0.05	0.05	0.05	0.05	0.05	0.05	0.05	m	Typical leaf width
$\mathcal{Z}_0$	0.0	1.3	1.3	1.3	1.3	1.3	1.3	m	Offset parameter for tree height allometry
$\mathcal{Z}_1$	0.7500	0.0388	0.0388	0.0444	0.0653	0.0496	0.0540	—	Slope coefficient for leaf biomass allometry
$\mathcal{Z}_2$	1	1	1	1	1	1	1	—	Exponent coefficient for leaf biomass allometry
$\mathcal{Z}_\infty$	0.478	27.140	27.140	22.790	22.680	25.180	23.387	m	Asymptote height (relative to Z_0 at $\lim_{\mathrm{DBH}\to\infty}$)
$z_{t_{\max}}$	0.454	27.113	27.113	22.767	22.657	25.155	23.364	m	Maximum attainable height
z_t^{Repro}	0.45	18.0	18.0	18.0	18.0	18.0	18.0	m	Plant height at reproductive maturity
$\Delta q_b^{\mathrm{Bond}}$	63.10	63.10	63.10	63.10	63.10	63.10	63.10	$\mathrm{J kg^{-1}\,K^{-1}}$	Specific heat associated with bonding between wood and water
Δw	0.016	0.016	0.016	0.016	0.016	0.016	0.016	$\mathrm{mol_W\,mol^{-1}}$	Leaf water deficit down-regulation parameter (stomatal conductance)
ϵ	0.080	0.080	0.080	0.080	0.080	0.080	0.080	—	Quantum yield
ρ_t	—	—	—	—	—	—	—	$\mathrm{g\,cm^{-3}}$	Wood density (currently not used)
$\hat{\sigma}^{\mathrm{FR}}$	0.0	0.0	0.0	0.0	0.0	0.0	0.0	—	Survivorship to fire disturbance
$\hat{\sigma}^{\mathrm{TF}}(z_t < 10\ \mathrm{m})$	0.25	0.10	0.10	0.10	0.10	0.10	0.10	—	Survivorship of small trees to tree fall disturbance
$\hat{\sigma}^{\mathrm{TF}}(z_t \geq 10\ \mathrm{m})$	0.0	0.0	0.0	0.0	0.0	0.0	0.0	—	Survivorship of large trees to tree fall disturbance
$\varsigma_R^{\mathrm{Leaf}}$	(0.110; 0.577, 0.040)	(0.110; 0.577, 0.030)			(0.110; 0.577, 0.050)			—	Leaf reflectance
$\varsigma_R^{\mathrm{Wood}}$	(0.160; 0.110, 0.040)	(0.110; 0.250; 0.100)						—	Wood reflectance
$\varsigma_T^{\mathrm{Leaf}}$	(0.160; 0.248; 0.000)							—	Leaf transmittance
$\varsigma_T^{\mathrm{Wood}}$	(0.028; 0.248; 0.000)	(0.001; 0.001; 0.000)						—	Wood transmittance
τ_l	2.0	0.333	0.333	0.333	—	—	—	$\mathrm{yr^{-1}}$	Leaf turnover rate (not applicable for hardwoods, which are deciduous)
τ_n	0.000	0.000	0.000	0.000	0.624	0.624	0.624	$\mathrm{yr^{-1}}$	Storage turnover rate
τ_r	2.0	3.927	4.118	3.800	5.773	5.083	5.071	$\mathrm{yr^{-1}}$	Fine-root turnover rate
τ_Δ	0.333	0.450	0.450	0.450	—	—	—	$\mathrm{dy^{-1}}$	Growth respiration factor (not applicable for hardwoods, which are deciduous)
χ	0.00	0.00	0.00	0.00	0.00	0.00	0.00	—	Mean orientation factor

Table S7: List of soil component properties (air, sand, silt, and clay), used to derive most soil-texture dependent properties. Most parameters are based on Monteith and Unsworth (2008); values for silt were unavailable and assumed to be intermediate between sand and clay. The volumetric fractions of the default soil texture types in ED-2.2 are listed in Table S8.

Symbol	Soil components				Units	Description
	Air	Sand	Silt	Clay		
q	1010	800	850	900	$\mathrm{J\,kg^{-1}\,K^{-1}}$	Specific heat
ρ	1.200	2660	2655	2650	$\mathrm{kg\,m^{-3}}$	Bulk density
Υ_{Q}	0.025	8.80	5.87	2.92	$\mathrm{W\,m^{-1}\,K^{-1}}$	Thermal conductivity

Table S8: List of volumetric fractions of sand, silt, and clay ($f_{\mathcal{V}}$) for the default soil texture types in ED-2.2 (Fig. S6). Component-specific properties of soils are listed in Table S7.

Class	Description	Volumetric fractions		
		Sand	Silt	Clay
Sa	Sand	0.920	0.050	0.030
LSa	Loamy sand	0.825	0.115	0.060
SaL	Sandy loam	0.660	0.230	0.110
SiL	Silt loam	0.200	0.640	0.160
L	Loam	0.410	0.420	0.170
SaCL	Sandy clay loam	0.590	0.140	0.270
SiCL	Silty clay loam	0.100	0.560	0.340
CL	Clayey loam	0.320	0.340	0.340
SaC	Sandy clay	0.520	0.060	0.420
SiC	Silty clay	0.060	0.470	0.470
C	Clay	0.200	0.200	0.600
Si	Silt	0.075	0.875	0.050
CC	Heavy clay	0.100	0.100	0.800
CSa	Clayey sand	0.375	0.100	0.525
CSi	Clayey silt	0.125	0.350	0.525

Table S9: Coefficients used in Eq. (S191) for each limitation and photosynthetic path. The special case in which the stomata are closed is also shown for reference.

Case	C_3 photosynthesis				C_4 photosynthesis			
	F^A	F^B	F^C	F^D	F^A	F^B	F^C	F^D
Closed stomata ($\dot{A}_k^{\varnothing}$)	0	0	0	1	0	0	0	1
RuBP-saturated ($\dot{A}_k^{\mathrm{RuBP}}$)	$\dot{V}_{C_k}^{\max}$	$-\dot{V}_{C_k}^{\max}\Gamma_k$	1	$\mathcal{K}_{\mathrm{ME}_k}$	0	$\dot{V}_{C_k}^{\max}$	0	1
CO_2-limited ($\dot{A}_k^{\mathrm{InSl}}$)	$\dot{V}_{C_k}^{\max}$	$-\dot{V}_{C_k}^{\max}\Gamma_k$	1	$\mathcal{K}_{\mathrm{ME}_k}$	$k_{\mathrm{PEP}}\dot{V}_{C_k}^{\max}$	0	0	1
Light-limited ($\dot{A}_k^{\mathrm{PAR}}$)	$\epsilon_k\ \dot{q}_k$	$-\epsilon_k\ \dot{q}_k\Gamma_k$	1	$2\Gamma_k$	0	$\epsilon_k\ \dot{q}_k$	0	1

S1 ED-2 developments since ED-2.0 and ED-2.2

In this Supplement, we list the main developments in the Ecosystem Demography Model version 2 (ED-2), with focus on mentioned in this manuscript (Fig. S3). The complete list of implementations, improvements, and code fixes are available on the GitHub website (`https://github.com/EDmodel/ED2`).

S1.1 Version 2.0 (ED-2.0)

This is the version described in Medvigy (2006); Medvigy et al. (2009), and it is the first version of the ED model that implements energy and water cycles at sub-daily scale. The biophysics core was adapted from the LEAF-2 land surface model (Walko et al., 2000), which is part of the Regional Atmospheric Model System (RAMS). The main differences in the ED-2.0 biophysics core include (1) solution of the energy and water cycle for each cohort and patch; (2) use of 4^{th} order Runge-Kutta solver to improve numerical stability. In addition, this version allowed leaf phenology to be prescribed from external data (Supplement S3.1.3). The photosynthesis solver was largely the same as in ED-1.0 (Moorcroft et al., 2001).

S1.2 Version 2.0.12 (ED-2.0.12)

Most developments between ED-2.0 and ED-2.0.12 relate to code organization and structure. ED-2.0 was partly written in C (legacy from ED-1) and partly written in Fortran (legacy from LEAF-2). To simplify the code and ensure data were correctly transferred between subroutines, we rewrote most of the code in Fortran. The only exceptions were a few file handling functions that remained in C because we could not find equivalent functions in Fortran.

In addition, this version uses Hierarchical Data Format 5 (HDF5) format and libraries (The HDF Group, 2016) to generate model outputs. HDF5 allows a more efficient framework to output variables in the dynamic patch and cohort structures. It also introduced an XML model parameter input file, rather than relying solely on hard-coded defaults, which makes it easier to perform model calibration, sensitivity analyses, and ensemble error propagation. Importantly, this was the last version of ED-2 that used temperature as prognostic variable for leaves and canopy air space.

S1.3 Version 2.1 (ED-2.1)

Most ED-2.1 developments aimed at improving the energy cycle representation in ED-2.1. Leaf enthalpy and canopy air space enthalpy replaced temperature as the prognostic variables (Eq. 4; Sec. 3.2.3-3.2.4). The main advantages of energy-related prognostic equations include: (1) simplification the numeric integration, as total energy changes must be equivalent to net energy flux; (2) improved conservation of energy when water fluxes are large and cause rapid changes in heat capacity of the thermodynamic systems; (3) elimination of singularity at the water's fusion point (0 °C), when enthalpy changes due to freezing or melting, but the temperature remains the same.

To ensure the model was thermodynamically consistent, we also: (1) implemented a mechanistic representation of heat capacity for vegetation (leaves and branches, Supplement S6.2) that is scaled with leaf and branch biomass (e.g. Dufour and van Mieghem, 1975); (2) replaced the original LEAF-2-based surface layer model (that was based on Louis, 1979) with the parameterization by Beljaars and Holtslag (1991), as the latter parameterization improved numerical stability of eddy covariance fluxes under thermally stable conditions; (3) included an option to prescribe silt, clay, and sand fractions to define site-specific soil texture characteristics (Supplement S9) instead of the original ED-2.0 implementation that required soils to be assigned to one of the 12 fixed classes originally defined in LEAF-2 (Walko et al., 2000); (4) implemented the capability of saving the entire ecosystem and thermodynamic state of the model into HDF5 files, which can be used to stop and start simulations and yield the same results of uninterrupted simulations, a desirable feature for simulations with long runtimes.

S1.4 Version 2.2 (ED-2.2)

The ED-2.2 version implemented several improvements and fixed inconsistencies in the representation of the energy, water, and carbon dioxide cycles. First, we redefined enthalpy (S5), to ensure that it would be a true thermodynamic state variable (i.e. path independent, see Dufour and van Mieghem, 1975), by making latent heat of vaporization a linear function of temperature (Eq. 72-73). Moreover, we identified missing components of the energy cycle that precluded the conservation: (1) the transfer of internal energy from soils to leaves before transpiration (Eq. 97); (2) the enthalpy exchange associated with vaporization and condensation also accounts the mass transfer of water between the thermodynamic systems (e.g. Eq. 75; 98). Furthermore, to ensure results from ED-2.2 consistently conserve mass and energy, we implemented detailed conservation verification during the model execution, which now reports any violation of energy, water, and carbon conservation, generates detailed output of the violation, and interrupts the simulation. Finally, to improve computational efficiency of the energy, water, and carbon cycle solvers at subdaily time steps, we implemented a shared-memory parallelization of the most computationally-

intensive subroutines. The parallelization was written to allow users to select any number of cores (depending on core availability), and it accounts for patch ages in order to balance the load among cores.

In addition, we rewrote the photosynthesis to allow temperature-dependent functions to be expressed as functions of Q_{10}. We retained the original Arrhenius-based functions as legacy options, but the new option increases the options for assimilating data into the model. The current Q_{10}-based parameters fix the low-temperature optimum in tropical plants previously noted by Rogers et al. (2017). Importantly, we rewrote the photosynthesis solver to ensure that it would always converge to a unique solution for net assimilation rate, stomatal conductance, and intercellular carbon dioxide concentration given the environmental conditions (Supplement S16).

The ED-2.2 version also includes improvements in the representation of conductances between different thermodynamic systems. First, the leaf boundary-layer conductance now accounts for differences in leaf and branch characteristics of each cohort, and to account for both free and forced convection under both laminar and turbulent flow (Supplement S14.2). Second, we implemented ground-to-canopy conductance formulations (Sellers et al., 1986; Massman, 1997; Massman and Weil, 1999) that account for the cumulative drag profile of vegetated areas obtained from the cohort structure, as well as the stability of the surface layer (Supplement S14.3).

Finally, in ED-2.2 we replaced the version control to GitHub, which makes the new code developments readily available to the scientific community and encourages users to post issues, code fixes and model improvements and developments to the main code repository in open and collaborative forums.

S2 Boundary conditions for the ecosystem dynamics equations

The boundary conditions for Eq. (2) and (3) are:

$$\underbrace{n_{fq}\left(\mathbf{C}_{f_0},a,t\right)}_{\text{Recruit}} = \frac{1}{\mathbf{g}_{f_0}\cdot\mathbf{1}}\left\{\underbrace{\int_{\mathbf{C_{f_0}}}^{\infty}\left(1-f_{\delta_f}\right)\ \varrho_f\ n_{fq}\mathrm{d}\mathbf{C}}_{\text{Local recruitment}} + \underbrace{\sum_{q'=1}^{N_Q}\left[\int_{\mathbf{C_{f_0}}}^{\infty}\int_0^{\infty} f_{\delta_f}\ \varrho_f\ n_{FQ'X'Y}\,\alpha_{fq'}\,\mathrm{d}a\,\mathrm{d}\mathbf{C}\right]}_{\text{Non-local, random dispersal}}\right\}, \tag{S1}$$

$$\underbrace{n_{fq}\left(\mathbf{C}_f,0,t\right)}_{\text{Population at new gap}} = \underbrace{\sum_{q'=1}^{N_Q}\left[\int_0^{\infty}\hat{\sigma}_{fq'}\,n_{fq'}\,\alpha_{q'}\,\mathrm{d}a\right]}_{\text{Disturbance Survivors}}, \tag{S2}$$

$$\underbrace{\alpha_q(0,t)}_{\text{Probability of new gap}} = \underbrace{\sum_{q'=1}^{N_Q} \lambda_{q'q}\,\alpha_{q'}\mathrm{d}a}_{\text{Disturbance rates}}, \tag{S3}$$

where $\mathbf{C}_{f_0}$ is the size of the smallest individual of PFT f; $\mathbf{g}_{f_0}$ is the growth rate for individuals of PFT f with size $\mathbf{C}_{f_0}$; $\mathbf{1}$ is the unity vector for size; ϱ_f is the recruitment rate, which depends on the PFT, size, and carbon balance; f_{δ_f} is the fraction of recruits of PFT f that are randomly dispersed instead of locally recruited; and $\hat{\sigma}_{fq}$ is size-dependent survivorship probability for a PFT f following a disturbance of type q (for a complete list of subscripts and variable meanings, refer to Tables S1 and S2). Both $\mathbf{g}_f$ and m_f are functions of the plant size and the individual's carbon balance. The individual's carbon balance depends on the environment perceived by each individual; in turn, the environment perceived by each individual is modulated by both the plant community living in the same gap and the general landscape environment. Likewise, the disturbance rates may be affected by the local plant community in the gap and the regional landscape environment.

S3 Long-term carbon dynamics and relation with carbon balance

S3.1 Leaf phenology

The phenological strategy of the plant functional types can be evergreen, drought-deciduous, or cold-deciduous. The plant's phenology strategy is defined by two functions: (i) the leaf elongation factor ($\hat{e}_{l_k}$), defined as the ratio between the environmentally-constrained leaf biomass and the potential (maximum) leaf biomass, and the rate of leaf shedding ($\omega_{l_k}(t)$) which can either be prognosed, or prescribed from observations.

S3.1.1 Evergreen plants

For evergreen PFTs, the elongation factor is always 1, the rate of leaf shedding ($\omega_{l_k}(t)$) is zero, and their rate of leaf turnover is governed by the PFT-dependent leaf turnover parameter (τ_{l_k}, see Eq. S12, and Tables S5-S6). The leaf phenology of tropical trees can also be represented by an empirical model that is driven by the seasonality of light availability (see Kim et al., 2012).

S3.1.2 Drought-deciduous tropical phenology

The drought-deciduous phenology assumes that leaf flushing and leaf senescence are controlled by the water availability in the rooting zone. The elongation factor $\hat{e}_{l_k}$ is determined by the following

parameterization:

$$\hat{e}_{l_k} = \begin{cases} 1 & \text{, if } s_{l_k} \geq 1 \\ s_{l_k} & \text{, if } 0.05 \leq s_{l_k} < 1 \\ 0 & \text{, if } s_{l_k} < 0.05 \end{cases}, \tag{S4}$$

$$s_{l_k} = \frac{1}{|z_{r_k}|\,\Delta t_{\mathrm{El}}} \int_{t'-\Delta t_{\mathrm{El}}}^{t'} \left(\sum_{j=j(z_{r_k})}^{N_G} \left\{ \frac{\max\left[0, \Psi_{g_j}(t') + \frac{1}{2}\left(z_{g_j} + z_{g_{j+1}}\right) - \Psi_{\mathrm{Wp}}\right]}{\Psi_{\mathrm{Ld}} - \Psi_{\mathrm{Wp}}} \right\} \right) \mathrm{d}t, \tag{S5}$$

where s_{l_k} is a 10-day running average of soil moisture accessed by cohort k (normalized by the difference between the water potential threshold and the wilting point), z_{r_k} is the rooting depth of cohort k (Supplement S18), Δt_{El} is the time scale for changes in phenology (assumed to be 10 days), $j(z_{r_k})$ is the soil layer containing the deepest roots of cohort k, Ψ_{g_j} is the soil matric potential at soil layer j, Ψ_{Ld} is the soil matric potential below which plants start shedding leaves (assumed -1.2 MPa), Ψ_{Wp} is the soil matric potential at the wilting point, and z_{g_j} is the depth of soil layer j ($z_{g_{N_G+1}} \equiv 0$, otherwise z_g is negative). Leaf shedding occurs whenever soil is drier than the threshold defined by Ψ_{Ld} and drought conditions are increasing. Specifically:

$$\omega_{l_k} = \frac{1}{\Delta t_{\mathrm{Phen}}} \max\left[0, \frac{C_{l_k}}{C^{\bullet}_{l_k}} - f_{\mathrm{El}}\right]. \tag{S6}$$

S3.1.3 Cold-deciduous phenology

The prognostic cold-deciduous leaf phenology approach is a thermal sum and chilling sum-based model identical to that of Albani et al. (2006), which, in turn, is based on Botta et al. (2000). At each patch, growing degree-days (GDD) are accumulated during the extended growing season ($\mathfrak{T}_{\mathrm{GS}}$, January–August for the Northern Hemisphere, and July–February for the Southern Hemisphere), and the chilling days (CHD) in the extended senescing season ($\mathfrak{T}_{\mathrm{SS}}$, November–June for the Northern Hemisphere, and May–December for the Southern Hemisphere):

$$\mathrm{GDD}(t) = \begin{cases} 0 & \text{, if } t \notin \mathfrak{T}_{\mathrm{GS}} \\ \sum_{t'=t_{\mathrm{GS}}(0)}^{t} \max\left(0, \overline{T}_c(t') - T_{\mathrm{Phen}}\right) & \text{, otherwise} \end{cases}, \tag{S7}$$

$$\mathrm{CHD}(t) = \begin{cases} 0 & \text{, if } \overline{T}_c(t) \geq T_{\mathrm{Phen}}, \text{ or } t \notin \mathfrak{T}_{\mathrm{SS}} \\ \mathrm{CHD}(t - \Delta t_{\mathrm{Phen}}) + 1 & \text{, otherwise} \end{cases}, \tag{S8}$$

where $\overline{T}_c$ is the daily average canopy air space temperature, $\Delta t_{\mathrm{Phen}} = 1$ day is the phenology time

step (Table 2), $t_{\mathrm{GS}}(0)$ is the beginning of the growing season, and $T_{\mathrm{Phen}} = 278.15$ K (5 °C) is the leaf phenology threshold (Albani et al., 2006). The valued elongation factor $\hat{e}_{l_k}$ is then determined by the following series of conditions:

$$\hat{e}_{l_k}(t) = \begin{cases} 0 & \text{, if } \overline{T}_s(t) < 275.15 \text{ K} \\ 0 & \text{, if } \overline{T}_s(t) < 284.30 \text{ K and } t_{\odot} < 655 \text{ min} \\ 1 & \text{, if GDD} \geq -68.0 + 638.0 \exp\left[-0.01\,\mathrm{CHD}(t)\right] \\ \hat{e}_{l_k}(t - \Delta t_{\mathrm{Phen}}) & \text{, otherwise} \end{cases}, \tag{S9}$$

where $t_{\odot}$ is the daytime duration.

If desired, cold-deciduous phenology can be prescribed rather than prognosed, as described in Medvigy et al. (2009) and Viskari et al. (2015). The timing of leaf onset and leaf senescence are empirically determined from either field observations or from remote sensing (e.g. Zhang et al., 2003) by fitting the following curves, which are then used to determine $\hat{e}_{l_k}$ in the model:

$$\hat{e}_{l_k} = \begin{cases} \dfrac{1}{1 + (y_0 t)^{y_1}} & \text{, if } t \in \mathfrak{T}_{\mathrm{GS}} \\ \dfrac{1}{1 + (y_2 t)^{y_3}} & \text{, if } t \in \mathfrak{T}_{\mathrm{SS}} \end{cases}, \tag{S10}$$

where y_0, y_1, y_2, and y_3 are empirical parameters, determined from data prior to running the ED-2.2 model and provided to the model as inputs; t is the time, provided as day of year (i.e. 1 for January 1st, 365 for December 31 in non-leap years, and 366 for December 31 in leap years); $\mathfrak{T}_{\mathrm{GS}}$ is the extended growing season (e.g. January–July for the Northern Hemisphere, July–January for the Southern Hemisphere); and $\mathfrak{T}_{\mathrm{SS}}$ is the senescing season (e.g. August–December for the Northern Hemisphere, February–June for the Southern Hemisphere).

S3.2 Carbon allocation to living tissues and non-structural carbon

The accumulated carbon balance (C_{Δ_k}, Eq. 25) over the phenology time step Δt_{Phen} is used to update the non-structural carbon storage (C_{n_k}) as well as the changes in carbon stocks of living tissues (leaves: C_{l_k}; fine roots C_{r_k} and sapwood C_{σ_k}) due to carbon allocation, turnover losses, and phenology. Changes in living tissues and non-structural carbon are interdependent and described by the following system of equations (see also Medvigy et al., 2009; Kim et al., 2012):

$$\frac{\mathrm{d}C_{n_k}}{\mathrm{d}t} = \frac{1}{\Delta t_{\mathrm{Phen}}} \left[\int_{t - \Delta t_{\mathrm{Phen}}}^{t} \frac{\mathrm{d}C_{\Delta_k}}{\mathrm{d}t} \mathrm{d}t' \right] + \left(f_{\mathrm{LD}}\, \omega_{l_k} - \gamma_{l_k} \right) C_{l_k} - \gamma_{r_k} C_{r_k} - \gamma_{\sigma_k} C_{\sigma_k} - \tau_{n_k} C_{n_k}, \tag{S11}$$

$$\frac{\mathrm{d}C_{l_k}}{\mathrm{d}t} = \left(\gamma_{l_k} - \tau_{l_k} - \omega_{l_k}\right) C_{l_k}, \tag{S12}$$

$$\frac{\mathrm{d}C_{r_k}}{\mathrm{d}t} = \left(\gamma_{r_k} - \tau_{r_k}\right) C_{r_k}, \tag{S13}$$

$$\frac{\mathrm{d}C_{\sigma_k}}{\mathrm{d}t} = \gamma_{\sigma_k} C_{\sigma_k}, \tag{S14}$$

where $\hat{e}_{l_k}$ is the elongation factor (Supplement S3.1); f_{LD} is the fraction of carbon retained from active leaf drop as storage, currently assumed to be 0.5; $(\gamma_{l_k}; \gamma_{r_k}; \gamma_{\sigma_k})$ are the growth rates of leaves, fine roots, and sapwood, respectively; $(\tau_{l_k}; \tau_{r_k}; \tau_{n_k})$ are the background turnover rates of leaves, fine roots, and non-structural carbon, and are typically assumed constant (Tables S5-S6; but see Kim et al., 2012); and ω_{l_k} is the phenology-driven leaf shedding rate (Supplement S3.1).

The allocation to living tissues depends on whether the plant carbon balance and environmental conditions are favorable for growing, and it is proportional to the amount of carbon needed by each pool to reach the expected carbon stock given size and environmental constrains (Supplement S18). First, let $\left(C^{\circledcirc}_{l_k}; C^{\circledcirc}_{r_k}; C^{\circledcirc}_{\sigma_k}\right)$ be the biomass increment needed to bring leaves, fine roots, and sapwood, respectively to the expected carbon stock given the plant size and PFT $\left(C^{\bullet}_{l_k}; C^{\bullet}_{r_k}; C^{\bullet}_{\sigma_k}\right)$:

$$C^{\circledcirc}_{l_k} = \max\left[0, \hat{e}_{l_k} C^{\bullet}_{l_k} - C_{l_k}\left(1 - \tau_{l_k}\Delta t_{\mathrm{Phen}}\right)\right], \tag{S15}$$

$$C^{\circledcirc}_{r_k} = \max\left[0, C^{\bullet}_{r_k} - C_{r_k}\left(1 - \tau_{r_k}\Delta t_{\mathrm{Phen}}\right)\right], \tag{S16}$$

$$C^{\circledcirc}_{\sigma_k} = \max\left[0, C^{\bullet}_{\sigma_k} - C_{\sigma_k}\right], \tag{S17}$$

$$C^{\circledcirc}_{\alpha_k} = C^{\circledcirc}_{l_k} + C^{\circledcirc}_{r_k} + C^{\circledcirc}_{\sigma_k}, \tag{S18}$$

where $C^{\circledcirc}_{\alpha_k}$ is the biomass increment needed to bring all living tissues to expected biomass given size and PFT, and Δt_{Phen} is the phenology time step (Table 2). Growth rates of leaves (γ_{l_k}), fine roots (γ_{r_k}) and sapwood (γ_{σ_k}) are proportional to the amount needed by each tissue to be brought back to the expected biomass given size and PFT, but also constrained by the amount of non-structural carbon (C_{n_k}) available:

$$\gamma_{l_k} = \max\left\{0, \frac{1}{\Delta t_{\mathrm{Phen}}} \frac{\hat{e}_{l_k} C^{\circledcirc}_{l_k}}{C^{\circledcirc}_{\alpha_k}} \min\left[C^{\circledcirc}_{\alpha_k}, C_{n_k}\left(1 - \tau_{n_k}\right) + C_{\Delta_k}\right]\right\}, \tag{S19}$$

$$\gamma_{r_k} = \max\left\{0, \frac{1}{\Delta t_{\mathrm{Phen}}} \frac{C^{\circledcirc}_{r_k}}{C^{\circledcirc}_{\alpha_k}} \min\left[C^{\circledcirc}_{\alpha_k}, C_{n_k}\left(1 - \tau_{n_k}\right) + C_{\Delta_k}\right]\right\}, \tag{S20}$$

$$\gamma_{\sigma_k} = \max\left\{0, \frac{1}{\Delta t_{\mathrm{Phen}}} \frac{C^{\circledcirc}_{\sigma_k}}{C^{\circledcirc}_{\alpha_k}} \min\left[C^{\circledcirc}_{\alpha_k}, C_{n_k}\left(1 - \tau_{n_k}\right) + C_{\Delta_k}\right]\right\}. \tag{S21}$$

When the cohorts are actively shedding leaves due to phenology, $(\gamma_{l_k}; \gamma_{r_k}; \gamma_{\sigma_k})$ are assumed to be

zero. In case carbon balance is sufficiently negative to consume the entire non-structural carbon pool, carbon stocks of living tissues will be depleted and mortality rates will increase (Supplement S3.4).

S3.3 Carbon allocation to structural tissues and reproduction

Growth of structural (C_{h_k}) and reproductive ($C_{\varrho k}$) tissues are calculated at the cohort dynamics time step (Δt_{CD}, Table 2), after the biomass of living tissues and phenology have been updated:

$$C_{h_k}(t) = C_{h_k}(t - \Delta t_{\mathrm{CD}}) + \gamma_{h_k} C_{n_k}(t)\,\Delta t_{\mathrm{CD}}, \tag{S22}$$

$$C_{\varrho k}(t) = \varrho_{t_k}\, C_{n_k}(t), \tag{S23}$$

$$\gamma_{h_k} = \frac{1}{\Delta t_{\mathrm{CD}}} - \varrho_{t_k} - \gamma_{n_k}, \tag{S24}$$

$$\varrho_{t_k} = \frac{1}{\Delta t_{\mathrm{CD}}} \begin{cases} 0.0 & \text{, if } z_{t_k} < z_{t_k}^{\mathrm{Repro}} \text{ or } \omega_{l_k} > 0 \\ f_{\varrho} & \text{, otherwise} \end{cases}, \tag{S25}$$

$$\gamma_{n_k} = \frac{1}{\Delta t_{\mathrm{CD}}} \begin{cases} 1.0 & \text{, if } \omega_{l_k} > 0 \\ f_n & \text{, otherwise} \end{cases}, \tag{S26}$$

where z_{t_k} is the cohort height (Supplement S18); $z_{t_k}^{\mathrm{Repro}}$ is the minimum height for reproduction, currently defined as the maximum height for grasses and 18 m for trees (based on Wright et al., 2005); f_{ϱ} is the fraction of carbon storage allocated for reproduction when trees are above minimum reproductive height, currently defined as 1.0 for grasses and 0.3 for tropical and temperate trees (Moorcroft et al., 2001); f_n is the fraction of carbon storage that is kept as storage, currently assumed to be 0 for grasses and temperate trees, and 0.1 for tropical trees; and ω_{l_k} is the phenology-driven leaf shedding rate (Supplement S3.1). The total reproduction biomass $C_{\varrho k}$ is transferred either to the patches' seed bank or to the soil carbon pools. The fraction that is transferred to the soil carbon pools is defined in terms of a mortality factor ($m_{\varrho k}$), by default equivalent to 95% in a month, which accounts for both the allocation to reproductive accessories (fruits, flowers, or cones), which are eventually lost, and the seedling mortality rate; the remainder ($1 - m_{\varrho k}$) is transferred to the seed bank. Carbon storage C_{n_k} is updated after carbon allocation to structural carbon and reproduction.

S3.4 Mortality rates

Following Moorcroft et al. (2001) and Albani et al. (2006), the individual-based mortality rate (m_{t_k}) of any cohort k is the sum of four terms:

$$m_{t_k} = \underbrace{m_{t_k}^{\mathrm{DI}}}_{\substack{\text{Aging}\\ \text{(Density-Independent)}}} + \underbrace{m_{t_k}^{\mathrm{DD}}}_{\substack{\text{Carbon starvation}\\ \text{(Density dependent)}}} + \underbrace{m_{t_k}^{\mathrm{CF}}}_{\text{Cold/Frost}} + \underbrace{m_{t_k}^{\mathrm{FR}}}_{\text{Fire}}. \tag{S27}$$

As in Moorcroft et al. (2001), density-independent mortality is the component attributable to aging of the cohort, and it depends both on the typical tree fall disturbance rate λ_{TF} (Table S4) and the cohort wood density:

$$m_{t_k}^{\mathrm{DI}} = \lambda_{\mathrm{TF}} + \frac{1}{\text{æ}}, \tag{S28}$$

$$\tag{S29}$$

where æ is a PFT-specific term to account for the excess mortality in addition to the background mortality due to plant life span (Tables S5-S6). For tropical broadleaf trees, æ is parameterized following Moorcroft et al. (2001):

$$\text{æ} = \frac{0.0933\,\rho_{\mathrm{LTR}}}{\lambda_{\mathrm{TF}}\,(\rho_{\mathrm{LTR}} - \rho_{t_k})}, \tag{S30}$$

where ρ_{t_k} ($\mathrm{g\,cm^{-3}}$) is the wood density of tropical broadleaf cohort k (Table S5), and ρ_{LTR} is the wood density for late-successional, tropical broadleaf trees (Table S5).

Mortality due to cold or frost is also determined through a phenomenological parameterization that linearly increases mortality when the monthly mean canopy air space temperature $\overline{T}_c$ falls below a temperature threshold (Albani et al., 2006):

$$m_{t_k}^{\mathrm{CF}} = 3.0\,\max\left[0, \min\left(1, 1 - \frac{\overline{T}_c - T_{F_k}}{5}\right)\right], \tag{S31}$$

where T_{F_k} is a cold temperature threshold that represents the plant hardiness to cold (Tables S5-S6).

Mortality due to fire in ED-2.2 follows the original implementation by Moorcroft et al. (2001), and assumes that while fire depends on local scale dryness, once it ignites, it can spread throughout the entire site. Unlike other mortality rates, here we take multiple patches into account (patches are denoted by subscript u). First, let $\lambda_{u,u_0}^{\mathrm{FR}}$ be the disturbance rate associated with fires affecting patch u (and creating patch u_0), defined as in Moorcroft et al. (2001):

$$\lambda_{u,u_0}^{\mathrm{FR}} = \mathcal{I} \sum_{u=1}^{N_P} \sum_{k=1}^{N_{T_u}} \left\{ \left[C_{ul_k} + f_{\mathrm{AG}_{uk}} \left(C_{u\sigma_k} + C_{uh_k} \right) \right] \mathcal{Y}_u \, \alpha_u \right\}, \tag{S32}$$

where N_P is the number of patches, N_{T_u} is the number of cohorts in patch u, $\mathcal{Y}_u$ is the binary ignition function, α_u is the relative area of patch u, and $\mathcal{I} = 0.5$ m^2 kgC^{-1} yr^{-1} is a phenomenological parameter that controls fire intensity, and $f_{\mathrm{AG}_{uk}}$ is the fraction of the tissue that is above ground (Tables S5-S6).

The ignition switch is defined in terms of the dryness of the environment, following the original formulation by Moorcroft et al. (2001), which uses soil moisture to estimate dryness:

$$\mathcal{Y}_u = \begin{cases} 1 & \text{, if } \left(\frac{1}{|z_{\mathrm{Fr}}|} \int_{z_{\mathrm{Fr}}}^{0} \vartheta_g \, \mathrm{d}z \right) < \vartheta_{\mathrm{Fr}} \\ 0 & \text{, otherwise} \end{cases}, \tag{S33}$$

where z_{Fr} is the maximum soil depth to consider when assessing dryness and ϑ_{Fr} is the average soil moisture below which ignition occurs. Both z_{Fr} and ϑ_{Fr} are adjustable parameters; default values are $z_{\mathrm{Fr}} = -0.50$ m and $\vartheta_{\mathrm{Fr}} = \vartheta\left(\Psi_{\mathrm{Fr}}\right)$ ($\Psi_{\mathrm{Fr}} = -1.4$ MPa). Once the fire disturbance rate is determined, mortality rate can be determined from the definition of disturbance rate (Moorcroft et al., 2001):

$$m_{ut_k}^{\mathrm{FR}} = \ln \left[\frac{1}{\hat{\sigma}_{ut_k}^{\mathrm{FR}} + \left(1 - \hat{\sigma}_{ut_k}^{\mathrm{FR}}\right) \exp\left(-\lambda_{u,u_0}^{\mathrm{FR}} \, \Delta t_{\mathrm{PD}}\right)} \right], \tag{S34}$$

where $\hat{\sigma}_{ut_k}^{\mathrm{FR}}$ is the survivorship fraction of cohort t_k of patch u following fire disturbance; this value is currently assumed to be zero for all plants in ED-2.2.

Density-dependent mortality rate ($m_{t_k}^{\mathrm{DD}}$) is called so because it describes the limitations of carbon uptake due to competition with other trees to access shared resources such as light and water. Similarly to Moorcroft et al. (2001), the density-dependent mortality rate is parameterized with a logistic function:

$$m_{t_k}^{\mathrm{DD}}(t) = \frac{y_1}{1 + \exp\left[y_2 \left(\frac{\overline{C}_{\Delta_k}}{\overline{C}_{\Delta_k}^{\bullet}} - y_3 \right) \right]}, \tag{S35}$$

where $(y_1; y_2; y_3) = (5.0, 20.0, 0.2)$ are the default (but adjustable) parameters for tropical plants; $\overline{C}_{\Delta_k}$ is the average carbon balance of cohort k over a 12-month period ending at time t, and $\overline{C}_{\Delta_k}^{\bullet}$ is

the average carbon balance the cohort would attain if neither light nor water were limiting carbon uptake. The current implementation includes only light and moisture, although the idea can be extended to any limiting resource.

S4 Input fluxes for soil carbon pools

Soil carbon is represented by three pools characterized by their typical decay rates: the fast soil carbon (subscript e_1), is comprised by metabolic litter (non-lignified leaf and fine-root litter); the intermediate soil carbon (subscript e_2) represents the decaying structural tissues and lignified materials, and the slow soil carbon (e_3) represents the dissolved soil organic matter. Changes in soil carbon content of the three pools are described by the following ordinary differential equations:

$$\frac{\mathrm{d}\dot{C}_{e_1}}{\mathrm{d}t} = \dot{C}_{t_k,e_1} + \dot{C}^{\bigstar}_{t_k,e_1} - \dot{C}_{e_1,c} - \dot{C}_{e_1,e_3}, \tag{S36}$$

$$\frac{\mathrm{d}\dot{C}_{e_2}}{\mathrm{d}t} = \dot{C}_{t_k,e_2} + \dot{C}^{\bigstar}_{t_k,e_2} - \dot{C}_{e_2,c} - \dot{C}_{e_2,e_3}, \tag{S37}$$

$$\frac{\mathrm{d}\dot{C}_{e_3}}{\mathrm{d}t} = \dot{C}_{e_1,e_3} + \dot{C}_{e_2,e_3} - \dot{C}_{e_3,c}, \tag{S38}$$

where $(\dot{C}_{t_k,e_1};\dot{C}_{t_k,e_2})$ are the influxes from cohorts to fast and structural soil carbon that are due to maintenance and shedding of living tissues; $(\dot{C}^{\bigstar}_{t_k,e_1};\dot{C}^{\bigstar}_{t_k,e_2})$ are the influxes from cohorts to fast and structural soil carbon that are due to mortality; $(\dot{C}_{e_1,c};\dot{C}_{e_2,c};\dot{C}_{e_3,c})$ are the effluxes from all soil carbon pools through heterotrophic respiration; and $(\dot{C}_{e_1,e_3};\dot{C}_{e_2,e_3})$ are the decay fluxes that are transported from fast and structural carbon pools to the soil organic matter pool.

Heterotrophic respiration terms are discussed in Section 4.8. The transport terms between cohorts and the fast and the structural carbon pools are defined as:

$$\dot{C}_{t_k,e_1} = \left(1-\text{£}_{l_k}\right)\left[(1-f_{\mathrm{LD}})\,\omega_{l_k}C_{l_k} + \tau_{l_k}C_{l_k} + \tau_{r_k}C_{r_k}\right], \tag{S39}$$

$$\dot{C}_{t_k,e_2} = \text{£}_{l_k}\left(f_{\mathrm{LD}}\,\omega_{l_k}C_{l_k} + \tau_{l_k}C_{l_k} + \tau_{r_k}C_{r_k}\right), \tag{S40}$$

$$\dot{C}^{\bigstar}_{t_k,e_1} = m_{t_k}\left[\left(1-\text{£}_{l_k}\right)\left(C_{l_k}+C_{r_k}\right) + \left(1-\text{£}_{h_k}\right)\left(C_{\sigma_k}+C_{h_k}\right) + C_{n_k}\right] + m_{\varrho_k}C_{\varrho_k}, \tag{S41}$$

$$\dot{C}^{\bigstar}_{t_k,e_2} = m_{t_k}\left[\text{£}_{l_k}\left(C_{l_k}+C_{r_k}\right) + \text{£}_{h_k}\left(C_{\sigma_k}+C_{h_k}\right)\right], \tag{S42}$$

where $(\text{£}_{l_k};\text{£}_{h_k})$ are the fraction of soft — leaves and fine roots — and woody — sapwood and hardwood — tissues that are lignified, and $(\tau_{l_k};\tau_{r_k})$ are the leaf and fine root turnover rates (Tables S5-S6); f_{LD} is the fraction of carbon reabsorbed by cohorts when shedding leaves (Table S4); ω_{l_k} is the phenology-driven leaf shedding rate; m_{t_k} is the mortality rate (Supplement S3.4); and m_{ϱ_k}

is the rate of loss associated with reproduction (reproductive accessories and seedling mortality; Supplement S3.3).

The decay rates that are transported from fast and structural pools to dissolved soil carbon pools are also determined from the complementary fraction of decay functions, i.e. the fraction of decay that is not lost through heterotrophic respiration (see Section 4.8):

$$\dot{C}_{e_j,e_3} = \frac{1 - f_{he_j}}{f_{he_j}} \dot{C}_{e_j,c}, \tag{S43}$$

where the subscript e_j corresponds to either the fast (e_1) or the structural (e_2) soil carbon; f_{he_j} is the fraction of decay that is lost through respiration (Table S4); and $\dot{C}_{e_j,c}$ is the heterotrophic respiration flux from these soil carbon pools.

S5 Definition of enthalpy as a state function

Enthalpy is an extensive thermodynamic variable, therefore the total enthalpy of any thermodynamic system consisting of two or more materials is the sum of enthalpies of each material. Likewise, enthalpy must increase linearly with mass, therefore the total enthalpy of any material (H_x) is defined as $H_x = X \cdot h_x$, where X is the mass of this material and h_x is the specific enthalpy of this material.

For any material other than water (hereafter, dry material), h_d is defined as zero when the dry material temperature is 0 K; for water, the zero level is also at 0 K, with the additional condition that water is completely frozen. The specific enthalpy for dry material (h_d), ice (h_i), liquid water (h_ℓ) and water vapor (h_v) are defined as:

$$h_d(T) = \underbrace{q_d \cdot T}_{\text{Heating}} \tag{S44}$$

$$h_i(T) = \underbrace{q_i \cdot T}_{\text{Heating ice}} \tag{S45}$$

$$h_\ell(T) = \underbrace{h_i(T_{i\ell})}_{\text{Ice enthalpy at melting point}} + \underbrace{l_{i\ell}(T_{i\ell})}_{\text{Melting ice}} + \underbrace{q_\ell\,(T - T_{i\ell})}_{\text{Heating liquid}} \tag{S46}$$

$$h_v(T) = \underbrace{h_\ell(T_{\ell v})}_{\text{Liquid enthalpy at vaporization point}} + \underbrace{l_{\ell v}(T_{\ell v})}_{\text{Vaporization}} + \underbrace{q_{pv}\,(T - T_{\ell v})}_{\text{Heating vapor}} \tag{S47}$$

where q_d, q_i and q_ℓ are the specific heats for dry material, ice and liquid water, respectively; q_{pv} is the specific heat at constant pressure for water vapor; $T_{i\ell}$ and $T_{\ell v}$ are the temperatures where ice

melted and liquid water vaporized; and $l_{i\ell}$ and $l_{\ell v}$ are the latent heat of melting and vaporization, respectively. Equation (S47) is still valid even when ice sublimates, because $l_{iv}(T) = l_{i\ell}(T) + l_{\ell v}(T)$ for any temperature T. By definition (e.g. Dufour and van Mieghem, 1975), the latent heat associated with phase change is the difference in enthalpy between the two phases at the temperature in which the phase change happens, therefore, we can determine the dependency of latent heat on temperature:

$$\left(\frac{\partial l_{\ell v}}{\partial T}\right)_p = \left(\frac{\partial h_v}{\partial T}\right)_p - \left(\frac{\partial h_\ell}{\partial T}\right)_p = q_{pv} - q_\ell, \tag{S48}$$

$$\left(\frac{\partial l_{i\ell}}{\partial T}\right)_p = \left(\frac{\partial h_\ell}{\partial T}\right)_p - \left(\frac{\partial h_i}{\partial T}\right)_p = q_\ell - q_i. \tag{S49}$$

If we further assume that the transition between ice and liquid phases can only occur at the water triple point (T_3), and that the latent heat of fusion $l_{i\ell 3} \equiv l_{i\ell}(T_3)$ and vaporization $l_{\ell v3} \equiv l_{\ell v}(T_3)$ are known (Table S3), we can combine Eq. (S44)-(S47) to obtain a generic state function for specific enthalpy h:

$$h = \frac{H}{D+W} = d\,q_d\,T + w\left[i\,q_i\,T + \ell\,q_\ell\,(T - T_{\ell 0}) + v\,q_{pv}\,(T - T_{v0})\right], \tag{S50}$$

$$d = \frac{D}{D+W}, \tag{S51}$$

$$w = \frac{W}{D+W}, \tag{S52}$$

$$T_{\ell 0} = T_3 - \frac{q_i\,T_3 + l_{i\ell 3}}{q_\ell}, \tag{S53}$$

$$T_{v0} = T_3 - \frac{q_i\,T_3 + l_{i\ell 3} + l_{\ell v3}}{q_{pv}}, \tag{S54}$$

where d and w are the specific mass of other materials and water, respectively, and i, ℓ, and v are fraction of ice, liquid water, and vapor, respectively. Importantly, (S50) does not contain any information about the temperature at which the phase changes had occurred, which is necessary because enthalpy must be a state function (i.e. path-independent).

Temperature T and phase fractions $(i;\ell;v)$ of any thermodynamic system are diagnosed from enthalpy. In the case of canopy air space, i, and ℓ are all assumed to be zero, and thus $v = 1$. The canopy air space temperature T_c is obtained by inverting Eq. S50 and using that $d = 1 - w$:

$$T_c = \frac{h_c + w\,q_{pv}\,T_{v0}}{(1-w)\,q_{pd} + w\,q_{pv}}. \tag{S55}$$

For other thermodynamic systems, v is assumed to be zero. To obtain the temperature and the liquid fraction, we eliminate i from Eq. (S50) by using that $i = 1 - \ell$, and define two critical values of specific enthalpy: h_{i3}, the enthalpy when the water is at the triple point temperature (T_3) but entirely frozen, and $h_{\ell 3}$, when water is entirely in liquid phase and still at triple point temperature:

$$h_{i3} = d\, q_d\, T_3 + w\, q_i\, T_3, \tag{S56}$$

$$h_{\ell 3} = h_{i3} + w\, l_{i\ell 3} = d\, q_d\, T_3 + w\, q_\ell\, (T_3 - T_{\ell 0})\,. \tag{S57}$$

Liquid water and ice can coexist when $T = T_3$, and this only occurs when $h_{i3} < h < h_{\ell 3}$. Therefore, we obtain T and ℓ by comparing the specific enthalpy with h_{i3} and $h_{\ell 3}$:

$$T = \begin{cases} \frac{h}{d\, q_d + w\, q_i} & \text{, if } h < h_{i3} \\ T_3 & \text{, if } h_{i3} \leq h \leq h_{\ell 3}\,, \\ \frac{h + w\, q_\ell\, T_{\ell 0}}{d\, q_d + w\, q_\ell} & \text{, if } h > h_{\ell 3} \end{cases} \tag{S58}$$

$$\ell = \begin{cases} 0 & \text{, if } h < h_{i3} \\ \frac{h - h_{i3}}{l_{i\ell 3}\, w} & \text{, if } h_{i3} \leq h \leq h_{\ell 3}\,. \\ 1 & \text{, if } h > h_{\ell 3} \end{cases} \tag{S59}$$

S6 Specific heat capacity of the thermodynamic systems

From Eq. (S50), we must know the mass and specific heats of each material for each thermodynamic system. For water, specific heat depends on the phase: q_i (ice); q_ℓ (liquid); q_{pv} (vapor at constant pressure); values are shown in Table S3. The specific heats of dry materials are defined below.

S6.1 Soil

Soil water of layer j is normally expressed in terms of liquid-equivalent volumetric fraction (ϑ_{g_j}), thus the bulk density of water in the layer is simply $\mathcal{W}_{g_j} = \rho_\ell \vartheta_{g_j}$. Dry soil is a combination of sand, silt, clay, and air filling any pore space not filled by water, and its bulk density $\mathcal{D}_{g_j}$ for each layer is based on Monteith and Unsworth (2008, Section 15.3):

$$\mathcal{D}_{g_j} = \left[\sum_{\kappa=0}^{3} \rho_\kappa \mathcal{V}_{0\kappa}\left(z_{g_j}\right) \right], \tag{S60}$$

$$\mathcal{V}_{0\kappa}\left(z_{g_j}\right) = \begin{cases} \vartheta_{\mathrm{Po}} - \vartheta_{g_j} \approx \frac{\vartheta_{\mathrm{Re}} + \vartheta_{\mathrm{Po}}}{2} & \kappa = 0 \\ f_{\mathcal{V}_\kappa}\left(1 - \vartheta_{\mathrm{Po}}\right) & \kappa \neq 0 \end{cases}, \tag{S61}$$

where κ indices 0, 1, 2, 3 correspond to air, sand, silt, and clay, respectively; ρ_κ (Table S7) and $\mathcal{V}_{0\kappa}$ (Table S8) are the specific gravity and the reference volumetric fraction of each component, and z_{g_j} is the depth of soil layer j. The volumetric soil content depends on the following texture-dependent variables: $f_{\mathcal{V}_\kappa}$, the soil texture-dependent, volumetric fraction of each soil component excluding water and air; ϑ_{Po}, the total porosity or maximum soil moisture and ϑ_{Re} is the residual water content, defined in Supplement S9. In reality, the volumetric fraction of air is not constant and depends on soil moisture; nevertheless, the total air mass is three orders of magnitude less than the solid materials, thus the contribution of varying air in the pore space to changes in specific heat is negligible. To reduce the maximum error associated with this assumption, we use the volumetric fraction corresponding to halfway between the minimum and maximum soil moisture.

Specific heat of dry soil of layer j (q_{dg_j}) is also determined following Monteith and Unsworth (2008), as the weighted average of the specific heats of the four components (Table S7):

$$q_{dg_j} = \frac{\sum_{\kappa=0}^{3} \left(\rho_\kappa \mathcal{V}_{0\kappa} q_\kappa\right)}{\sum_{\kappa=0}^{3} \left(\rho_\kappa \mathcal{V}_{0\kappa}\right)}. \tag{S62}$$

S6.2 Vegetation

In ED-2.2, vegetation biomass of the different tissues is usually expressed in $\mathrm{kg_C\,m^{-2}}$; for the energy budget, however, we must account for the total internal mass ($\mathrm{kg\,m^{-2}}$) because internal energy is also stored in non-carbon material, including the interstitial and intracellular water of leaves and above ground wood (internal water). Internal water is considered a plant functional trait that remains constant throughout the simulations, although it can be different for different plant functional types. The extensive mass of the vegetation tissue (D_{t_k}) for any cohort k is given by:

$$D_{t_k} = D_{l_k} + D_{b_k}, \tag{S63}$$

$$D_{l_k} = \frac{1}{\mathcal{B}_C} C_{l_k} \left(1 + \mathcal{B}_{Wl}\right), \text{ and} \tag{S64}$$

$$D_{b_k} = \frac{1}{\mathcal{B}_C} f_{\mathrm{AG}} C_{b_k} \left(1 + \mathcal{B}_{Wb}\right), \text{ and} \tag{S65}$$

where $\mathcal{B}_C = 2.0$ is the conversion from carbon to oven dry biomass, following Baccini et al. (2012); n_{t_k} is the demographic density of cohort k (plant m^{-2}); C_{l_k} and C_{b_k} are the carbon biomass of leaves and wood for each cohort ($\mathrm{kg_C\,m^{-2}}$), respectively; D_{l_k} and D_{b_k} are the extensive internal mass leaves and wood, respectively; f_{AG} is the fraction of woody biomass that is above ground (assumed 0.7 for all tree PFTs); and $\mathcal{B}_{Wl} = 0.7$ (Forest Products Laboratory, 2010) and $\mathcal{B}_{Wb} = 1.85$ (Kursar et al., 2009) are the water to oven-dry mass ratios for leaves and wood.

The vegetation specific heat excluding intercepted water (q_{dt_k}) is based on the Gu et al. (2007) parameterization and determined by the weighted average of leaves and wood specific heats, which in turn are weighted averages of the specific heat of the oven-dry materials and water:

$$q_{dt_k} = \frac{1}{D_{t_k}} \left[D_{l_k} \frac{q_l^{(\mathrm{OD})} + \mathcal{B}_{Wl} q_\ell}{1 + \mathcal{B}_{Wl}} + D_{b_k} \left(\frac{q_b^{(\mathrm{OD})} + \mathcal{B}_{Wb} q_\ell}{1 + \mathcal{B}_{Wb}} + \Delta q_b^{\mathrm{Bond}} \right) \right] \tag{S66}$$

where $q_l^{(\mathrm{OD})}$ and $q_b^{(\mathrm{OD})}$ are the specific heats of oven-dry leaves and wood, respectively. The default values are taken from Forest Products Laboratory (2010) and Jones (2014) and assumed the same for all PFTs (Tables S5-S6); and $\Delta q_b^{\mathrm{Bond}}$ is a term included by Gu et al. (2007) and Forest Products Laboratory (2010) to represent the additional heat capacity associated with the bonding between wood and water (Tables S5-S6). Although $q_b^{(\mathrm{OD})}$ and $\Delta q_b^{\mathrm{Bond}}$ are both functions of temperature in Gu et al. (2007), we further simplified them to constants in ED-2.2, using their original equations at 15 °C (Tables S5-S6). In addition, using q_ℓ as the specific heat for water is equivalent to assuming that internal water does not freeze.

S6.3 Canopy air space

The specific heat at constant pressure of the canopy air space (q_{pc}) is determined similarly to the vegetation and soils, as the weighted average between dry air and water vapor:

$$q_{pc} = \left(1 - w_c\right) q_{pd} + w_c q_{pv}, \tag{S67}$$

where q_{pd} and q_{pv} are the specific heats of dry air and water vapor at constant pressure (Table S3).

S7 Snowpack depth dynamics

In addition to enthalpy and total water, we must also track the changes in snowpack depth of each layer (Δz_{s_j}) and density (ρ_{s_j}) over time. The ordinary differential equation that governs changes in depth over time is defined as:

$$\frac{\mathrm{d}\left(\Delta z_{s_j}\right)}{\mathrm{d}t} = \begin{cases} \underbrace{\rho_{wa}\dot{W}_{a,s_j}}_{\substack{\text{Throughfall}\\ \text{precipitation}\\ (4.2)}} + \underbrace{\left(\sum_{k=1}^{N_T}\rho_{wt_k}\dot{W}_{t_k,s_j}\right)}_{\substack{\text{Canopy dripping}\\ \text{from cohorts}\\ (4.2)}} - \underbrace{\rho_{ws_j}\dot{W}_{s_j,o}}_{\substack{\text{Surface runoff}\\ (4.1)}} - \underbrace{\rho_{wx}\dot{W}_{s_j,c}}_{\substack{\text{Surface water}\\ \text{evaporation}\\ (4.5.2 \text{ and } 4.5.3)}} - \underbrace{\delta_{s_1 s_j}\rho_{ws_j}\dot{W}_{s_1,g_{N_G}}}_{\substack{\text{Surface water}\\ \text{percolation}\\ (4.1)}} & \text{, if } s_j = s_{N_S} \\ 0 & \text{, otherwise} \end{cases}, \tag{S68}$$

$$\rho_{ws_j} = \frac{W_{s_j}}{\Delta z_{s_j}} \tag{S69}$$

$$\rho_{wx} = \begin{cases} \rho_{ws_{N_S}} & \text{, if } \dot{W}_{s_{N_S},c} \geq 0 \\ \rho_{wc} & \text{, if } \dot{W}_{s_{N_S},c} < 0 \end{cases} \tag{S70}$$

where $\delta_{s_j s_{j'}}$ is the Kronecker delta for comparing two TSW layers s_j and $s_{j'}$ (1 if $s_j = s_{j'}$, 0 otherwise), ρ_{wa} is the precipitation density, ρ_{wt_k} is the canopy interception density, ρ_{wc} is the density of condensing water vapor. Precipitation density is defined based on Jin et al. (1999), but slightly modified to make it continuous:

$$\rho_{wa} = \frac{\rho_{ia}\rho_\ell}{\ell_a\rho_{ia} + (1-\ell_a)\,\rho_\ell}, \tag{S71}$$

$$\rho_{ia} = \begin{cases} 169.16 & \text{, if } T_a > 275.16 \text{ K} \\ 50. + 1.7\left(T_a - 258.16\right)^{1.5} & \text{, if } 258.16 \text{ K} < T_a \leq 275.66 \text{ K} \\ 50. & \text{, if } T_a \leq 258.16 \text{ K} \end{cases}, \tag{S72}$$

where ρ_ℓ is the density of liquid water (Table S3). For the canopy dripping flux, water density is similar to Eq. (S71), except that we assume the density of frozen water to be the same as frost density (ρ_*, Table S3). A similar assumption is done for water condensing from canopy air space, with the additional assumption that the liquid fraction of condensation is the same as the liquid fraction of the top TSW layer:

$$\rho_{wt_k} = \frac{\rho_*\rho_\ell}{\ell_{t_k}\rho_* + (1-\ell_{t_k})\,\rho_\ell}, \tag{S73}$$

$$\rho_{wc} = \frac{\rho_* \rho_\ell}{\ell_{s_{N_S}} \rho_* + \left(1 - \ell_{s_{N_S}}\right) \rho_\ell}. \tag{S74}$$

The maximum allowed number of snow layers is determined by the user, but the actual number of snow layers is dynamically determined, following the same algorithm as Walko et al. (2000). Multiple layers only exist when ice is present, otherwise a single layer ($N_S = 1$) is enforced. When ice is present, the model selects N_S to be the maximum number of layers that satisfies $W_{s_j} \geq 5\ \mathrm{kg_W\,m^{-2}}$ for all layers $s_j, j \in 1, 2, \ldots, N_S$, to ensure numerical stability. The layer thickness distribution (Δz_{s_j}) for any given N_S is defined as:

$$\Delta z_{s_j} = z_s \frac{2^{\min(j-1, N_S - j)}}{2^{\lfloor \frac{N_S+1}{2} \rfloor} + 2^{\lfloor \frac{N_S}{2} \rfloor} - 2}, \tag{S75}$$

$$z_s = \sum_{j=1}^{N_S} \Delta z_{s_j}, \tag{S76}$$

where z_s is the total depth of the snow, and $\lfloor x \rfloor$ is the floor function (i.e. the nearest integer value to x that is not greater than x). The layer distribution described by Eq. (S75) ensures that the layers near the ground and near the canopy air space are thinner than the intermediate layers, to improve the representation of exchanges between the snowpack and the canopy air space, soils, and incoming irradiance (Walko et al., 2000).

S8 Canopy-Air-Space Pressure

Canopy-air-space pressure p_c is assumed to remain constant throughout the integration time step ($\Delta t_{\mathrm{Thermo}}$). At the end of the time step, the air pressure above canopy p_a is updated using the meteorological forcing, at which time p_c and h_c are also updated. To determine p_c, we combine three assumptions:

1. Both canopy air space and the air above are a mix of two perfect gases, dry air and water vapor (Dufour and van Mieghem, 1975):

$$p = \rho\, \mathcal{R} \left[\frac{1}{\mathcal{M}_d} (1 - w) + \frac{1}{\mathcal{M}_w} w \right] T = \rho\, \frac{\mathcal{R}}{\mathcal{M}_d} T_{\mathcal{V}}, \tag{S77}$$

$$T_{\mathcal{V}} = T \left[1 - \left(1 - \frac{\mathcal{M}_d}{\mathcal{M}_w} w \right) \right], \tag{S78}$$

where $\mathcal{R}$ is the universal gas constant, and $\mathcal{M}_d$ and $\mathcal{M}_w$ are the molar masses of dry air and

water (Table S3); and $T_{\mathcal{V}}$ is the virtual temperature, which is the temperature that pure dry air would be at if pressure and density were the same as the observed air:

2. p_c instantaneously changes when p_a is updated, and this update does not involve any exchange of mass or energy. This is equivalent to assuming that potential temperature of the canopy air space θ_c and air aloft θ_a do not change when pressure is updated, even if enthalpy and temperature change. Potential temperature, approximated to the potential temperature of dry air, is defined as:

$$\theta = T\left(\frac{p_0}{p}\right)^{\frac{\mathcal{R}}{\mathcal{M}_d q_{pd}}}, \tag{S79}$$

where p_0 is the reference pressure level and q_{pd} is the specific heat of dry air at constant pressure (Table S3).

3. The layer between canopy air space depth $\bar{z}_c$ and reference height of the free air z_a is in hydrostatic equilibrium:

$$\frac{\partial p}{\partial z} = -\rho\, g, \tag{S80}$$

where g is the gravity acceleration (Table S3).

Combining these three assumptions and defining $\theta_{\mathcal{V}} \equiv \theta(T_{\mathcal{V}})$ yields:

$$p_c = \left[p_a^{\frac{\mathcal{R}}{\mathcal{M}_d q_{pd}}} + \frac{g\,(z_a - \bar{z}_c)}{q_{pd}\overline{\theta_{\mathcal{V}}}} p_0^{\frac{\mathcal{R}}{\mathcal{M}_d q_{pd}}}\right]^{\frac{\mathcal{M}_d q_{pd}}{\mathcal{R}}}, \tag{S81}$$

where $\overline{\theta_{\mathcal{V}}}$ is the virtual potential temperature averaged between z_a and $\bar{z}_c$. Once pressure is updated at the biophysics time step, temperature and enthalpy are also updated using Eq. (S79) and Eq. (S50), respectively. Because canopy air pressure is known at all times, canopy air density ρ_c can be determined diagnostically using Eq. (S77).

S9 Soil thermal and hydraulic properties

Most of the soil hydraulic properties in ED-2.2 are derived from LEAF-3 (Walko et al., 2000) and use the soil classification based on the United States Department of Agriculture (e.g. Cosby et al.,

1984). Soils in tropical forests often fall under the *Clay* class of the USDA classification, even though their sand, silt, and clay fractions often vary significantly from the average values of this class. To avoid large deviations from observations, we further split the original *Clay* class into four categories, named as *Clayey sand*, *Clayey silt*, *Clay*, and *Heavy Clay*, as shown in Fig. S6; the default fractions of each component for the default soil texture types in ED-2.2 are listed in Table S8. In addition to the standard classes, the model can derive site-specific properties based on the actual clay, silt, and sand fractions, which can be provided directly by the user.

The main hydraulic properties follow the parameterization by Cosby et al. (1984), shown here for reference:

$$\vartheta_{\mathrm{Po}} = 0.0505 - 0.0142\, f_{\mathcal{V}_{\mathrm{Sand}}} - 0.0037\, f_{\mathcal{V}_{\mathrm{Clay}}}, \tag{S82}$$

$$\Psi_{\mathrm{Po}} = -0.01 \cdot 10^{2.17 - 1.58\, f_{\mathcal{V}_{\mathrm{Sand}}} - 0.63\, f_{\mathcal{V}_{\mathrm{Clay}}}}, \tag{S83}$$

$$b = 3.10 - 0.3 \cdot f_{\mathcal{V}_{\mathrm{Sand}}} + 15.7 \cdot f_{\mathcal{V}_{\mathrm{Clay}}}, \tag{S84}$$

$$\Upsilon_{\Psi_{\mathrm{Po}}} = 6.817 \times 10^{-6} \cdot 10^{-0.60 + 1.26\, f_{\mathcal{V}_{\mathrm{Sand}}} - 0.64\, f_{\mathcal{V}_{\mathrm{Clay}}}}, \tag{S85}$$

where $f_{\mathcal{V}_{\mathrm{Sand}}}$ and $f_{\mathcal{V}_{\mathrm{Clay}}}$ are the volumetric fraction of sand and clay, respectively; ϑ_{Po} ($\mathrm{m}^3_{\mathrm{W}}\,\mathrm{m}^{-3}$) is the volumetric soil porosity (maximum soil moisture possible), $\Upsilon_{\Psi_{\mathrm{Po}}}$ (m) is the soil matric potential at porosity, b is the slope of the logarithmic water retention curve (Clapp and Hornberger, 1978), and $\Upsilon_{\Psi}^{(\mathrm{Po})}$ ($\mathrm{kg_W\,m^{-2}\,s^{-1}}$) is the soil hydraulic conductivity at bubbling pressure, assumed to occur when soil moisture $\vartheta = \vartheta_{\mathrm{Po}}$.

The equation that describes soil matric potential as a function of soil moisture is taken from Clapp and Hornberger (1978); soil hydraulic conductivity is defined after Brooks and Corey (1964), with an additional correction term applied to hydraulic conductivity to reduce conductivity in case the soil is partially or completely frozen:

$$\Psi = \Psi_{\mathrm{Po}} \left(\frac{\vartheta_{\mathrm{Po}}}{\vartheta} \right)^{b}, \tag{S86}$$

$$\Upsilon_{\Psi} = \left[10^{-7(1-\ell)} \right] \Upsilon_{\Psi_{\mathrm{Po}}} \left(\frac{\vartheta}{\vartheta_{\mathrm{Po}}} \right)^{2b+3}, \tag{S87}$$

where ℓ is the fraction of liquid water of soil moisture.

Additional reference points are determined using the above equations combined with Eq. (S86) and (S87). The permanent wilting point ϑ_{Wp} and residual soil moisture ϑ_{Re} are defined as the soil moisture when soil matric potential is equivalent to -1.5 and -3.1 MPa, respectively:

$$\vartheta_{\mathrm{Wp}} = \vartheta_{\mathrm{Po}} \cdot \left(-\frac{g\,\rho_\ell\,\Psi_{\mathrm{Po}}}{1.5 \cdot 10^6} \right)^{\frac{1}{b}}, \tag{S88}$$

$$\vartheta_{\mathrm{Re}} = \vartheta_{\mathrm{Po}} \cdot \left(-\frac{g\,\rho_\ell\,\Psi_{\mathrm{Po}}}{3.1 \cdot 10^6} \right)^{\frac{1}{b}}, \tag{S89}$$

where g is the gravity acceleration and ρ_ℓ is the density of liquid water (Table S3).

Field capacity (ϑ_{Fc}) is often defined from soil matric potential (e.g. Hodnett and Tomasella, 2002; Saxton and Rawls, 2006). However, this definition is based on field measurements and the definition of ϑ_{Fc} from soil matric potential can substantially across studies, with values ranging from -0.1 kPa to -0.5 kPa (Romano and Santini, 2002). In ED-2.2, we follow Romano and Santini (2002) and define field capacity in terms of hydraulic conductivity, and assume that the drainage flux of water becomes negligible at hydraulic conductivity of 0.1 $\mathrm{kg_W\,m^{-2}\,day^{-1}}$:

$$\vartheta_{\mathrm{Fc}} = \vartheta_{\mathrm{Po}} \cdot \left(\frac{1.16 \cdot 10^{-9}}{\Upsilon_{\Psi_{\mathrm{Po}}}} \right)^{\frac{1}{2\,b+3}}. \tag{S90}$$

Soil thermal conductivity at soil layer j ($\Upsilon_{\mathrm{Q}_{g_j}}$) is a function of the soil texture and soil moisture, and is determined using the *de Vries* weighted average of conductivities of each constituent of the soil (e.g. Parlange et al., 1998):

$$\Upsilon_{\mathrm{Q}_{g_j}} = \frac{\sum_{\kappa=0}^{3} \left[\left(\frac{3\,\Upsilon_{\mathrm{Q}_\ell}}{2\,\Upsilon_{\mathrm{Q}_\ell} + \Upsilon_{\mathrm{Q}_\kappa}} \right) \mathcal{V}_\kappa\left(z_{g_j}\right) \Upsilon_{\mathrm{Q}_\kappa} \right] + \vartheta_{g_j} \Upsilon_{\mathrm{Q}_\ell}}{\sum_{\kappa=0}^{3} \left[\left(\frac{3\,\Upsilon_{\mathrm{Q}_\ell}}{2\,\Upsilon_{\mathrm{Q}_\ell} + \Upsilon_{\mathrm{Q}_\kappa}} \right) \mathcal{V}_\kappa\left(z_{g_j}\right) \right] + \vartheta_{g_j}}, \tag{S91}$$

$$\mathcal{V}_\kappa\left(z_{g_j}\right) = \begin{cases} \vartheta_{\mathrm{Po}} - \vartheta_{g_j} & \kappa = 0 \\ \mathcal{V}_\kappa^{\mathrm{Dry}}\left(1 - \vartheta_{\mathrm{Po}}\right) & \kappa \neq 0 \end{cases}, \tag{S92}$$

where $\mathcal{V}_\kappa\left(z_{g_j}\right)$ is the volumetric fraction for soil components air, sand, silt, and clay ($\kappa = 0, 1, 2, 3$, respectively) at soil layer j; $\Upsilon_{\mathrm{Q}_\kappa}$ is the thermal conductivity for air, sand, silt, and clay (Table S7), respectively; $\Upsilon_{\mathrm{Q}_\ell}$ is the thermal conductivity of water (Table S3); $\mathcal{V}_\kappa^{\mathrm{Dry}}$ is the dry matter volumetric fraction; and ϑ_{Po} is the soil porosity. In Eq. (S91), the weights are the product between the volumetric fraction and a function that represents both the ratio of the thermal gradient of the soil constituents and the thermal gradient of water and the shape of each soil constituent (Camillo and Schmugge, 1981); in ED-2.2 we assume all particles to be spherical.

S10 Thermal and hydraulic properties of temporary surface water

The fraction of ground covered by the temporary surface water (f_{TSW}) is determined following Niu and Yang (2007), with the same coefficients used in the Community Land Model (NCAR-CLM Oleson et al., 2013):

$$f_{\mathrm{TSW}} = \begin{cases} 0 & \text{if } N_S = 0 \\ \tanh\left[\frac{\sum_{j=1}^{N_S} z_{s_j}}{2.5 z_{0\varnothing}} \left(\frac{\overline{\rho}_s}{\rho_{\circledast}}\right)^{-1.0}\right] & \text{if } N_S > 0 \end{cases}, \tag{S93}$$

$$\overline{\rho}_s = \frac{\sum_{j=1}^{N_S} W_{s_j}}{\sum_{j=1}^{N_S} z_{s_j}}, \tag{S94}$$

where N_S is the number of temporary surface water layers, z_{s_j} (m) is the vertical position of the temporary surface water layer j; W_{s_j} ($\mathrm{kg\,m^{-2}}$) is the water mass of temporary surface water layer j, $z_{0\varnothing}$ is the bare soil roughness (Table S4); $\rho_{\circledast}$ is the reference density of fresh snow (Table S3).

The thermal conductivity of each temporary surface water layer ($\Upsilon_{\mathrm{Q}_{s_j}}$) is a function of the layer temperature T_{s_j} and the bulk layer density ρ_{ws_j} (Eq. S69), and is found using the same parameterization as LEAF-2 (Walko et al., 2000):

$$\Upsilon_{\mathrm{Q}_{s_j}} = y_0 \cdot \left[y_1 + y_2\,\rho_{ws_j} + y_3\,\left(\rho_{ws_j}\right)^2 + y_4\,\left(\rho_{ws_j}\right)^3\right] \cdot \exp\left(y_5\,T_{s_j}\right), \tag{S95}$$

where $(y_0; y_1; y_2; y_3; y_4; y_5) = \left(1.093\times10^{-3}; 0.03; 3.03\times10^{-4}; -1.77\times10^{-7}; 2.25\times10^{-9}; 0.028\right)$ are empirical constants.

S11 Optical properties of vegetation, soil, and temporary surface water.

The inverse of the optical depth per unit of plant area index (μ) for a radiation beam coming from any given angle of incidence Z is determined from the same parameterization described by Sellers (1985) and Oleson et al. (2013):

$$\mu\left(Z, \chi_k\right) = \frac{\cos Z}{E(Z, \chi_k)}, \tag{S96}$$

where $E(Z, \chi_k)$ is the average projection of all leaves and branches onto the horizontal, defined

after Goudriaan (1977):

$$E\left(Z,\chi_k\right) = Y_{1_k} + Y_{2_k}\cos Z, \tag{S97}$$

$$Y_{1_k} = 0.5 - 0.633\,\chi_k - 0.33\,\chi_k^2, \tag{S98}$$

$$Y_{2_k} = 0.877\left(1 - 2Y_{1_k}\right), \tag{S99}$$

where Z is 0 when the beam is coming from the zenith and π when coming from the nadir (Fig. 4 in the main text); and χ_k is the mean orientation of leaves and branches, a PFT-dependent parameter that ranges from -1 (vertical leaves) to +1 (horizontal leaves), with 0 corresponding to spherically distributed leaves (Tables S5-S6). Equation (S97) is valid only when $-0.4 \leq \chi_k \leq 0.6$, which is the case for most plants in the wild (Goudriaan, 1977), and also all plant functional types in ED-2.2.

In the case of direct radiation, $\mu_k^{\odot} = \mu(Z^{\odot}, \chi_k)$, where $Z^{\odot}$ is the solar zenith angle, whereas all angles between 0 and $\pi/2$ contribute equally to downward diffuse radiation. In the case of upward radiation, the actual angles are between $\pi/2$ and π; in practice, the contribution of each angle is similar to the downward hemisphere except for the sign, hence the negative sign on the left-hand side of Eq. (47) in the main text. The contribution of all different zenith angles is represented by $\overline{\mu}_k$, which is the average across all possible angles (Sellers, 1985):

$$\overline{\mu}_k = \int_0^{\frac{\pi}{2}} \frac{\cos Z}{E\left(Z,\chi_k\right)} \sin Z\,\mathrm{d}Z = \frac{1}{Y_{2_k}}\left[1 + \frac{Y_{1_k}}{Y_{2_k}} \ln\left(\frac{Y_{1_k}}{Y_{1_k} + Y_{2_k}}\right)\right]. \tag{S100}$$

The scattering parameters ς_{mk}, β_{mk} and $\beta_{mk}^{\odot}$ for each band m and cohort k are found using the same formulation as the Community Land Model (CLM, Oleson et al., 2013), which is mostly derived from Goudriaan (1977) and Sellers (1985). The scattering coefficient is defined as:

$$\varsigma_{mk} = \varsigma_{R_{mk}} + \varsigma_{T_{mk}}, \tag{S101}$$

where $\varsigma_{R_{mk}}$ and $\varsigma_{T_{mk}}$ are the PFT- and spectral-band-dependent reflectance and transmittance, respectively (Tables S5-S6). The cohort parameters are found by taking the weighted average of the PFT-dependent, leaf ($\varsigma_{R_{mk}}^{\mathrm{Leaf}}$; $\varsigma_{T_{mk}}^{\mathrm{Leaf}}$) and branchwood ($\varsigma_{R_{mk}}^{\mathrm{Wood}}$; $\varsigma_{T_{mk}}^{\mathrm{Wood}}$) properties, using $f_{\mathrm{Clump}_k}\Lambda_k$ and Ω_k as weights, respectively.

Both the bulk diffuse backscattering β_{mk} and forwarding scattering $1 - \beta_{mk}$ contain contributions from reflectance and transmittance because leaves and branches are not perfectly horizontal; therefore the fraction depends on the mean leaf and branch inclination relative to the horizontal plane ($\mathcal{A}_k$), which is related to the leaf orientation by the same approximation used by Oleson et al. (2013):

$$\beta_{mk} = \frac{1}{2\,\varsigma_{mk}} \left[\varsigma_{R_{mk}} + \varsigma_{T_{mk}} + \left(\varsigma_{R_{mk}} - \varsigma_{T_{mk}} \right) \cos^2 \mathcal{A}_k \right], \tag{S102}$$

$$\cos \mathcal{A}_k \approx \frac{1 + \chi_k}{2}. \tag{S103}$$

For direct radiation, backscattering $\beta_{mk}^{\odot}$ and single-scattering albedo $\varsigma_{mk}^{\odot}$ are the same as Sellers (1985) and Oleson et al. (2013), and are determined by taking the limit $\varsigma_{mk} \to 0$ of Eq. (46) and (47) in the main text, assuming isotropic scattering of leaves and branches, and the projected area from Eq. (S97):

$$\beta_{mk}^{\odot} = \frac{\overline{\mu}_k + \mu_k^{\odot}}{\overline{\mu}_k} \frac{\varsigma_{mk}^{\odot}}{\varsigma_{mk}}, \tag{S104}$$

$$\begin{aligned} \frac{\varsigma_{mk}^{\odot}}{\varsigma_{mk}} &= \frac{1}{2} \int_0^{\frac{\pi}{2}} \frac{E\left(Z^{\odot}, \chi_k\right) \cos Z}{E\left(Z^{\odot}, \chi_k\right) \cos Z + E\left(Z, \chi_k\right) \cos Z^{\odot}} \sin Z \, \mathrm{d}Z \\ &= \frac{1}{2\left(1 + Y_{2_k}\,\mu_k^{\odot}\right)} \left\{ 1 - \frac{Y_{1_k}\,\mu_k^{\odot}}{1 + Y_{2_k}\,\mu_k^{\odot}} \ln \left[\frac{1 + \left(Y_{1_k} + Y_{2_k}\right) \mu_k^{\odot}}{Y_{1_k}\,\mu_k^{\odot}} \right] \right\}. \end{aligned} \tag{S105}$$

The effective ground scattering coefficient ς_{m0} is the weighted average of the exposed soil scattering and the combined backscattering of temporary surface water and soil scattering of irradiance transmitted through the temporary surface water:

$$\varsigma_{m0} = \left(1 - f_{\mathrm{TSW}}\right) \varsigma_{R_{mg}} + f_{\mathrm{TSW}}\, \varsigma_{R_{ms}} \left(1 + \varsigma_{T_{ms}}\, \varsigma_{R_{mg}}\right), \tag{S106}$$

where f_{TSW} is the fraction of ground covered by temporary surface water, $\varsigma_{R_{mg}}$ is the reflectance of the top soil layer; and $\varsigma_{R_{ms}}$ and $\varsigma_{T_{ms}}$ are the reflectance and transmittance of the temporary surface water, respectively. Soil reflectance is a function of the soil color and volumetric soil moisture at the topmost layer, determined from the same parameterization and soil color classes as in Oleson et al. (2013):

$$\varsigma_{R_{mg}} = \min \left[\varsigma_{R_m}^{\mathrm{Po}} + 0.11 - 0.40\, \vartheta_{g_{N_G}}, \varsigma_{R_m}^{\mathrm{Re}} \right], \tag{S107}$$

where $\varsigma_{R_m}^{\mathrm{Re}}$ and $\varsigma_{R_m}^{\mathrm{Po}}$ are the soil color-dependent reflectance for dry and saturated soils, respectively.

The temporary surface water reflectance $\varsigma_{R_{ms}}$ depends on the liquid fraction, snow grain size and age, impurities, and the direction of incoming radiation, but here we simply assume a linear interpolation of soil reflectance at saturation and pure snow reflectance ($\varsigma_{R_{ms}}^{\circledast}$; Table S4), assumed constant for each band:

$$\varsigma_{R_{ms}} = \varsigma^{\circledast}_{R_{ms}} + \ell_{s_{N_S}} \left(\varsigma^{\mathrm{Po}}_{R_m} - \varsigma^{\circledast}_{R_{ms}} \right). \tag{S108}$$

Following Verseghy (1991) and Walko et al. (2000), the transmissivity of intercepted irradiance for PAR and NIR is solved following Beer's law, with a direction-independent extinction coefficient:

$$\varsigma_{T_{ms}} = \begin{cases} \exp\left(-\frac{\sum_{j=1}^{N_S} \Delta\bar{z}_{s_j}}{f_{\mathrm{TSW}} \overline{\mu}_s} \right) & \text{, if } m \in (1,2) \\ 0 & \text{, if } m = 3 \end{cases}, \tag{S109}$$

where $\overline{\mu}_s = 0.05\,\mathrm{m}$ is the inverse of the optical depth per unit of temporary surface water depth, defined here to be the same coefficient used by Verseghy (1991) and Walko et al. (2000), and the additional f^{-1}_{TSW} term accounts for the clumping of the temporary surface water, when the water does not cover all ground. Temporary surface water is assumed to be opaque for the TIR band ($m = 3$), following Walko et al. (2000).

S12 Solving the two-stream linear system of canopy radiation in ED-2.2.

Because we assume that the optical properties are constant within each layer, it is possible to find an analytical solution for the full profile of direct and diffuse radiation. First, let $\dot{Q}^{\odot}_{mk}$, $\dot{Q}^{\Downarrow}_{mk}$, and $\dot{Q}^{\Uparrow}_{mk}$ be the solution for band m and interface k immediately beneath the cohort (i.e. at $\tilde{\Phi} = \tilde{\Phi}_k$), and $\dot{Q}^{\odot}_{0_{mk}}$, $\dot{Q}^{\Downarrow}_{0_{mk}}$, and $\dot{Q}^{\Uparrow}_{0_{mk}}$ be the solution for band m and interface k immediately above the cohort (i.e. at $\tilde{\Phi} = 0$), as shown in Fig. 4. The direct radiation profile within each layer is simply given by:

$$\dot{Q}^{\odot}_{mk} = \dot{Q}^{\odot}_{0_{mk}} \exp\left(-\frac{\tilde{\Phi}_k}{\mu^{\odot}_k} \right), \tag{S110}$$

$$\dot{Q}^{\odot}_{0_{mk}} = \dot{Q}^{\odot}_{m(k+1)}, \tag{S111}$$

$$\dot{Q}^{\odot}_{m(N_T+1)} = \dot{Q}^{\odot}_{m(\infty,a)}, \tag{S112}$$

where $\dot{Q}^{\odot}_{m(\infty,a)}$ is the above-canopy, incoming direct radiation for band m and serves as the top boundary condition. Because the value at interface $N_T + 1$ is known, it is possible to determine all levels by integrating the layers from top to bottom.

For the diffuse components, an analytic solution can be found by defining two auxiliary variables $\dot{Q}^{+}_{mk} \equiv \dot{Q}^{\Downarrow}_{mk} + \dot{Q}^{\Uparrow}_{mk}$ and $\dot{Q}^{-}_{mk} = \dot{Q}^{\Downarrow}_{mk} - \dot{Q}^{\Uparrow}_{mk}$. By subtracting (adding) Eq. (46) from (to) Eq. (47), and using Eq. (S110)-(S112) we obtain:

$$\frac{\mathrm{d}\dot{Q}^{+}_{mk}}{\mathrm{d}\tilde{\Phi}} = -\frac{1-(1-2\beta_{mk})\,\varsigma_{mk}}{\overline{\mu}_k}\,\dot{Q}^{-}_{mk} + \frac{\left(1-2\beta^{\odot}_{mk}\right)\,\varsigma_{mk}}{\mu^{\odot}_{mk}}\,\dot{Q}^{\odot}_{m(k+1)}, \tag{S113}$$

$$\frac{\mathrm{d}\dot{Q}^{-}_{mk}}{\mathrm{d}\tilde{\Phi}} = -\frac{1-\varsigma_{mk}}{\overline{\mu}_k}\dot{Q}^{+}_{mk} + \frac{\varsigma_{mk}}{\mu^{\odot}_{k}}\,\dot{Q}^{\odot}_{m(k+1)} + \frac{2\,(1-\varsigma_{mk})}{\overline{\mu}_k}\,\dot{Q}^{\blacklozenge}_{mk}. \tag{S114}$$

By differentiating Eq. (S113) and Eq. (S114) and substituting the first derivatives by Eq. (S114) and Eq. (S113), we obtain two independent, second-order ordinary differential equations:

$$\frac{\mathrm{d}^2\dot{Q}^{+}_{mk}}{\mathrm{d}\tilde{\Phi}^2} = \varkappa^2_{mk}\,\dot{Q}^{+}_{mk} + \kappa^{+}_{mk}\exp\left(-\frac{\tilde{\Phi}}{\mu^{\odot}_{k}}\right) - 2\varkappa^2_{mk}\,\dot{Q}^{\blacklozenge}_{ik}, \tag{S115}$$

$$\frac{\mathrm{d}^2\dot{Q}^{-}_{mk}}{\mathrm{d}\tilde{\Phi}^2} = -\varkappa^2_{mk}\,\dot{Q}^{-}_{mk} + \kappa^{-}_{mk}\exp\left(-\frac{\tilde{\Phi}}{\mu^{\odot}_{k}}\right), \tag{S116}$$

where

$$\varkappa^2_{mk} = \frac{\left[1-(1-2\beta_{mk})\,\varsigma_{mk}\right](1-\varsigma_{mk})}{\overline{\mu}^2_k}, \tag{S117}$$

$$\kappa^{+}_{mk} = -\left[\frac{1-(1-2\beta_{mk})\,\varsigma_{mk}}{\overline{\mu}_k} + \frac{1-2\beta^{\odot}_{mk}}{\mu^{\odot}_{k}}\right]\frac{\varsigma_{mk}\,\dot{Q}^{\odot}_{m(k+1)}}{\mu^{\odot}_{k}}, \tag{S118}$$

$$\kappa^{-}_{mk} = -\left[\frac{(1-\varsigma_{mk})\left(1-2\beta^{\odot}_{mk}\right)}{\overline{\mu}_k} + \frac{1}{\mu^{\odot}_{k}}\right]\frac{\varsigma_{mk}\,\dot{Q}^{\odot}_{m(k+1)}}{\mu^{\odot}_{k}}. \tag{S119}$$

The solution of Eq. (S115)-(S116) is the combination of the homogeneous and the particular solution, and can be determined analytically:

$$\dot{Q}^{+}_{mk}\left(\tilde{\Phi}\right) = x^{+-}_{mk}\exp\left(-\varkappa_{mk}\tilde{\Phi}\right) + x^{++}_{mk}\exp\left(+\varkappa_{mk}\tilde{\Phi}\right) + \frac{\kappa^{+}\,{\mu^{\odot}_{k}}^2}{1-\varkappa^2_{mk}\,{\mu^{\odot}_{k}}^2}\exp\left(-\frac{\tilde{\Phi}}{\mu^{\odot}_{k}}\right) + 2\,\dot{Q}^{\blacklozenge}_{mk} \tag{S120}$$

$$\dot{Q}^{-}_{mk}\left(\tilde{\Phi}\right) = x^{--}_{mk}\exp\left(-\varkappa_{mk}\tilde{\Phi}\right) + x^{-+}_{mk}\exp\left(+\varkappa_{mk}\tilde{\Phi}\right) + \frac{\kappa^{-}\,{\mu^{\odot}_{k}}^2}{1-\varkappa^2_{mk}\,{\mu^{\odot}_{k}}^2}\exp\left(-\frac{\tilde{\Phi}}{\mu^{\odot}_{k}}\right) \tag{S121}$$

where x^{+-}_{mk}, x^{++}_{mk}, x^{--}_{mk}, and x^{-+}_{mk} are coefficients to be determined. We can reduce the number of

coefficients to two by differentiating Eq. (S120)-(S121) and comparing them to Eq. (S113)-(S114), and using the fact that they must be equal for any $\tilde{\Phi}$, $\mu_k^{\odot}$, $\varkappa_{mk}$, and $\dot{Q}_{mk}^{\blacklozenge}$. We call these parameters $x_{m(2k-1)}$ and $x_{m(2k)}$, $k \in \{1,2,\ldots,N_T\}$. By further recalling the definition of $\dot{Q}_{mk}^{+}$ and $\dot{Q}_{mk}^{-}$, we obtain the profile of downward and upward diffuse irradiances:

$$\dot{Q}_{mk}^{\Downarrow}\left(\tilde{\Phi}\right) = x_{m(2k-1)}\, Ð_{mk}^{+} \exp\left(-\varkappa_{mk}\tilde{\Phi}\right) + x_{m(2k)}\, Ð_{mk}^{-} \exp\left(+\varkappa_{mk}\tilde{\Phi}\right) + Þ_{mk}^{+} \exp\left(-\frac{\tilde{\Phi}}{\mu_k^{\odot}}\right) + \dot{Q}_{mk}^{\blacklozenge}, \tag{S122}$$

$$\dot{Q}_{mk}^{\Uparrow}\left(\tilde{\Phi}\right) = x_{m(2k-1)}\, Ð_{mk}^{-} \exp\left(-\varkappa_{mk}\tilde{\Phi}\right) + x_{m(2k)}\, Ð_{mk}^{+} \exp\left(+\varkappa_{mk}\tilde{\Phi}\right) + Þ_{mk}^{-} \exp\left(-\frac{\tilde{\Phi}}{\mu_k^{\odot}}\right) + \dot{Q}_{mk}^{\blacklozenge}, \tag{S123}$$

where

$$Ð_{mk}^{\pm} = \frac{1}{2}\left[1 \pm \sqrt{\frac{1-\varsigma_{mk}}{1-(1-2\beta_{mk})\,\varsigma_{mk}}}\right], \tag{S124}$$

$$Þ_{mk}^{\pm} = \frac{\left(\kappa_{mk}^{+} \pm \kappa_{mk}^{-}\right)\mu_k^{\odot 2}}{2\left(1-\varkappa_{mk}^{2}\,\mu_k^{\odot 2}\right)}. \tag{S125}$$

To determine all vector elements $\left(x_{m(2k-1)}, x_{m(2k)}\right); k \in \{1,2,\ldots,N_T,N_T+1\}$ we need three independent systems of $2N_T+2$ equations (one system of equations for each spectral band). For $k \in \{1,2,\ldots,N_T\}$, the solution must meet the boundary conditions for all middle interfaces (Fig. 4), with one additional boundary condition for upward radiation coming out of the ground (Line 1), and another for incoming downward radiation from above the canopy (Line $2N_T+2$):

$$\begin{array}{lll}
\text{Line 1:} & \dot{Q}_{m1}^{\Uparrow} - \varsigma_{m0}\left(\dot{Q}_{mk}^{\Downarrow} + \dot{Q}_{mk}^{\odot}\right) - (1-\varsigma_{m0})\,\dot{Q}_{m0}^{\blacklozenge} = 0 & \\
\text{Line } 2k: & \dot{Q}_{0_{mk}}^{\Downarrow} - \dot{Q}_{m(k+1)}^{\Downarrow} = 0 & , \; k \in \{1,2,\ldots,K=N_T\} \\
\text{Line } 2k+1: & \dot{Q}_{0_{mk}}^{\Uparrow} - \dot{Q}_{m(k+1)}^{\Uparrow} = 0 & , \; k \in \{1,2,\ldots,K=N_T\} \\
\text{Line } 2N_T+2: & \dot{Q}_{0_{m(N_T+1)}}^{\Downarrow} - \dot{Q}_{m(\infty,a)}^{\Downarrow} = 0 &
\end{array} \tag{S126}$$

where ς_{i0} is the ground (soil and temporary surface water) scattering coefficient (Section S11), $\dot{Q}_{m0}^{\blacklozenge}$ is the ground black body emission, and $\dot{Q}_{m(\infty,a)}^{\Downarrow}$ is the above-canopy, downward diffuse radiation for the band. For the top boundary condition, it is also assumed that $\tilde{\Phi}_{N_T+1} = 0$; $\overline{\mu}_{N_T+1} = 1$; $\dot{Q}_{m(N_T+1)}^{\blacklozenge} = 0$; $\varsigma_{m(N_T+1)} = 1$ (no absorption or emission); and $\beta_{m(N_T+1)} = \beta_{m(N_T+1)}^{\odot} = 0$ (all ir-

radiance is transmitted). Because $\varsigma_{m(N_T+1)} = 1$ creates singularities for $Đ^{\pm}_{m(N_T+1)}$, we use the limit $\varsigma_{m(N_T+1)} \to 0$, so that $Đ^{+}_{m(N_T+1)} = 1$ and $Đ^{-}_{m(N_T+1)} = 0$. Substituting Eq. (S110)-(S112) and Eq.(S122)-(S123) into Eq. (S126) yields

$$\mathbf{S}_m \cdot \mathbf{x}_m = \mathbf{y}_m, \tag{S127}$$

where $\mathbf{x}_m = \left(x_{m1}, x_{m2}, \ldots, x_{m(2N_T+1)}, x_{m(2N_T+2)}\right)$ are the constants from Eq. (S122) and Eq. (S123); $\mathbf{S}_m$ is a $(2N_T+2) \times (2N_T+2)$ sparse matrix with following non-zero elements:

$$\begin{array}{lll}
S_{m(1,1)} = \left(Đ^{-}_{m1} - \varsigma_{m0} Đ^{+}_{m1}\right) \exp\left(-\varkappa_{m1} \tilde{\Phi}_1\right) & & \\
S_{m(1,2)} = \left(Đ^{+}_{m1} - \varsigma_{m0} Đ^{-}_{m1}\right) \exp\left(+\varkappa_{m1} \tilde{\Phi}_1\right) & & \\
S_{m(2k,2k-1)} = Đ^{+}_{mk} & ,k \in (1,2,\ldots,N_T+1) & \\
S_{m(2k,2k)} = Đ^{-}_{mk} & ,k \in (1,2,\ldots,N_T+1) & \\
S_{m(2k,2k+1)} = -Đ^{+}_{m(k+1)} \exp\left(-\varkappa_{m(k+1)} \tilde{\Phi}_{m(k+1)}\right) & ,k \in (1,2,\ldots,N_T) & \\
S_{m(2k,2k+2)} = -Đ^{-}_{m(k+1)} \exp\left(+\varkappa_{m(k+1)} \tilde{\Phi}_{m(k+1)}\right) & ,k \in (1,2,\ldots,N_T) & \\
S_{m(2k+1,2k-1)} = Đ^{-}_{mk} & ,k \in (1,2,\ldots,N_T+1) & \\
S_{m(2k+1,2k)} = Đ^{+}_{mk} & ,k \in (1,2,\ldots,N_T+1) & \\
S_{m(2k+1,2k+1)} = -Đ^{-}_{m(k+1)} \exp\left(-\varkappa_{m(k+1)} \tilde{\Phi}_{m(k+1)}\right) & ,k \in (1,2,\ldots,N_T) & \\
S_{m(2k+2,2k+2)} = -Đ^{+}_{m(k+1)} \exp\left(+\varkappa_{m(k+1)} \tilde{\Phi}_{m(k+1)}\right) & ,k \in (1,2,\ldots,N_T) &
\end{array}, \tag{S128}$$

and $\mathbf{y}_m = \left(y_{m1}, y_{m2}, \ldots, y_{m(2N_T+1)}, y_{m(2N_T+2)}\right)$, where

$$\begin{array}{lll}
y_{m1} = \varsigma_{m0} \dot{Q}^{\odot}_{m1} + (1-\varsigma_{m0}) \left(\dot{Q}^{\blacklozenge}_{m0} - \dot{Q}^{\blacklozenge}_{m1}\right) - \left(Ṗ^{-}_{m1} - \varsigma_{m0} Ṗ^{+}_{m1}\right) \exp\left(-\frac{\tilde{\Phi}}{\mu^{\odot}_1}\right) & & \\
y_{m(2k)} = Ṗ^{+}_{m(k+1)} \exp\left(-\frac{\tilde{\Phi}_{k+1}}{\mu^{\odot}_{k+1}}\right) - Ṗ^{+}_{mk} + \dot{Q}^{\blacklozenge}_{m(k+1)} - \dot{Q}^{\blacklozenge}_{mk} & ,k \in (1,2,\ldots,N_T) & \\
y_{m(2k+1)} = Ṗ^{-}_{m(k+1)} \exp\left(-\frac{\tilde{\Phi}_{k+1}}{\mu^{\odot}_{k+1}}\right) - Ṗ^{-}_{mk} + \dot{Q}^{\blacklozenge}_{m(k+1)} - \dot{Q}^{\blacklozenge}_{mk} & ,k \in (1,2,\ldots,N_T) & \\
y_{m(2N_T+2)} = \dot{Q}^{\Downarrow}_{m(\infty,a)} - Ṗ^{+}_{m(N_T+1)} - \dot{Q}^{\blacklozenge}_{m(N_T+1)} & &
\end{array}. \tag{S129}$$

S13 Overview of the momentum transfer model

The momentum transfer model must first quantify two characteristic scales associated with the vertical structure of the vegetation, namely the displacement height (z_d) and the roughness length (z_0). The displacement height is defined according to Shaw and Pereira (1982) and represents the effective height of the mean drag from all cohorts and soil surface. The roughness length is defined

after Raupach (1994, 1995) and represents the limit above the displacement height below which the typical logarithmic-based, surface layer wind profile is no longer valid. When the patch contains cohorts, we determine z_d and z_0 by adapting the model proposed by Massman (1997). This model is convenient because it does not assume fixed vegetation structures, therefore it can be determined and updated based on the demography of each patch. In ED-2.2, we use the discrete form of the original formulation, assuming that cohorts are dispersed uniformly in their patch space, such that the leaf and branch area indices are homogeneous in the horizontal plane for any given patch. The canopy environment is split in a fixed vertical grid with N_C layers spanning from the ground to the maximum vegetation height.

In the original formulation by Massman (1997), the displacement height is normalized by the canopy height; in ED-2.2 we apply a correction to scale the height with the effective canopy depth ($\bar{z}_c$) while accounting for the contribution from all cohorts including the tallest cohort (z_{t_1}):

$$z_d = \bar{z}_c \left\{ 1 - \frac{1}{z_{t_1}} \sum_{j=1}^{N_C} \left[\exp\left(-2 \frac{\Xi_{N_C} - \Xi_j}{\xi_{\text{sfc}}} \right) \Delta z_{c_j} \right] \right\}, \tag{S130}$$

$$z_0 = (\bar{z}_c - z_d) \exp\left(-\kappa \sqrt{\frac{2}{\xi_{\text{sfc}}}} + \tilde{\psi}_0 \right), \tag{S131}$$

where κ is the von Kármán constant (Table S3); $\Delta z_{c_j} = z_{c_j} - z_{c_{j-1}}$ is the layer thickness ($z_{c_0} = 0$); ξ_{sfc} is the vegetated surface drag coefficient, which is related to the ratio of the wind speed at the top cohort and the surface (Albini, 1981); Ξ_j is the cumulative cohort drag area per unit of ground area at layer j; and $\tilde{\psi}_0$ is the flux profile function of momentum at the roughness height (see Supplement S14.1), here approximated to 0.190 as in Raupach (1995).

Following Massman (1997), ξ_{sfc}, ξ_{c_j} and Ξ_{c_j} are defined as:

$$\xi_{\text{sfc}} = 2 \left[y_1 + y_2 \exp\left(y_3 \Xi_{c_{N_C}} \right) \right]^2, \tag{S132}$$

$$\Xi_{c_j} = \sum_{j'=1}^{j} \left(\frac{\xi_{c_{j'}}}{\mathcal{P}_{c_{j'}}} \phi_{c_{j'}} \Delta z_{c_{j'}} \right), \tag{S133}$$

$$\phi_{c_j} = \sum_{k=1}^{N_T} \left(\begin{cases} 0 & \text{, if } z_{t_k} < z_{c_{j-1}} \text{ or } z_{t_k}^- > z_{c_j} \\ \dfrac{\Phi_{t_k}}{\min\left(z_{c_j}, z_{t_k}\right) - \max\left(z_{t_k}^-, z_{c_{j-1}}\right)} & \text{, otherwise} \end{cases} \right), \tag{S134}$$

where ξ_{c_j} is the leaf-level drag coefficient due to cohorts at layer j; and $(y_1; y_2; y_3) = (0.320; 0.264; 15.1)$ are empirical constants (Massman, 1997). The sheltering factor for momentum ($\mathcal{P}_j$) accounts for the effects of adjacent leaves interfering in the viscous flow of air. The plant (leaves and wood)

area density function at layer j (ϕ_j) is calculated assuming that the leaf and branch-wood area indices of individual cohorts are evenly distributed between the height of the crown bottom $z_{t_k}^-$ and the cohort height z_{t_k}, as determined by the allometric equations (see Supplement S18).

Wohlfahrt and Cernusca (2002) pointed out that the drag coefficient ξ and the shelter factor $\mathcal{P}$ are not completely separable, and provided a functional form of the combined ratio instead of describing ξ and $\mathcal{P}$ independently. The function used in ED-2.2 is an adaptation of the original fit as a function of plant area density function (Wohlfahrt and Cernusca, 2002), using a logistic function to reduce the number of parameters (Fig. S7):

$$\frac{\xi_{c_j}}{\mathcal{P}_{c_j}} = y_4 + \frac{y_5}{1+\exp\left(y_6\,\phi_{c_j}\right)}, \tag{S135}$$

where $(y_4; y_5; y_6) = (0.086; 1.192; 0.480)$.

In case no above-ground vegetation exists (i.e. a patch with no cohorts), we assume that the roughness height $z_{0\varnothing}$ is the bare soil roughness z_{0g} plus any snow or water standing on top of the ground z_{0s}:

$$z_{0\varnothing} = z_{0g}\,(1 - f_{\mathrm{TSW}}) + z_{0s} f_{\mathrm{TSW}}; \tag{S136}$$

the default values of z_{0g} and z_{0s} are available in Table S4.

S14 Derivation of conductances

S14.1 Canopy air space conductance

To obtain the conductance at the top of the canopy air space, we solve the surface layer model that is based on the Monin-Obukhov similarity theory (Monin and Obukhov, 1954; Foken, 2006). First, we define the momentum ($\dot{U}_{a,c}$) and buoyancy ($\dot{\Theta}_{a,c}$) fluxes between the free atmosphere and the canopy air space at the top of the canopy air space. Following (Monteith and Unsworth, 2008), these fluxes can be represented either by the gradient or the eddy flux form:

$$\dot{U}_{a,c} = \rho_c K_U \frac{\partial u}{\partial z} = \rho_c \overline{u'_z u'_{\mathbf{x}}}, \tag{S137}$$

$$\dot{\Theta}_{a,c} = -\rho_c K_\Theta q_{p_c} \frac{\partial \theta_\mathcal{V}}{\partial z} = -\rho_c\, q_{p_c}\, \overline{u'_z \theta'_\mathcal{V}}, \tag{S138}$$

where K_U and K_Θ are the eddy diffusivities of momentum and buoyancy, respectively; $u_{\mathbf{x}}$ is the

horizontal wind speed, u_z is the vertical velocity; $\theta_{\mathcal{V}}$ is the virtual potential temperature; and q_{p_c} is the specific heat of the canopy air space (Supplement S6.3). The eddy diffusivities of enthalpy, moisture and CO_2 are assumed to be the same as the buoyancy, a common assumption based on observations (Stull, 1988).

The Monin-Obukhov similarity theory is based on the Buckingham's Π-theory (Stull, 1988), which requires as many fundamental scales as fundamental dimensions. The fundamental dimensions are the canopy air density (ρ_c) and three characteristic scales, namely the friction velocity ($u^\star$), characteristic virtual temperature gradient ($\theta^\star_{\mathcal{V}}$), and the diffusivity-corrected Obukhov length $\mathcal{L}$ (Panofsky, 1963):

$$u^\star = \sqrt{\frac{\dot{U}_{a,c}}{\rho}} = \sqrt{\left|\overline{u'_{\mathbf{x}} u'_z}\right|}, \tag{S139}$$

$$\theta^\star_{\mathcal{V}} = -\frac{1}{\kappa u^\star}\frac{\dot{\Theta}_{a,c}}{\rho\, q_{p_c}} = -\frac{\overline{u'_z \theta'_{\mathcal{V}}}}{u^\star}, \tag{S140}$$

$$\mathcal{L} = \frac{1}{\mathrm{Pr}}\frac{\dot{U}_{a,c}}{\dot{\Theta}_{a,c}}\frac{\theta_{\mathcal{V}_0}}{g}\frac{u^\star}{\kappa} \approx \frac{(\theta_{\mathcal{V}_a} + \theta_{\mathcal{V}_c})\, u^{\star 2}}{2\,\kappa\, g\, \theta^\star_{\mathcal{V}}}, \tag{S141}$$

where κ is the von Kármán constant, g is the gravity acceleration, and $\mathrm{Pr} \equiv K_U / K_\Theta$ is the turbulent Prandtl number (Table S3-S4). Another important dimensionless quantity is the bulk Richardson number Ri_B, defined as:

$$\mathrm{Ri}_B = \frac{2\, g\, (z^\star - z_0)\, (\theta_{\mathcal{V}_a} - \theta_{\mathcal{V}_c})}{(\theta_{\mathcal{V}_a} + \theta_{\mathcal{V}_c})\, u_a^2}, \tag{S142}$$

where $z^\star \equiv z_a - z_d$, z_a is the reference height, z_d is the displacement height, and z_0 is the roughness scale; both z_d and z_0 are determined by the momentum transfer model based on Massman (1997) (Supplement S13). The bulk Richardson number is informative on whether the layer between the canopy air space and the reference height z_a is unstable, neutral, or stable.

To determine the three remaining unknowns ($u^\star; \theta^\star_{\mathcal{V}}; \mathcal{L}$), we start from the general definition of dimensionless length scale ζ and two particular cases:

$$\zeta(z) = \frac{z - z_d}{\mathcal{L}}, \tag{S143}$$

$$\zeta^\star = \frac{z^\star}{\mathcal{L}} = \zeta_0 + \kappa \mathrm{Ri}_B \left(\frac{u_a}{u^\star}\right)^2 \frac{\theta^\star_{\mathcal{V}}}{\theta_{\mathcal{V}_a} - \theta_{\mathcal{V}_c}}, \tag{S144}$$

$$\zeta_0 = \frac{z_0}{\mathcal{L}} = \frac{z_0}{z^\star}\zeta^\star, \tag{S145}$$

where $z^\star = z_a - z_d$, where z_a (m) is the reference height above canopy, typically the height where the meteorological forcing measurements would be located in an eddy covariance tower; z_d is the displacement height (Eq. S130); z_0 (m) is the roughness length (Eq. S131); κ is the von Kármán constant (Table S3), Ri_B is the bulk Richardson number (Eq. S142); u_a is the wind speed at the reference height z_a; and $\theta_{\mathcal{V}_a}$ and $\theta_{\mathcal{V}_c}$ are the virtual temperature at the reference height and the canopy air space, respectively.

By choosing an appropriate combination of factors, Monin and Obukhov (1954) have shown that the dimensionless gradients of wind and temperature (here based on virtual potential temperature and the accounting for the Prandtl number) can be written as a function of the characteristic scales and dimensionless stability functions for momentum (φ_U) and heat (φ_Θ), which can be thought as correction factors for the logarithmic wind profile under non-neutral conditions (Monteith and Unsworth, 2008):

$$\frac{\partial}{\partial \zeta}\left(\frac{u_{\mathbf{x}}}{u^\star}\right) = \frac{1}{\kappa\,\zeta}\varphi_U(\zeta), \tag{S146}$$

$$\frac{\partial}{\partial \zeta}\left(\frac{\theta_{\mathcal{V}}}{\theta^\star_{\mathcal{V}}}\right) = \frac{\mathrm{Pr}}{\kappa\,\zeta}\varphi_\Theta(\zeta). \tag{S147}$$

Following Panofsky (1963), if we define the flux profile functions for momentum (ψ_U) and heat (ψ_Θ):

$$\psi_U(\zeta) = \int_0^\zeta \frac{1-\varphi_U(\zeta')}{\zeta'}\,\mathrm{d}\zeta', \tag{S148}$$

$$\psi_\Theta(\zeta) = \int_0^\zeta \frac{1-\varphi_\Theta(\zeta')}{\zeta'}\,\mathrm{d}\zeta', \tag{S149}$$

and integrate Eq. (S146)-(S147) between ζ_0, where wind is assumed to be zero, and any reference level ζ using the Leibniz integration rule, we obtain the horizontal wind and virtual potential temperature profile functions:

$$u_{\mathbf{x}}(\zeta) = \frac{u^\star}{\kappa}\left[\ln\left(\frac{\zeta}{\zeta_0}\right) - \psi_U(\zeta) + \psi_U(\zeta_0)\right], \tag{S150}$$

$$\theta_{\mathcal{V}}(\zeta) = \theta_{\mathcal{V}_c} + \frac{\mathrm{Pr}\,\theta^\star_{\mathcal{V}}}{\kappa}\left[\ln\left(\frac{\zeta}{\zeta_0}\right) - \psi_\Theta(\zeta) + \psi_\Theta(\zeta_0)\right]. \tag{S151}$$

If we substitute Eq. (S150)-(S151) for the specific case when $\zeta = \zeta^\star$ into Eq. (S144), we obtain an equation where the only unknown is $\zeta^\star$:

$$\zeta^{\star} = \frac{\mathrm{Ri}_B}{\mathrm{Pr}} \left(\frac{z^{\star}}{z^{\star} - z_0} \right) \frac{\left[\ln\left(\frac{\zeta^{\star}}{\zeta_0} \right) - \psi_U\left(\zeta^{\star}\right) + \psi_U\left(\zeta_0\right) \right]^2}{\ln\left(\frac{\zeta^{\star}}{\zeta_0} \right) - \psi_{\Theta}\left(\zeta^{\star}\right) + \psi_{\Theta}\left(\zeta_0\right)}. \tag{S152}$$

The ED-2.2 model uses the empirical parameterization of the originally developed by Beljaars and Holtslag (1991). For the unstable cases, Beljaars and Holtslag (1991) used the Businger-Dyer flux profile equations (Businger et al., 1971). For the stable cases, Beljaars and Holtslag (1991) implemented an empirical formulation that improved the vertical mixing between the canopy air space and the air above under stable conditions:

$$\psi_U\left(\zeta\right) = \begin{cases} 2\ln\left[\frac{1+Y(\zeta)}{2}\right] + \ln\left[\frac{1+Y^2(\zeta)}{2}\right] - 2\arctan\left[Y(\zeta)\right] + \frac{\pi}{2} & \text{, if } \mathrm{Ri}_B < 0 \\ y_1\zeta + y_2\left(\zeta - \frac{y_3}{y_4}\right)\exp\left(-y_4\zeta\right) + \frac{y_2 y_3}{y_4} & \text{, if } \mathrm{Ri}_B \geq 0 \end{cases}, \tag{S153}$$

$$\psi_{\Theta}\left(\zeta\right) = \begin{cases} 2\ln\left[\frac{1+Y^2(\zeta)}{2}\right] & \text{, if } \mathrm{Ri}_B < 0 \\ 1 - \left(1 - \frac{y_1}{y_5}\zeta\right)^{y_5} + x_2\left(\zeta - \frac{y_3}{y_4}\right)\exp\left(-y_4\zeta\right) + \frac{y_2 y_3}{y_4} & \text{, if } \mathrm{Ri}_B \geq 0 \end{cases}, \tag{S154}$$

$$Y(\zeta) = \sqrt[4]{1 - y_6\zeta}, \tag{S155}$$

where $\mathbf{y} = \left(-1; -\frac{2}{3}; 5; 0.35; \frac{3}{2}; 13\right)$ are empirical and adjustable parameters. Equation (S152) cannot be solved analytically, therefore $\zeta^{\star}$ is calculated using a root-finding technique. Once $\zeta^{\star}$ is determined, we can find $u^{\star}$ using Eq. (S150), and define the canopy conductance G_c ($\mathrm{m\,s^{-1}}$) using Eq. (S151) as the starting point, similarly to Oleson et al. (2013):

$$G_c = \frac{u^{\star}\,\theta_{\mathcal{V}}^{\star}}{\theta_{\mathcal{V}_a} - \theta_{\mathcal{V}_c}} = \frac{\kappa\, u^{\star}}{\mathrm{Pr}\left[\ln\left(\frac{\zeta^{\star}}{\zeta_0}\right) - \psi_{\Theta}\left(\zeta^{\star}\right) + \psi_{\Theta}\left(\zeta_0\right)\right]}. \tag{S156}$$

S14.2 Derivation leaf and wood boundary layer conductances

Following Monteith and Unsworth (2008), convection can be of two types: forced convection, which depends on mechanic mixing associated with the fluid velocity; and free convection, which is due to buoyancy of the boundary layer fluid. Although convection is often dominated by either forced or free convection, in ED-2.2 we always assume that the total conductance is a simple combination of forced and free convection conductances as if they were parallel:

$$G_{Qx_k} = G_{Qx_k}^{\text{Free}} + G_{Qx_k}^{\text{Forced}}, \tag{S157}$$

where x_k can be either the leaf (λ_k) or the branch wood (β_k) boundary layer. For each convective regime, we define the conductance in terms of the Nusselt number Nu, a dimensionless number that corresponds to the ratio between heat exchange through convection and conduction:

$$G_{Qx_k} = \frac{\eta_c \,\mathrm{Nu}}{x^\star}. \tag{S158}$$

where η_c is the thermal diffusivity of canopy air space and $x^\star$ is the characteristic size of the obstacle. For leaves, the characteristic size $x^\star_{\lambda_k}$ is a PFT-dependent constant corresponding to the typical leaf width , whereas for branch wood the typical size $x^\star_{\beta_k}$ is assumed to be the typical diameter of twigs (Tables S5-S6).

Free convection is a result of the thermal gradient between the obstacle surface and the fluid, and this is normally expressed in terms of the Grashof number Gr, a dimensionless index that relates buoyancy and viscous forces. In ED-2.2 we use the same empirical functions as Monteith and Unsworth (2008), using flat plate geometry for leaves and horizontal cylinder geometry for branch wood:

$$\mathrm{Nu}_{\lambda_k}^{(\text{Free})} = \max\left[\underbrace{0.50\,\mathrm{Gr}_{\lambda_k}^{\frac{1}{2}}}_{\text{Laminar}}, \underbrace{0.13\,\mathrm{Gr}_{\lambda_k}^{\frac{1}{3}}}_{\text{Turbulent}}\right], \tag{S159}$$

$$\mathrm{Nu}_{\beta_k}^{(\text{Free})} = \max\left[\underbrace{0.48\,\mathrm{Gr}_{\beta_k}^{\frac{1}{2}}}_{\text{Laminar}}, \underbrace{0.09\,\mathrm{Gr}_{\beta_k}^{\frac{1}{3}}}_{\text{Turbulent}}\right], \tag{S160}$$

$$\mathrm{Gr}_{x_k} = \frac{\varepsilon_c\, g\, \left(x^\star_{x_k}\right)^3}{\nu_c^2}\, |T_{x_k} - T_c|\,, \tag{S161}$$

where ε_c is the thermal dilatation coefficient for the canopy air space and ν_c is the kinematic viscosity of the canopy air space; x_k represents either the leaf (λ_k) or wood (β_k) surface; and g is the gravity acceleration. Like in Monteith and Unsworth (2008), thermal diffusivity and dynamic viscosity (both in $\mathrm{m^2\,s^{-1}}$) are assumed to be linear functions of the canopy air space temperature:

$$\eta_c = 1.89 \cdot 10^{-5}\left[1 + 0.007\,(T_c - T_0)\right], \tag{S162}$$

$$\nu_c = 1.33 \cdot 10^{-5}\left[1 + 0.007\,(T_c - T_0)\right], \tag{S163}$$

where the first term on the right hand side are the reference values at temperature $T_0 = 273.15\,\mathrm{K}$. Under the assumption that canopy air space is a perfect gas, thermal dilatation is $\varepsilon_c = T_c^{-1}$ (Dufour and van Mieghem, 1975).

For forced convection the flow of air through the object at different temperature causes the heat exchange, therefore Nusselt number is written as a function of the Reynolds number Re, a dimensionless index that relates inertial and viscous forces. Like in the free convection case, we use the same empirical functions as Monteith and Unsworth (2008) and the same shapes as the free convection case:

$$\mathrm{Nu}_{\lambda_k}^{(\mathrm{Forced})} = \max\left[\underbrace{0.60\,\mathrm{Re}_{\lambda_k}^{0.5}}_{\text{Laminar}}, \underbrace{0.032\,\mathrm{Re}_{\lambda_k}^{0.8}}_{\text{Turbulent}}\right], \tag{S164}$$

$$\mathrm{Nu}_{\beta_k}^{(\mathrm{Forced})} = \max\left[\underbrace{0.32 + 0.51\,\mathrm{Re}_{\beta_k}^{0.52}}_{\text{Laminar}}, \underbrace{0.24\,\mathrm{Re}_{\beta_k}^{0.60}}_{\text{Turbulent}}\right], \tag{S165}$$

$$\mathrm{Re}_{x_k} = \frac{u_{t_k} x^{\star}_{x_k}}{\eta_c}, \tag{S166}$$

where u_{t_k} is the wind speed experienced by the cohort k, and x_k represents either the leaf (λ_k) or wood (β_k) surface.

The wind profile within the canopy air space is determined in two steps. Above the tallest cohort, we assume that the wind can be determined from the similarity theory; from Eq. (S143) we define $\zeta_{c_j} = \zeta\left(z_{c_j}\right)$, and use wind profile function from the similarity theory (Eq. S150) to determine the wind speed at the top of the vegetated layer $u_{c_{N_C}} = u\left(\zeta_{c_{N_C}}\right)$. Within the canopy, we estimate the wind speed reduction using the wind profile as a function of cumulative drag (Ξ_j; Albini, 1981; Massman, 1997); the wind speed experienced by the cohort is the average wind between the layers where the bottom ($\hat{z}_{t_k}$) and top (z_{t_k}) of the crown are located:

$$u_{c_j} = u_{c_{N_C}} \exp\left(-\frac{\Xi_{c_{N_C}} - \Xi_{c_j}}{\xi_{\mathrm{sfc}}}\right) \tag{S167}$$

$$u_{t_k} = \max\left[0.25\,\mathrm{m\,s^{-1}}, \frac{u_{c_{N_C}}}{z_{c_j(k)} - z_{c_{\hat{j}}(k)}} \sum_{j'=\hat{j}(k)}^{j(k)} \left(u_{c_{j'}} \Delta z_{c_{j'}}\right)\right], \tag{S168}$$

where $c_{\hat{j}(k)}$ and $c_j(k)$ are the canopy air space layers corresponding to the bottom and top of the cohort's crown. The minimum wind speed of $0.25\,\mathrm{m\,s^{-1}}$ is imposed to avoid conductance to become unrealistically low and to account for some mixing due to gusts when the mean wind

is very weak. Once the heat conductance is determined, we use the same vapor to heat ratio as Leuning et al. (1995) to calculate the water vapor conductance:

$$G_{Wx_k} = 1.075\, G_{Qx_k}, \tag{S169}$$

where x_k represents either the leaf (λ_k) or wood (β_k) surface. Similarly, we define the CO_2 boundary layer conductance for leaves using the ratio of diffusivities and convection between water and CO_2 ($f_{G\lambda}$, Table S4), following Cowan and Troughton (1971):

$$\hat{G}_{W\lambda_k} = f_{G\lambda}\, \hat{G}_{C\lambda_k}. \tag{S170}$$

S14.3 Derivation of surface conductance

The total resistance between the surface and the canopy air space is a combination of the air resistance if the surface were bare, and the resistance due to the presence of the vegetated canopy, assuming that these resistances are serial and thus additive (as mentioned by Walko et al., 2000); using that conductance is the inverse of resistance:

$$\frac{1}{G_{\text{Sfc}}} = \frac{1}{G_{\text{Bare}}} + \frac{1}{G_{\text{Veg}}}, \tag{S171}$$

where G_{Sfc} is the total surface conductance, G_{Bare} is the bare-ground equivalent conductance, and G_{Veg} is the conductance associated with vegetation presence. The bare ground conductance G_{Bare} can be approximated to be G_c (Eq. S156; see also Sellers et al., 1996). Two methods have been implemented conductance due to vegetation presence, one based on the Simple Biosphere Model (SiB-2, Sellers et al., 1996) ($G_{\text{Veg}}^{\text{SiB}}$), and one based on Massman and Weil (1999) ($G_{\text{Veg}}^{\text{MW99}}$), which incorporates the second-order closure method that accounts for the amount of shear in the sublayer above the canopy and the geometric attributes that define the drag of air. Results in the main text used the SiB-2 based vegetation conductance.

S14.3.1 SiB-2 based vegetation conductance

In the SiB-2 based approach, we assume that the total resistance due to vegetation presence (inverse of conductance G_{Veg}) is equivalent to the total contribution of diffusivity from ground to the top of vegetated layer:

$$\frac{1}{G_{\text{Veg}}^{\text{SiB}}} = \int_{z_{0\varnothing}}^{z_{t_k}} \frac{1}{K_\Theta(z)} \mathrm{d}z \approx \sum_{j=1}^{N_C} \frac{\text{Pr}}{K_{U_{c_j}}} \Delta z_{c_j}, \tag{S172}$$

$$z_{0\varnothing} = z_{0s} f_{\text{TSW}} + z_{0g} (1 - f_{\text{TSW}}), \tag{S173}$$

where $j = 1, 2, \ldots, N_C$ are the discrete vertical layers used to describe the canopy air space, Δz_{c_j} is the thickness of canopy air space layer j, the index $z_{0\varnothing}$ is combined contribution to roughness from the temporary surface water (z_{0s}) and bare-ground (z_{0g}), f_{TSW} is the fraction of ground covered by temporary surface water, K_Θ is the eddy diffusivity for heat, $K_{U_{c_j}}$ is the eddy diffusivity for momentum of canopy air space layer j, $\text{Pr} = K_U K_\Theta^{-1}$ is the Prandtl number (Table S4; Businger et al., 1971). We further assume that $K_{U_{c_j}}$ is proportional to u_{c_j}, the horizontal wind speed at canopy air space layer j, and that Y_U is the scaling factor, i.e. $K_{U_{c_j}} \equiv Y_U u_{\mathbf{x}}$ (Sellers et al., 1986), and that within the vegetated layer the winds are determined through Eq. (S167). Therefore, Eq. (S172) becomes

$$\frac{1}{G_{\text{Veg}}^{\text{SiB}}} = \sum_{j=1}^{N_C} \left[\frac{\text{Pr}}{Y_U u_{c_j}} \exp\left(\frac{\Xi_{c_{N_C}} - \Xi_{c_j}}{\xi_{\text{Sfc}}} \right) \right], \tag{S174}$$

where ξ_{Sfc} is the drag coefficient of vegetated surfaces (Eq. S132) and Ξ_{c_j} is the cumulative cohort drag area per unit of ground area at layer j (Eq. S133). If we assume that Y_U is constant and the wind profile is continuous, and combine Eq. (S137), Eq. (S139), Eq. (S146), and Eq. (S148) at the dimensionless length scale $\zeta(z_{c_{N_C}}) = \zeta_{c_{N_C}}$ (Eq. S143), Y_U can be estimated as:

$$Y_U = \frac{\kappa u^\star (z_{t_1} - z_d)}{u_{c_{N_C}}} \frac{1}{1 - \zeta_{c_{N_C}} \frac{\partial \psi_U}{\partial \zeta}(\zeta_{c_{N_C}})}. \tag{S175}$$

S14.3.2 Second Order Closure of Turbulent Transport from the Surface to Canopy

The method of Massman and Weil (1999) is a second-order closure method that derives $G_{\text{Veg}}^{\text{MW99}}$ from the shear in the sub-layer above the canopy and the geometric attributes of the canopy that define the drag of fluid. Massman and Weil (1999) base their method on some key simplifications to the the turbulent kinetic energy (TKE) budget equation: (1) no horizontal variability exists within any given patch (horizontal homogeneity); (2) the turbulent flow has proportional isotropy, i.e., the variance in each of the three wind directions is proportional to TKE.

$$\mathrm{TKE} = \frac{1}{2}\left[\underbrace{\sigma_{u_x}^2 + \sigma_{u_y}^2}_{\sigma_{u_\mathbf{x}}^2} + \sigma_{u_z}^2\right], \tag{S176}$$

$$\sigma_{u_\mathbf{x}}^2 = \overline{u'_\mathbf{x} u'_\mathbf{x}}, \tag{S177}$$

$$\sigma_{u_z}^2 = \overline{u'_z u'_z}, \tag{S178}$$

where $u_\mathbf{x} = \sqrt{u_x^2 + u_y^2}$ is the horizontal wind along the direction of the mean wind, and $u'_?$ is the departure from the mean wind in any of the wind directions. With the horizontal homogeneity and proportional isotropy assumptions, it is possible to derive an analytical solution to the TKE budget, and ultimately obtain an analytical solution for the vertical profile of standard deviation of wind speed (Eq. 10 of Massman and Weil, 1999):

$$\sigma_{u_k}(z_{c_j}) = \mathcal{S}_{u_k}\, y\, u^\star \left\{ Y_1 \exp\left[-\frac{3\left(\Xi_{c_{N_C}} - \Xi_{c_j}\right)}{\xi_{\mathrm{Sfc}}}\right] + Y_2 \exp\left[-\frac{\sqrt{3}\, y\left(\Xi_{c_{N_C}} - \Xi_{c_j}\right)}{\beta}\right]\right\}^{\frac{1}{3}}, \tag{S179}$$

$$y = \left(\mathcal{S}_x^2 + \mathcal{S}_y^2 + \mathcal{S}_z^2\right)^{-\frac{1}{2}}, \tag{S180}$$

$$Y_1 = -\frac{3\beta\,(2\,\xi_{\mathrm{Sfc}})^{\frac{1}{2}}}{3\beta^2\, y - y^3\,\xi_{\mathrm{Sfc}}^2}, \tag{S181}$$

$$Y_2 = \frac{1}{y^3} - Y_1, \tag{S182}$$

where Ξ_c is the cumulative drag profile (Eq. S133); ξ_{Sfc} is the vegetated surface drag coefficient (Eq. S132); and $\left(\mathcal{S}_{u_x}; \mathcal{S}_{u_y}; \mathcal{S}_{u_z}\right) = (2.40; 1.90; 1.25)$ are adjustable parameters that represent the ratio between above-canopy velocity variance and the momentum flux, taken from Raupach et al. (1991) as in Massman and Weil (1999); and the u_k subscript represents one of the wind directions (u_x, u_y, or u_z). In addition, the empirical β represents a joint eddy mixing length scale for both shear- and wake-driven turbulence. A sensitivity study of β using the ED-2.2 model implementation found that this parameter should be between 0.01 and 0.03 (Knox, 2012) to ensure that the turbulence intensity ($\imath_U = \sigma_{u_z}/u_\mathbf{x}$) is stable over the canopy depth as it approaches the soil surface. These values of β are also similar to the value of 0.05 found by Massman and Weil (1999). Depending on the the magnitude of ξ_{Sfc} and the choice of β, it is possible that Eq. (S179) yields negative (non-physical) values of σ_{u_k}; to avoid unrealistic solutions, β is dynamically set in ED-2.2. The model assigns an initial guess of $\beta = 0.03$ and, in case the solution is non-physical, it iteratively reduces the parameter until σ_{u_k} becomes positive.

Similar to the heat conductance between leaves, branches and the canopy air space (Section S14.2), the conductance between ground and canopy air space is related to the Nusselt number (Nu), following Eq. (S158). To account for the effects of both free (buoyant) convection and forced (mechanic) convection, the Nusselt number is parameterized as a function of the Reynolds (Re) and the Prandtl (Pr) numbers, with an additional modification to account for turbulence intensity (ι_U) (Sauer and Norman, 1995; Massman and Weil, 1999). To ensure that the conductance encompasses the entire canopy air space, we use the average turbulence intensity ($\overline{\iota_U}$) between the soil surface and the canopy air space depth (z_c):

$$\overline{\iota_U} = \frac{1}{z_c} \sum_{j=1}^{N_C} \frac{\sigma_{u_z}\left(z_{c_j}\right)}{u_{\mathbf{x}}\left(z_{c_j}\right)} \Delta z_{c_j}, \tag{S183}$$

$$G_{\text{Veg}}^{\text{MW99}} = z_0^{1/2} \left(1 + 2\,\overline{\iota_U}\right) \frac{\eta_c}{x_{\text{Veg}}^{\star}} \text{Re}^{b_1} \text{Pr}^{b_2} u_{\mathbf{x}}(z_{t_1}) \sqrt{\frac{u_{\mathbf{x}}\left(z_0\right)}{u_{\mathbf{x}}\left(z_{t_1}\right)}}. \tag{S184}$$

where $(b_1; b_2) = (-1/2; -2/3)$ (Sauer and Norman, 1995); and $x_{\text{Veg}}^{\star}$ is the mixing length scale for vegetated surface, and z_0 is the roughness length scale (Eq. S131).

S15 Phase equilibrium (saturation) of water vapor

The partial pressure of water vapor at phase equilibrium (p_{Sat}) is solely a function of temperature, following the Clapeyron equation (Dufour and van Mieghem, 1975; Murphy and Koop, 2005). Whether the phase equilibrium of water vapor refers to ice-vapor ($p_{vi}^{\equiv}$) or liquid-vapor ($p_{v\ell}^{\equiv}$) transitions also depends on the temperature, and in ED-2.2, we use the law of minimum:

$$p_{\text{Sat}}(T) = \min\left[p_{vi}(T), p_{v\ell}(T)\right]. \tag{S185}$$

Both p_{vi} and $p_{v\ell}$ are defined after the parameterization by (Murphy and Koop, 2005), which have high degree of accuracy ($< 0.05\%$) between 123 K and 332 K, and thus includes all the range of near-surface temperatures solved by ED-2.2:

$$p_{vi}(T) = \exp\left[9.550426 - \frac{5723.265}{T} + 3.53068 \ln(T) - 0.00728332\,T\right], \tag{S186}$$

$$p_{v\ell}(T) = \exp\left\{Y_1(T) + Y_2(T) \tanh\left[0.0415\,(T - 218.8)\right]\right\}, \tag{S187}$$

$$Y_1(T) = 54.842763 - \frac{6763.22}{T} - 4.210 \ln(T) + 0.000367\,T, \tag{S188}$$

$$Y_2(T) = 53.878 - \frac{1331.22}{T} - 9.44523 \ln(T) + 0.014025\,T. \tag{S189}$$

Importantly, Eq. (S186) and Eq. (S187) yield the same value (within $4.1 \cdot 10^{-6}\%$ accuracy) at the water's triple point, which guarantees continuity of Eq. (S185).

The saturation specific humidity $w^{=}$ is obtained using Eq. (S185) and the definition of specific humidity:

$$w_{\mathrm{Sat}}(T,p) = \frac{\mathcal{M}_w\, p_{\mathrm{Sat}}(T)}{\mathcal{M}_d\,[p - p_{\mathrm{Sat}}(T)] + \mathcal{M}_w\, p_{\mathrm{Sat}}(T)}, \tag{S190}$$

where $\mathcal{M}_d$ and $\mathcal{M}_w$ are the molar masses of dry air and water, respectively (Tab S3).

S16 Solver for the CO_2 assimilation rates and transpiration

Variables w_{l_k}, $\dot{V}_{C_k}^{\max}$, $\dot{R}_k$, ϖ_k, $\mathcal{K}_{O_k}$, $\mathcal{K}_{C_k}$, Γ_k, and $\mathcal{K}_{\mathrm{ME}_k}$ are functions of leaf temperature and canopy air space pressure, and thus can be determined directly. In constrast, nine variables are unknown for each limitation case as well as for the case when the stomata are closed: $\dot{E}_k$, $\dot{A}_k$, $\dot{V}_{C_k}$, $\dot{V}_{O_k}$, c_{l_k}, c_{λ_k}, w_{λ_k}, $\hat{G}_{Wl_k}$, and $\hat{G}_{Cl_k}$. To solve the remaining unknowns, we first substitute Eq. (82) and either Eq. (85), Eq. (87) or Eq. (89) into Eq. (81) and write a general functional form for $\dot{A}_k$, similarly to Medvigy (2006), that is a function of only one unknown, c_{l_k}:

$$\dot{A}_k\left(c_{l_k}\right) = \frac{F_k^{\mathrm{A}}\, c_{l_k} + F_k^{\mathrm{B}}}{F_k^{\mathrm{C}}\, c_{l_k} + F_k^{\mathrm{D}}} - \dot{R}_k, \tag{S191}$$

where parameters F depend on the limitation and the photosynthetic pathway, as shown in Table S9.

We then combine Eq. (76) and Eq. (S170) to eliminate $\hat{G}_{Cl_k}$ and c_{λ_k}, and write an alternative equation for $\hat{G}_{Wl_k}$:

$$\hat{G}_{Wl_k} = \frac{f_{Gl}\,\hat{G}_{W\lambda_k}\,\dot{A}_k}{\hat{G}_{W\lambda_k}\left(c_c - c_{l_k}\right) - f_{G\lambda}\,\dot{A}_k}. \tag{S192}$$

To eliminate c_{λ_k} and w_{λ_k} from Eq. (91), we use Eq. (76) and Eq. (77). Then, we eliminate $\hat{G}_{Wl_k}$ by replacing the left hand side of Eq. (91) by the alternative Eq. (S192), yielding to the following function $\mathcal{F}(c_{l_k})$ for which we seek the solution $\mathcal{F}(c_{l_k}) = 0$:

$$\mathcal{F}(c_{l_k}) = \mathcal{F}_1(c_{l_k})\,\mathcal{F}_2(c_{l_k})\,\mathcal{F}_3(c_{l_k}) - 1, \tag{S193}$$

$$\mathcal{F}_1(c_{l_k}) = \frac{\left(f_{Gl} - f_{G\lambda}\,\dfrac{\hat{G}^{\varnothing}_{Wl_k}}{\hat{G}_{W\lambda_k}}\right)\dot{A}_k - \hat{G}^{\varnothing}_{Wl_k}\left(c_c - c_{l_k}\right)}{m_k \dot{A}_k}, \tag{S194}$$

$$\mathcal{F}_2(c_{l_k}) = \frac{\hat{G}_{W\lambda_k}\left(c_c - \Gamma_k\right) - f_{G\lambda}\,\dot{A}_k}{\hat{G}_{W\lambda_k}\left(c_c - c_{l_k}\right) + \left(f_{Gl} - f_{G\lambda}\right)\dot{A}_k}, \tag{S195}$$

$$\mathcal{F}_3(c_{l_k}) = 1 + \frac{w_c - w_{l_k}}{\Delta w_k}\,\frac{\hat{G}_{W\lambda_k}\left(c_c - c_{l_k}\right) - f_{G\lambda}\,\dot{A}_k}{\hat{G}_{W\lambda_k}\left(c_c - c_{l_k}\right) + \left(f_{Gl} - f_{G\lambda}\right)\dot{A}_k}. \tag{S196}$$

For the limitation cases in which Eq. (S191) does not depend on c_{l_k}, Eq. (S193) is reduced to a quadratic equation. For the other cases, Eq. (S193) becomes a fifth-order polynomial, which cannot be solved algebraically. Nevertheless, Eq. (S193) is still convenient because it highlights the range of plausible solutions, corresponding to the singularities associated with $\mathcal{F}_1$ and $\mathcal{F}_2$ — the singularities associated with $\mathcal{F}_3$ requires c_{l_k} to exceed c_c, which could be only achieved with negative $\hat{G}_{l_k w}$ or $\dot{A}_k < -\dot{M}_k$, and none of them are meaningful. Function $\mathcal{F}_1$ is singular when $\dot{A}_k = 0$; from Eq. (S192), this would require $\hat{G}_{Wl_k}$ to be 0, unless $c_{l_k} = c_c$. Function $\mathcal{F}_2$ is singular when $\dot{A}_k = \hat{G}_{C\lambda_k}\left(c_c - c_{l_k}\right)$; from Eq. (S192), this happens only when $c_{l_k} = c_c$ or at $\lim_{\hat{G}_{Wl_k}\to\infty}$. The singularities for when $c_c \neq c_{l_k}$ are obtained by substituting Eq. (S191) into Eq. (76), and by taking the $\lim_{\hat{G}_{Wl_k}\to 0}\left(\dot{A}_k\right)$ and $\lim_{\hat{G}_{Wl_k}\to\infty}\left(\dot{A}_k\right)$:

$$c^{\min}_{l_k} + \frac{F^{\mathrm{D}}_k \dot{M}_k - F^{\mathrm{B}}_k}{F^{\mathrm{C}}_k \dot{M}_k - F^{\mathrm{A}}_k} = 0, \tag{S197}$$

$$\left(c^{\max}_{l_k}\right)^2 + \frac{\hat{G}_{C\lambda_k} F^{\mathrm{D}}_k + F^{\mathrm{B}}_k - F^{\mathrm{C}}_k\left(\hat{G}_{C\lambda_k} c_c + \dot{M}_k\right)}{\hat{G}_{C\lambda_k} F^{\mathrm{C}}_k}\, c^{\max}_{l_k} + \frac{F^{\mathrm{B}}_k - F^{\mathrm{D}}_k\left(\hat{G}_{C\lambda_k} c_c + \dot{M}_k\right)}{\hat{G}_{C\lambda_k} F^{\mathrm{C}}_k} = 0. \tag{S198}$$

From Eq. (S198) up to two roots are possible, but normally only one is plausible. In case both values are greater than c_c, we use c_c as the upper boundary, because c_c is also a singularity; otherwise the root between $c^{\min}_{l_k}$ and c_c is selected. If none of them are in this range, then there is no viable solution for this limitation, and we assume that the stomata must be closed. Once the boundaries are defined, we seek the solution in the $\left]c^{\min}_{l_k}; c^{\max}_{l_k}\right[$ interval, where there is only one possible solution, as illustrated in Fig. S8.

Once all cases are determined, the solution is determined by a law of minimum (Collatz et al., 1991, 1992; Moorcroft et al., 2001):

$$\dot{A}_k = \min\left(\dot{A}_k^{\mathrm{RuBP}}, \dot{A}_k^{\mathrm{InSL}}, \dot{A}_k^{\mathrm{PAR}}\right), \tag{S199}$$

$$\dot{E}_k = \dot{E}_k^{L\star}, \tag{S200}$$

where $L\star$ is the limiting case chosen in Eq. (S199). When available light or c_{l_k} is near or below their compensation point, it is possible that none of the limiting cases yields a viable solution. In this case, we assume that photosynthesis cannot occur and that stomata are closed.

S17 Soil moisture limitation on photosynthesis

The stomatal conductance equation by Leuning (1995) was developed using well-watered seedlings, therefore it does not consider soil moisture limitation, which can be important in seasonally dry ecosystems. To account for soil water stress, we define a phenomenological scaling function f_{Wl_k} (wilting factor). The functional form of f_{Wl_k} follows the previous versions of ED (Moorcroft et al., 2001; Medvigy et al., 2009). However, in ED-2.2 we define water availability ($W^{\star}_{g_j}$) in terms of soil matric potential, similarly to CLM (Oleson et al., 2013), which produces a more gradual transition from no-stress conditions to completely closed stomata as soil moisture approaches the wilting point (Fig. S9).

In ED-2.2, the wilting factor f_{Wl_k} is defined as:

$$f_{Wl_k} = \frac{1}{1+\dfrac{\mathrm{Demand}}{\mathrm{Supply}}} = \frac{1}{1+\dfrac{\mathcal{M}_w \Lambda_k \dot{E}_k}{\hat{G}_{r_k} C_{r_k} W^{\star}_{g_{j0}}}}, \tag{S201}$$

$$W^{\star}_{g_j} = \sum_{j'=j}^{N_G} \left[\rho_\ell \left(\vartheta_{\mathrm{Fc}} - \vartheta_{\mathrm{Wp}}\right) \Psi^{\star}_{g_{j'}} \Delta z_{g_{j'}}\right], \tag{S202}$$

$$\Psi^{\star}_{g_j} = \ell_{g_j} \frac{\max\left[\min\left(\Psi_{g_j} + \frac{z_{g_j}+z_{g_{j+1}}}{2}, \Psi_{\mathrm{Fc}}\right), \Psi_{\mathrm{Wp}}\right] - \Psi_{\mathrm{Wp}}}{\Psi_{\mathrm{Fc}} - \Psi_{\mathrm{Wp}}}, \tag{S203}$$

where $\hat{G}_{r_k}$ ($\mathrm{m^2\,kg_C^{-1}\,s^{-1}}$) is a PFT-dependent scaling parameter related to fine root conductance (Tables S5-S6); $\mathcal{M}_w$ is the molar mass of water (Table S3); $\dot{E}_k$ ($\mathrm{mol_W\,m_{Leaf}^{-2}\,s^{-1}}$) is the leaf-level transpiration rate if soil moisture is not limiting; C_{r_k} ($\mathrm{kg_C\,m^{-2}}$) is the fine root biomass per individual; Λ_k ($\mathrm{m^2\,m^{-2}}$) is the leaf area index of cohort k; $W^{\star}_{g_j}$ ($\mathrm{kg_W\,m^{-2}}$) is the available water for photosynthesis integrated from soil layer j to surface; $j0$ is the deepest soil layer that the cohort k can access water; z_{g_j} and Δz_{g_j} are the depth and thickness of soil layer j (z_{g_j} is always negative, and Δz_{g_j} is always positive); ρ_ℓ ($\mathrm{kg_w m^{-3}}$) is the density of liquid water; ϑ_{Fc} and ϑ_{Wp} ($\mathrm{m^3\,m^{-3}}$)

are the volumetric soil moistures at field capacity and at permanent wilting point, Ψ_{g_j} (m) is the matric potential of layer j, $\Psi_{\rm Fc}$ and $\Psi_{\rm Wp}$ (m) are the matric potentials at field capacity and wilting point, $\Psi^{\star}_{g_j}$ (unitless) is a factor that represents the reduction of available water due to force needed to extract the water.

S18 Allometric equations

In ED-2.2, size is defined by a suite of dimensions, including tree height z_{t_k} and rooting depth z_{r_k} which directly affect the cohort access to light and water, and the carbon stocks in different tissues. Most allometric equations use the diameter at the breast height (DBH, cm) as the size-dependent explanatory variable. The only time DBH becomes the dependent variable is when the code calculates the growth of structural tissues ($\Delta t_{\rm CD}$): structural carbon stocks are updated based on the cohort's net carbon balance, and DBH is calculated to be consistent with the updated structural carbon stocks.

The tree height of any cohort k (z_{t_k}) is determined through a modified Weibull function:

$$z_{t_k} = \min\left\{z_{t_{\max}}, \mathcal{Z}_0 + \mathcal{Z}_\infty\left[1 - \exp\left(-\mathcal{Z}_1 \cdot \mathrm{DBH}_k^{\mathcal{Z}_2}\right)\right]\right\}, \tag{S204}$$

where $\mathcal{Z}_0$, $\mathcal{Z}_1$, $\mathcal{Z}_2$, and $\mathcal{Z}_\infty$ are PFT-dependent coefficients; and $z_{t_{\max}}$ is the maximum tree height, imposed to avoid excessive extrapolation of the allometric equations for carbon stocks. The coefficients are shown in Tables S5-S6; coefficients for tropical trees are provided by Poorter et al. (2006) allometric equation for moist forests in Bolivia; coefficients for temperate trees are from Albani et al. (2006).

The tree height at the bottom of the crown ($z^{-}_{t_k}$) is based on Poorter et al. (2006), and it is currently applied to tropical, subtropical, and temperate trees. For grasses, we fix the height to 1% of the total height, to avoid numeric singularities while assuming that most of the grass vertical profile has leaves:

$$z^{-}_{t_k} = \begin{cases} \max\left(0.05, 0.01\, z_{t_k}\right) & \text{, if cohort } k \text{ is grass} \\ \max\left(0.05, z_{t_k} - 0.31\, z_{t_k}^{1.098}\right) & \text{, if cohort } k \text{ is tree} \end{cases}. \tag{S205}$$

Maximum leaf biomass ($C^{\bullet}_{l_k}$, $\mathrm{kg\,m^{-2}}$), corresponding to the state when leaves are fully flushed:

$$C^{\bullet}_{l_k} = n_{t_k}\, \mathcal{C}_{0 l_k} \mathrm{DBH}_k^{\mathcal{C}_{1 l_k}}, \tag{S206}$$

where n_{t_k} (plant m^{-2}) is the plant demographic density, and $\mathcal{C}_{0l}$ and $\mathcal{C}_{1l}$ are the PFT-dependent coefficients (Tables S5-S6). For tropical PFTs, the default parameters are derived from the allometric equations presented by Cole and Ewel (2006) and Calvo-Alvarado et al. (2008) for several commercial species in Costa Rica; for temperate PFTs, the default parameters are the same as in Albani et al. (2006) and Medvigy et al. (2009).

Maximum root biomass ($C^{\bullet}_{r_k}$, kg m^{-2}) and maximum sapwood biomass ($C^{\bullet}_{\sigma_k}$, kg m^{-2}) are determined from $C^{\bullet}_{l_k}$ using the same functional form as Moorcroft et al. (2001), whose formulation of sapwood biomass was was based on the pipe model by Shinozaki et al. (1964a,b):

$$C^{\bullet}_{r_k} = f_{r_k} C^{\bullet}_{l_k}, \tag{S207}$$

$$C^{\bullet}_{\sigma_k} = \frac{\mathrm{SLA}_k}{f_{\sigma_k}} z_{t_k} C^{\bullet}_{l_k}, \tag{S208}$$

where f_{r_k} and f_{σ_k} are PFT-dependent parameters, currently assumed to be the same as in the original ED-1 (Moorcroft et al., 2001, Tables S5-S6); SLA (Tables S5-S6) is the specific leaf area, determined from Kim et al. (2012) fit of specific leaf area as a function of leaf turnover rate, using the GLOPNET leaf economics dataset (Wright et al., 2004).

Total structural (heartwood) biomass (C_{h_k}, kg$_\mathrm{C}$ m^{-2}) functional form is the same functional form for all PFTs. For temperate PFTs, the parameters are the same as in Albani et al. (2006) and Medvigy et al. (2009). For tropical PFTs, the parameters are based on Baker et al. (2004) equation of above-ground biomass, which is in turn based on the allometric equation by Chave et al. (2001) for French Guiana. This allometric equation was used instead of the allometric equation based on Chambers et al. (2001) because in ED-2.2 the function relating C_{h_k} and DBH_k must be bijective (i.e. given n_{t_k}, each DBH_k is associated with a single value of C_{h_k} and vice versa), which cannot be attained with the polynomial fits of higher order. Structural biomass was assumed to be the difference between above-ground biomass and the biomass of leaves and 70% of the total sapwood, corresponding to the above-ground fraction. The estimate was fitted against DBH, yielding to:

$$C_{h_k} = \begin{cases} n_{t_k} \mathcal{C}_{0h_k} \mathrm{DBH}^{\mathcal{C}_{1h_k}} & \text{, if } \mathrm{DBH}_k \leq \mathrm{DBH}_{\mathrm{Crit}} \\ n_{t_k} \mathcal{C}_{2h_k} \mathrm{DBH}^{\mathcal{C}_{3h_k}} & \text{, if } \mathrm{DBH}_k > \mathrm{DBH}_{\mathrm{Crit}} \end{cases}, \tag{S209}$$

where $\mathrm{DBH}_{\mathrm{Crit}}$ is the minimum DBH that results in $z_{t_k} = 35.0$ m, and the coefficients $\mathcal{C}_{0h}$, $\mathcal{C}_{1h}$, $\mathcal{C}_{2h}$, $\mathcal{C}_{3h}$ are defined for each PFT (Tables S5-S6).

The size-dependent rooting depth (z_{r_k}) is defined from an exponential function that allows tree depths to reach 5 m once trees reach canopy size ($z_{t_k} = 35$ m):

$$z_{r_k} = -1.114\,\mathrm{DBH}_k^{0.422}. \tag{S210}$$

The maximum rooting depth is shallow compared to Nepstad et al. (1994) results, however it produces a rooting profile similar to other dynamic global vegetation models, and reflects that little variation in soil moisture exists at very deep layers (Christoffersen, 2013).

Leaf area index (Λ_k, $\mathrm{m}^2_{\mathrm{Leaf}}\,\mathrm{m}^{-2}$) is determined from leaf biomass and specific leaf area:

$$\Lambda_k = \mathrm{SLA}_k\, C_{l_k}, \tag{S211}$$

where n_k ($\mathrm{plant}\,\mathrm{m}^{-2}$) is the demographic density of cohort k.

No allometric equation was found for wood area index (Ω_k, $\mathrm{m}^2_{\mathrm{Wood}}\,\mathrm{m}^{-2}$) for evergreen forests. We assumed the same allometric equation for temperate zone by Hörmann et al. (2003) for trees, and imposed maximum area at $\mathrm{DBH}_{\mathrm{Crit}}$, similarly to C_{l_k}:

$$\Omega_k = \begin{cases} 0 & \text{if cohort } k \text{ is grass} \\ n_k\, 0.0096\, \min\left(\mathrm{DBH}, \mathrm{DBH}_{\mathrm{Crit}}\right)^{2.0947} & \text{if cohort } k \text{ is broadleaf tree} \\ n_k\, 0.02765\, \min\left(\mathrm{DBH}, \mathrm{DBH}_{\mathrm{Crit}}\right)^{1.9769} & \text{if cohort } k \text{ is conifer} \end{cases}. \tag{S212}$$

Crown area index (X_k, $\mathrm{m}^2_{\mathrm{Crown}}\,\mathrm{m}^{-2}$) is also based on Poorter et al. (2006), but re-written so it is a function of DBH_k. Like in the previous cases, crown area was capped at $\mathrm{DBH}_{\mathrm{Crit}}$, and local crown area was not allowed to exceed 1.0 or to be less than the leaf area index:

$$X_k = \begin{cases} \min\left[1.0, \max\left(\Lambda_k, n_k\, 1.126\, \mathrm{DBH}^{1.052}\right)\right] & \text{if cohort is tropical/subtropical} \\ \min\left[1.0, \max\left(\Lambda_k, n_k\, 2.490\, \mathrm{DBH}^{0.807}\right)\right] & \text{if cohort is temperate} \end{cases}. \tag{S213}$$

References

Albani, M., Medvigy, D., Hurtt, G. C., and Moorcroft, P. R.: The contributions of land-use change, CO_2 fertilization, and climate variability to the eastern US carbon sink, Glob. Change Biol., 12, 2370–2390, doi:10.1111/j.1365-2486.2006.01254.x, 2006.

Albini, F. A.: A phenomenological model for wind speed and shear stress profiles in vegetation cover layers, J. Appl. Meteor., 20, 1325–1335, doi:10.1175/1520-0450(1981)020<1325:APMFWS>2.0.CO;2, 1981.

Baccini, A., Goetz, S. J., Walker, W. S., Laporte, N. T., Sun, M., Sulla-Menashe, D., Hackler, J., Beck, P. S. A., Dubayah, R., Friedl, M. A., Samanta, S., and Houghton, R. A.: Estimated carbon dioxide emissions from tropical deforestation improved by carbon-density maps, Nature Clim. Change, 2, 182–185, doi:10.1038/nclimate1354, 2012.

Baker, T. R., Phillips, O. L., Malhi, Y., Almeida, S., Arroyo, L., Di Fiore, A., Erwin, T., Killeen, T. J., Laurance, S. G., Laurance, W. F., Lewis, S. L., Lloyd, J., Monteagudo, A., Neill, D. A., Patiño, S., Pitman, N. C. A., M. Silva, J. N., and Vásquez Martínez, R.: Variation in wood density determines spatial patterns in Amazonian forest biomass, Glob. Change Biol., 10, 545–562, doi:10.1111/j.1365-2486.2004.00751.x, 2004.

Beljaars, A. C. M. and Holtslag, A. A. M.: Flux parameterization over land surfaces for atmospheric models, J. Appl. Meteor., 30, 327–341, doi:10.1175/1520-0450(1991)030<0327:FPOLSF>2.0.CO;2, 1991.

Botta, A., Viovy, N., Ciais, P., Friedlingstein, P., and Monfray, P.: A global prognostic scheme of leaf onset using satellite data, Glob. Change Biol., 6, 709–725, doi:10.1046/j.1365-2486.2000.00362.x, 2000.

Brooks, R. H. and Corey, A. T.: Hydraulic properties of porous media, Hydrology Papers 3, Colorado State University, Fort Collins, U.S.A., 1964.

Businger, J. A., Wyngaard, J. C., Izumi, Y., and Bradley, E. F.: Flux-profile relationships in the atmospheric surface layer, J. Atmos. Sci., 28, 181–189, doi:10.1175/1520-0469(1971)028<0181:FPRITA>2.0.CO;2, 1971.

Calvo-Alvarado, J. C., McDowell, N. G., and Waring, R. H.: Allometric relationships predicting foliar biomass and leaf area:sapwood area ratio from tree height in five Costa Rican rain forest species, Tree Physiol., 28, 1601–1608, doi:10.1093/treephys/28.11.1601, 2008.

Camillo, P. and Schmugge, T. J.: A computer program for the simulation of heat and moisture flow in soils, Technical Memorandum TM-82121, NASA, Greenbelt, United States, 1981.

Chambers, J. Q., dos Santos, J., Ribeiro, R. J., and Higuchi, N.: Tree damage, allometric relationships, and above-ground net primary production in central Amazon forest, Forest Ecol. Manag., 152, 73–84, doi:10.1016/S0378-1127(00)00591-0, 2001.

Chave, J., Riéra, B., and Dubois, M.-A.: Estimation of biomass in a neotropical forest of French Guiana: spatial and temporal variability, J. Trop. Ecol., 17, 79–96, doi:10.1017/S0266467401001055, 2001.

Christoffersen, B. O.: The ecohydrological mechanisms of resilience and vulnerability of Amazonian tropical forests to water stress, Ph.d. dissertation, University of Arizona, Tucson, AZ, USA, URL http://hdl.handle.net/10150/293566, 2013.

Clapp, R. B. and Hornberger, G. M.: Empirical equations for some soil hydraulic properties, Water Resour. Res., 14, 601–604, doi:10.1029/WR014i004p00601, 1978.

Cole, T. G. and Ewel, J. J.: Allometric equations for four valuable tropical tree species, Forest Ecol. Manag., 229, 351–360, doi:10.1016/j.foreco.2006.04.017, 2006.

Collatz, G., Ribas-Carbo, M., and Berry, J.: Coupled photosynthesis-stomatal conductance model for leaves of C_4 plants, Aust. J. Plant Physiol., 19, 519–538, doi:10.1071/PP9920519, 1992.

Collatz, G. J., Ball, J., Grivet, C., and Berry, J. A.: Physiological and environmental regulation of stomatal conductance, photosynthesis and transpiration: a model that includes a laminar boundary layer, Agric. For. Meteorol., 54, 107–136, doi:10.1016/0168-1923(91)90002-8, 1991.

Cosby, B. J., Hornberger, G. M., Clapp, R. B., and Ginn, T. R.: A statistical exploration of the relationships of soil moisture characteristics to the physical properties of soils, Water Resour. Res., 20, 682–690, doi:10.1029/WR020i006p00682, 1984.

Cowan, I. and Troughton, J.: The relative role of stomata in transpiration and assimilation, Planta, 97, 325–336, doi:10.1007/BF00390212, 1971.

Dufour, L. and van Mieghem, J.: Thermodynamique de l'atmosphère, Institut Royal Météorologique de Belgique, Gembloux, Belgium, 2 edn., in French, 1975.

Foken, T.: 50 years of the Monin–Obukhov similarity theory, Boundary-Layer Meteorol., 119, 431–447, doi:10.1007/s10546-006-9048-6, 2006.

Forest Products Laboratory: Wood handbook – wood as an engineering material, General Technical Report FPL-GTR-190, U.S. Department of Agriculture, Madison, WI, doi:10.2737/FPL-GTR-190, 2010.

Goudriaan, J.: Crop meteorology: a simulation study, Ph.D. thesis, Wageningen University and Research Centre, Wageningen, Netherlands, URL http://library.wur.nl/WebQuery/clc/104086, 1977.

Gu, L., Meyers, T., Pallardy, S. G., Hanson, P. J., Yang, B., Heuer, M., Hosman, K. P., Liu, Q., Riggs, J. S., Sluss, D., and Wullschleger, S. D.: Influences of biomass heat and biochemical energy storages on the land surface fluxes and radiative temperature, J. Geophys. Res., 112, D02 107, doi:10.1029/2006JD007425, 2007.

Hodnett, M. and Tomasella, J.: Marked differences between van Genuchten soil water-retention parameters for temperate and tropical soils: a new water-retention pedo-transfer functions developed for tropical soils, Geoderma, 108, 155–180, doi:10.1016/S0016-7061(02)00105-2, 2002.

Hörmann, G., Irrgan, S., Jochheim, H., Lukes, M., Meesenburg, H., Müller, J., Scheler, B., Scherzer, J., Schüler, G., Schultze, B., Strohbach, B., Suckow, F., Wegehenkel, M., and Wessolek, G.: Wasserhaushalt von Waldökosystemen: methodenleitfaden zur bestimmung der wasserhaushaltskomponenten auf level II-Flächen, Technical note, Bundesministerium für Verbraucherschutz, Ernährung und Landwirtschaft (BMVEL), Bonn, Germany, URL `http://www.wasklim.de/download/Methodenband.pdf`, in German, 2003.

Jin, J., Gao, X., Sorooshian, S., Yang, Z.-L., Bales, R., Dickinson, R. E., Sun, S.-F., and Wu, G.-X.: One-dimensional snow water and energy balance model for vegetated surfaces, Hydrol. Process., 13, 2467–2482, doi:10.1002/(SICI)1099-1085(199910)13:14/15<2467::AID-HYP861>3.0.CO;2-J, 1999.

Jones, H. G.: Plants and Microclimate: A quantitative approach to environmental plant physiology, Cambridge Univ. Press, Cambridge, UK, 3rd edn., doi:10.1017/CBO9780511845727, 2014.

Kim, Y., Knox, R. G., Longo, M., Medvigy, D., Hutyra, L. R., Pyle, E. H., Wofsy, S. C., Bras, R. L., and Moorcroft, P. R.: Seasonal carbon dynamics and water fluxes in an Amazon rainforest, Glob. Change Biol., 18, 1322–1334, doi:10.1111/j.1365-2486.2011.02629.x, 2012.

Knox, R. G.: Land conversion in Amazonia and Northern South America; influences on regional hydrology and ecosystem response, Ph.D. dissertation, Massachusetts Institute of Technology, Cambridge, MA, URL `https://dspace.mit.edu/handle/1721.1/79489`, 2012.

Kursar, T. A., Engelbrecht, B. M. J., Burke, A., Tyree, M. T., EI Omari, B., and Giraldo, J. P.: Tolerance to low leaf water status of tropical tree seedlings is related to drought performance and distribution, Funct. Ecol., 23, 93–102, doi:10.1111/j.1365-2435.2008.01483.x, 2009.

Leuning, R.: A critical appraisal of a combined stomatal-photosynthesis model for C_3 plants, Plant Cell Environ., 18, 339–355, doi:10.1111/j.1365-3040.1995.tb00370.x, 1995.

Leuning, R., Kelliher, F. M., de Pury, D. G. G., and Schulze, E.-D.: Leaf nitrogen, photosynthesis, conductance and transpiration: scaling from leaves to canopies, Plant Cell Environ., 18, 1183–1200, doi:10.1111/j.1365-3040.1995.tb00628.x, 1995.

Louis, J.-F.: A parametric model of vertical eddy fluxes in the atmosphere, Boundary-Layer Meteorology, 17, 187–202, doi:10.1007/BF00117978, 1979.

Massman, W. J.: An analytical one-dimensional model of momentum transfer by vegetation of arbitrary structure, Boundary-Layer Meteorol., 83, 407–421, doi:10.1023/A:1000234813011, 1997.

Massman, W. J. and Weil, J. C.: An analytical one-dimensional second-order closure model of turbulence statistics and the Lagrangian time scale within and above plant canopies of arbitrary structure, Boundary-Layer Meteorol., 91, 81–107, doi:10.1023/A:1001810204560, 1999.

Medvigy, D. M.: The state of the regional carbon cycle: results from a constrained coupled ecosystem-atmosphere model, Ph.D. dissertation, Harvard University, Cambridge, MA, 2006.

Medvigy, D. M., Wofsy, S. C., Munger, J. W., Hollinger, D. Y., and Moorcroft, P. R.: Mechanistic scaling of ecosystem function and dynamics in space and time: Ecosystem Demography model version 2, J. Geophys. Res.-Biogeosci., 114, G01 002, doi:10.1029/2008JG000812, 2009.

Monin, A. S. and Obukhov, A. M.: Osnovnye zakonomernosti turbulentnogo pere- meshivanija v prizemnom sloe atmosfery (Basic laws of turbulent mixing in the atmosphere near the ground), Trudy Geofiz. Inst. AN SSSR, 24, 163–187, URL `http://mcnaughty.com/keith/papers/Monin_and_Obukhov_1954.pdf`, original in Russian. Translation available at the URL, 1954.

Monteith, J. L. and Unsworth, M. H.: Principles of environmental physics, Academic Press, London, 3rd edition edn., 418 pp., 2008.

Moorcroft, P. R., Hurtt, G. C., and Pacala, S. W.: A method for scaling vegetation dynamics: The Ecosystem Demography model (ED), Ecol. Monogr., 71, 557–586, doi:10.1890/0012-9615(2001)071[0557:AMFSVD]2.0.CO;2, 2001.

Murphy, D. M. and Koop, T.: Review of the vapour pressures of ice and supercooled water for atmospheric applications, Quart. J. Royal Meteorol. Soc., 131, 1539–1565, doi:10.1256/qj.04.94, 2005.

Nepstad, D. C., de Carvalho, C. R., Davidson, E. A., Jipp, P. H., Lefebvre, P. A., Negreiros, G. H., da Silva, E. D., Stone, T. A., Trumbore, S. E., and Vieira, S.: The role of deep roots in the hydrological and carbon cycles of Amazonian forests and pastures, Nature, 372, 666–669, doi:10.1038/372666a0, 1994.

Niu, G.-Y. and Yang, Z.-L.: An observation-based formulation of snow cover fraction and its evaluation over large North American river basins, J. Geophys. Res.-Atmos., 112, D21 101, doi:10.1029/2007JD008674, 2007.

Oleson, K. W., Lawrence, D. M., Bonan, G. B., Drewniak, B., Huang, M., Koven, C. D., Levis, S., Li, F., Riley, W. J., Subin, Z. M., Swenson, S. C., Thornton, P. E., Bozbiyik, A., Fisher, R., Heald, C. L., Kluzek, E., Lamarque, J.-F., Lawrence, P. J., Leung, L. R., Lipscomb, W., Muszala, S., Ricciuto, D. M., Sacks, W., Sun, Y., Tang, J., and Yang, Z.-L.: Technical description of version 4.5 of the Community Land Model (CLM), Technical Report NCAR/TN-503+STR, NCAR, Boulder, CO, doi:10.5065/D6RR1W7M, 420pp., 2013.

Panofsky, H. A.: Determination of stress from wind and temperature measurements, Quart. J. Royal Meteorol. Soc., 89, 85–94, doi:10.1002/qj.49708937906, 1963.

Parlange, M., Cahill, A., Nielsen, D., Hopmans, J., and Wendroth, O.: Review of heat and water movement in field soils, Soil Till. Res., 47, 5–10, doi:10.1016/S0167-1987(98)00066-X, 1998.

Poorter, L., Bongers, L., and Bongers, F.: Architecture of 54 moist-forest tree species: traits, trade-offs, and functional groups, Ecology, 87, 1289–1301, doi:10.1890/0012-9658(2006)87[1289:AOMTST]2.0.CO;2, 2006.

Raupach, M. R.: Simplified expressions for vegetation roughness length and zero-plane displacement as functions of canopy height and area index, Boundary-Layer Meteorol., 71, 211–216, doi:10.1007/BF00709229, 1994.

Raupach, M. R.: Corrigenda, Boundary-Layer Meteorol., 76, 303–304, doi:10.1007/BF00709356, 1995.

Raupach, M. R., Antonia, R. A., and Rajagopalan, S.: Rough-wall turbulent boundary layers, Appl. Mech. Rev., 44, 1–25, doi:10.1115/1.3119492, 1991.

Rogers, A., Medlyn, B. E., Dukes, J. S., Bonan, G., von Caemmerer, S., Dietze, M. C., Kattge, J., Leakey, A. D. B., Mercado, L. M., Niinemets, U., Prentice, I. C., Serbin, S. P., Sitch, S., Way, D. A., and Zaehle, S.: A roadmap for improving the representation of photosynthesis in Earth system models, New Phytol., 213, 22–42, doi:10.1111/nph.14283, 2017.

Romano, N. and Santini, A.: Field, in: Methods of soil analysis: Part 4 physical methods, edited by Dane, J. H. and Topp, G. C., SSSA Book Series 5.4, chap. 3.3.3, pp. 721–738, Soil Science Society of America, Madison, WI, 2002.

Sauer, T. and Norman, J.: Simulated canopy microclimate using estimated below-canopy soil surface transfer coefficients, Agric. For. Meteorol., 75, 135–160, doi:10.1016/0168-1923(94)02208-2, 1995.

Saxton, K. E. and Rawls, W. J.: Soil water characteristic estimates by texture and organic matter for hydrologic solutions, Soil Sci. Soc. Am. J., 70, 1569–1578, doi:10.2136/sssaj2005.0117, 2006.

Sellers, P. J.: Canopy reflectance, photosynthesis and transpiration, Int. J. Remote Sens., 6, 1335–1372, doi:10.1080/01431168508948283, 1985.

Sellers, P. J., Mintz, Y., Sud, Y. C., and Dalcher, A.: A Simple Biosphere model (SIB) for use within general circulation models, J. Atmos. Sci., 43, 505–531, doi:10.1175/1520-0469(1986)043<0505:ASBMFU>2.0.CO;2, 1986.

Sellers, P. J., Randall, D. A., Collatz, G. J., Berry, J. A., Field, C. B., Dazlich, D. A., Zhang, C., Collelo, G. D., and Bounoua, L.: A revised land surface parameterization (SiB2) for atmospheric GCMs. Part I: model formulation, J. Climate, 9, 676–705, doi:10.1175/1520-0442(1996)009<0676:ARLSPF>2.0.CO;2, 1996.

Shaw, R. H. and Pereira, A.: Aerodynamic roughness of a plant canopy: A numerical experiment, Agric. For. Meteorol., 26, 51–65, doi:10.1016/0002-1571(82)90057-7, 1982.

Shinozaki, K., Yoda, K., Hozumi, K., and Kira, T.: A quantitative analysis of plant form – the pipe model theory. I. Basic analyses, Jpn. J. Ecol., 14, 97–105, doi:10.18960/seitai.14.3_97, 1964a.

Shinozaki, K., Yoda, K., Hozumi, K., and Kira, T.: A quantitative analysis of plant form – the pipe model theory. II. Further evidence of the theory and its application in forest ecology, Jpn. J. Ecol., 14, 133–139, doi:10.18960/seitai.14.4_133, 1964b.

Stull, R. B.: An introduction to boundary layer meteorology, vol. 13 of *Atmospheric and Oceanographic Sciences Library*, Springer Netherlands, Dordrecht, Netherlands, doi:10.1007/978-94-009-3027-8, 1988.

The HDF Group: Hierarchical data format, version 5, URL `http://www.hdfgroup.org/HDF5/`, 2016.

Verseghy, D. L.: Class—A Canadian land surface scheme for GCMS. I. Soil model, Intl. J. Climatol., 11, 111–133, doi:10.1002/joc.3370110202, 1991.

Viskari, T., Hardiman, B., Desai, A. R., and Dietze, M. C.: Model-data assimilation of multiple phenological observations to constrain and predict leaf area index, Ecol. Appl., 25, 546–558, doi:10.1890/14-0497.1, 2015.

Walko, R. L., Band, L. E., Baron, J., Kittel, T. G. F., Lammers, R., Lee, T. J., Ojima, D., Pielke, R. A., Taylor, C., Tague, C., Tremback, C. J., and Vidale, P. L.: Coupled atmosphere–biophysics–hydrology models for environmental modeling, J. Appl. Meteor., 39, 931–944, doi:10.1175/1520-0450(2000)039<0931:CABHMF>2.0.CO;2, 2000.

Wohlfahrt, G. and Cernusca, A.: Momentum transfer by a mountain meadow canopy: a simulation analysis based on Massman's (1997) model, Boundary-Layer Meteorol., 103, 391–407, doi:10.1023/A:1014960912763, 2002.

Wright, I. J., Reich, P. B., Westoby, M., Ackerly, D. D., Baruch, Z., Bongers, F., Cavender-Bares, J., Chapin, T., Cornelissen, J. H. C., Diemer, M., Flexas, J., Garnier, E., Groom, P. K., Gulias, J., Hikosaka, K., Lamont, B. B., Lee, T., Lee, W., Lusk, C., Midgley, J. J., Navas, M.-L., Niinemets, U., Oleksyn, J., Osada, N., Poorter, H., Poot, P., Prior, L., Pyankov, V. I., Roumet, C., Thomas, S. C., Tjoelker, M. G., Veneklaas, E. J., and Villar, R.: The worldwide leaf economics spectrum, Nature, 428, 821–827, doi:10.1038/nature02403, 2004.

Wright, S. J., Jaramillo, M. A., Pavon, J., Condit, R., Hubbell, S. P., and Foster, R. B.: Reproductive size thresholds in tropical trees: variation among individuals, species and forests, J. Trop. Ecol., 21, 307–315, doi:10.1017/S0266467405002294, 2005.

Zhang, X., Friedl, M. A., Schaaf, C. B., Strahler, A. H., Hodges, J. C. F., Gao, F., Reed, B. C., and Huete, A.: Monitoring vegetation phenology using MODIS, Remote Sens. Environ., 84, 471–475, doi:10.1016/S0034-4257(02)00135-9, 2003.